Identification and characterization of novel filament-forming proteins in cyanobacteria

Benjamin L. Springstein[1]*, Christian Woehle[1‡], Julia Weissenbach[1‡‡], Andreas O. Helbig[2], Tal Dagan[1], Karina Stucken[3]*

[1] Institute of General Microbiology, Christian-Albrechts-Universität zu Kiel, Kiel, Germany

[2] Institute for Experimental Medicine, Christian-Albrechts-Universität zu Kiel, Kiel, Germany

[3] Department of Food Engineering, University of La Serena, La Serena, Chile.

‡ Present address: Max Planck Institute for Plant Breeding Research, Max Planck-Genome-Center Cologne, Cologne, Germany

‡‡ Present address: Faculty of Biology, Technion-Israel Institute of Technology, Haifa, 32000, Israel

* Corresponding authors: BLS: bspringstein@ifam.uni-kiel.de; KS: kstucken@userena.cl

Abstract

Filament-forming proteins in the bacterial cytoskeleton function in stabilization and localization of proteinaceous complexes and replicons. Research of the cyanobacterial cytoskeleton is focused on the bacterial tubulin (FtsZ) and actin (MreB). Nonetheless, the diverse colony morphologies and cell types in cyanobacteria suggest the presence of additional cytoskeletal proteins. Here we present two novel filament-forming proteins in cyanobacteria. Surveying cyanobacterial genomes for coiled-coil-rich proteins (CCRPs), we observed a higher proportion of CCRPs in filamentous cyanobacteria in comparison to unicellular cyanobacteria. We identified nine protein families with putative intermediate filament (IF) properties. Polymerization assays revealed four polymer-forming proteins *in vitro* and three polymer-forming proteins *in vivo*. Fm7001 from *Fischerella muscicola* PCC 7414 polymerized *in vitro* and formed filaments in different *in vivo* systems. Functional analysis of Fm7001 suggests that it has IF-like properties. Additionally, we identified a tetratricopeptide repeat protein, All4981 in *Anabaena* sp. PCC 7120 that polymerized into filaments *in vivo* and *in vitro*. All4981 interacts with other known cytoskeletal proteins and is indispensable for *Anabaena*. Our results expand the repertoire of known prokaryotic filament-forming CCRPs and demonstrate that cyanobacterial CCRPs are involved in cell morphology, motility, cytokinesis and colony integrity.

Author Summary

The phylum Cyanobacteria is characterized by a large morphological diversity, ranging from coccoid or rod-shaped unicellular species to complex filamentous multicellular species. Many species of multicellular cyanobacteria can undergo cell differentiation and changes in their cell shape. Despite this diversity, very few molecular mechanisms underlying the cyanobacterial morphological plasticity are known. Among these, the cytoskeletal proteins FtsZ and MreB are important regulators of cyanobacterial cell shape and viability. Also, the multicellular phenotype of filamentous cyanobacteria has been linked to prokaryotic gap-junction analogs, the septal junctions. The significance of our research is the identification and characterization of a novel

cyanobacterial cytoskeletal repertoire of IF-like proteins that will aid in the characterization of the morphological complexity of cyanobacteria. Thus, our survey leads to a broader understanding of the underlying principles of cyanobacterial morphotypes and will serve as a starting point for future research to further unravel the complex morphologies unique to this phylum.

Introduction

Species in the phylum Cyanobacteria present a wide morphological diversity, ranging from unicellular to multicellular organisms. Unicellular cyanobacteria of the *Synechocystis* and *Synechococcus* genera are characterized by a round or rod-shaped morphology, respectively, and many strains are motile. Species of the Nostocales order are multicellular and differentiate specialized cells, known as heterocysts, which fix atmospheric nitrogen under aerobic conditions. Within the Nostocales, species of the Nostocaceae (e.g., *Anabaena*, *Nostoc*) form linear filaments, while cells in the Hapalosiphonaceae and Chlorogloepsidaceae divide in more than one plane to form true-branching or multiseriate filaments (e.g. as in *Fischerella* or *Chlorogloeopsis*, respectively) (Rippka *et al.*, 1979). Notably, cells within a single filament (termed trichome) of a multicellular cyanobacterium can differ in size, form or cell wall composition (Rippka *et al.*, 1979). Cells in the *Anabaena* sp. PCC 7120 (hereafter *Anabaena*) trichome are linked by a shared peptidoglycan sheet and an outer membrane (Wilk *et al.*, 2011). The cells communicate and exchange nutrients through intercellular cell-cell connections, called septal junctions, thought to be comprised of the septal junction proteins SepJ, FraC and FraD (reviewed by Herrero, Stavans and Flores, 2016). SepJ is essential for the multicellular phenotype in the heterocystous cyanobacterium *Anabaena* (Flores *et al.*, 2007; Nayar *et al.*, 2007). Studies of the molecular basis of cyanobacterial morphogenesis have so far focused on the function of FtsZ and MreB, the prokaryotic homologs of tubulin and actin, respectively (Wagstaff and Löwe, 2018). FtsZ, which is organized in a multi-protein complex called the divisome, is a key regulator of cell division and septal peptidoglycan (PG) biogenesis (Bi and Lutkenhaus, 1991; Wagstaff and Löwe, 2018). In *Anabaena* and in the

coccoid cyanobacterium *Synechocystis* sp. PCC 6803 (*Synechocystis*), FtsZ is an essential cellular component (Zhang *et al.*, 1995). The FtsZ cellular concentration in *Anabaena* is tightly controlled by a so far undescribed protease (Lopes Pinto *et al.*, 2011). Apart from its function in cell division, the FtsZ-driven divisome also mediates the localization of SepJ (Ramos-León *et al.*, 2015). MreB, which similar to FtsZ is also organized in a multi-protein complex called the elongasome, is a key mediator of longitudinal PG biogenesis controlling cell shape (Jones, Carballido-López and Errington, 2001; Wagstaff and Löwe, 2018). In cyanobacteria, MreB has been shown to have a role in cell shape determination in *Anabaena*, nonetheless, it is dispensable for cell viability (Hu *et al.*, 2007). In contrast, MreB is essential in *Synechococcus* sp. PCC 7942 (*Synechococcus*) where partially segregated mutants display a coccoid morphology, resembling *E. coli mreB* deletion strains (Kruse, Bork-Jensen and Gerdes, 2005; Jain, Vijayan and O'Shea, 2012).

IF proteins exhibit an intrinsic nucleotide-independent polymerization capability *in vitro* that is mediated by the high frequency of coiled-coil-rich regions in their amino acid sequence (Shoeman and Traub, 1993; Fuchs and Weber, 1994; Löwe and Amos, 2009; Wagstaff and Löwe, 2018). Eukaryotic IF proteins are generally characterized by a conserved domain buildup consisting of discontinuous coiled-coil segments that form a central rod domain. This rod domain is N- and C-terminally flanked by globular head and tail domains of variable length (Fuchs and Weber, 1994; Herrmann *et al.*, 1996; Herrmann and Aebi, 2004). Crescentin, a bacterial IF-like CCRP from *Caulobacter crescentus*, exhibits a striking domain similarity to eukaryotic IF proteins. Crescentin filaments that align at the inner cell curvature are essential for the typical crescent-like cell shape of *C. crescentus*, possibly by locally exuding a constriction force which coordinates the MreB-driven peptidoglycan (PG) synthesis machinery (Ausmees, Kuhn and Jacobs-Wagner, 2003; Cabeen *et al.*, 2009; Charbon, Cabeen and Jacobs-Wagner, 2009). Reminiscent of eukaryotic IF proteins, crescentin was found to assemble into filamentous structures *in vitro* in a nucleotide-independent manner (Ausmees, Kuhn and Jacobs-Wagner, 2003). However, so far, no crescentin homologs have been found in other bacteria, indicating that non-spherical or rod-shaped prokaryotic morphologies are

putatively controlled by other cytoskeletal proteins of assumed IF-like origin (Bagchi *et al.*, 2008; Wickstead and Gull, 2011). Apart from crescentin, many other coiled coil-rich proteins (CCRPs) with IF-like functions have been identified to polymerize into filamentous structures and to perform cytoskeletal roles, however, none of them resembled the eukaryotic IF domain architecture (reviewed by Lin & Thanbichler, 2013). Examples are two proteins from *Streptomyces coelicolor* whose function has been studied in more detail: FilP and Scy (Bagchi *et al.*, 2008; Walshaw, Gillespie and Kelemen, 2010; Holmes *et al.*, 2013). Gradients of FilP filaments localize at the tip of a growing hyphae and contribute to cellular stiffness (Bagchi *et al.*, 2008). Scy forms patchy clusters at the sites of novel tip-formation and, together with the scaffolding CCRP DivIVA, orchestrates polar hyphal growth (Holmes *et al.*, 2013). Together with FilP and a cellulose-synthase, these proteins form the polarisome, which guides peptidoglycan biogenesis and hyphal tip growth (Flärdh *et al.*, 2012; Hempel *et al.*, 2012; Holmes *et al.*, 2013). Another example are four CCRPs in the human pathogen *Helicobacter pylori*, which were found to assemble into filaments *in vitro* and *in vivo* and to determine the helical cell shape as well as cell motility (Waidner *et al.*, 2009; Specht *et al.*, 2011). Consequently, filament-forming CCRPs with cytoskeletal functions have been found in numerous prokaryotes with different cellular morphologies. The presence of intermediate filament (IF)-like proteins in the cyanobacterial cytoskeleton is so far understudied. Thus, here we search for IF-like CCRPs in cyanobacteria using a computational prediction of CCRPs and functionally characterize putative IF-like proteins by *in vitro* and *in vivo* assays in morphologically diverse cyanobacteria.

Results

Coiled-coil rich proteins are widespread in cyanobacteria

For the computational prediction of putative filament-forming proteins, we surveyed 364 cyanobacterial genomes including 1,225,314 protein-coding sequences (CDSs). All CDSs in the cyanobacterial genomes where clustered by sequence similarity into families of homologous proteins (see Methods). The frequency of CCRPs in each CDS was calculated using the COILS algorithm (Lupas, Van Dyke and Stock, 1991). The algorithm yielded a list of 28,737 CDSs with high coiled-coil content (≥80 amino acids in coiled-coil conformation; Supplementary File 1). CCRPs were predicted in 158,466 protein families covering all cyanobacterial species. To examine the overall distribution of CCRPs in cyanobacterial genomes, we investigated 1,504 families of homologous proteins that include at least three CCRP members (Fig. 1). Notably, most protein families (1,142; 76%) include CCRP and non-CCRP members, indicating that IF-like properties might differ among homologous proteins. The presence/absence pattern of families including CCRPs further shows that those are less abundant in picocyanobacterial genomes (SynProCya group) in comparison to the remaining specie in the phylum. Furthermore, the proportion of CCRPs in the genome is significantly higher in filamentous cyanobacteria in comparison to unicellular cyanobacteria ($P=2.65x10^{-46}$ using Kruskal-Wallis test and Tukey test with $\alpha=0.05$). This indicates that a high frequency of CCRPs is one of the characteristics of multicellular cyanobacteria.

For the experimental validation, the complete list of CCRPs was filtered to include candidates from freshwater unicellular and filamentous cyanobacteria that are amenable to genetic modification, including *Thermosynechococcus elongatus* BP-1 (*Thermosynechococccus*), *Synechocystis*, *Synechococcus*, *Anabaena* and *Fischerella muscicola* PCC 7414 (*Fischerella*). The remaining CCPRs were further sorted to include proteins having similar properties to known prokaryotic IF-like proteins (e.g., crescentin, FilP) and are annotated as hypothetical proteins with an unknown function. An additional *Fischerella* CDS, Fm7001, was added to the list as earlier analyses suggested that it has a cell shape-

147 determining function. The preliminary filtration resulted in a list of nine candidates, which we
148 investigated experimentally here (Fig. 1 and Supplementary Fig. 1 and Supplementary Table
149 1). Candidate coding sequences vary in size and range from ca. 280 amino acids
150 (Synpcc7942_2039, abbreviated Syc2039) to ca. 650 amino acids (All4981). The coiled-coil
151 domain distribution is variable among the candidates in both coiled-coil domain count and
152 length. The presence of homologs across all cyanobacterial morphotypes serves as a hint for
153 universal protein function while a restricted distribution in specific subsections or morphotypes
154 indicates a functional specialization within the respective taxon. An example for such species-
155 specific candidate in our list is *slr7083* that is encoded on the pSYSA toxin-antitoxin plasmid
156 in *Synechocystis*, similarly to *parM* and *tubZ*, which mediate plasmid segregation (Larsen *et*
157 *al.*, 2007; Bharat *et al.*, 2015). In contrast, the homologous proteins Synpcc7942_1139
158 (abbreviated Syc1139) and Slr1301 are highly conserved and have homologous proteins
159 among all cyanobacterial groups (Fig. 1), including CypS from *Anabaena* (Springstein *et al.*,
160 2019). Slr1301 was also previously identified to be involved in *Synechocystis* twitching motility
161 in a transposon mutant library (Bhaya *et al.*, 2001).

162 **Cyanobacterial CCRPs assemble into diverse filamentous structures *in vitro***

163 A major characteristic of filament-forming proteins is their ability to self-polymerize into
164 filaments intra and extra-cellularly (Fuchs and Weber, 1994; Köster *et al.*, 2015). Unlike actin
165 and tubulin, IFs are able to form filamentous structures *in vitro* in a nucleotide-independent
166 manner without additional co-factors upon renaturation from a denaturing buffer (Herrmann
167 and Aebi, 2000; Köster *et al.*, 2015). To examine the self-polymerization property of the nine
168 CCRPs, we purified His_6-tagged CCRPs under denaturing conditions and subjected them to
169 subsequent renaturation. When applicable, the purified proteins were labeled with NHS-
170 Fluorescein and the formation of *in vitro* filaments was assessed by epifluorescence or bright
171 field microscopy. Several candidates did not form discernible structures *in vitro* and were
172 consequently excluded from further investigation (including Slr6096, Tlr0420 and Fm6009,
173 Supplementary Fig. 2). The remaining CCRPs assembled *in vitro* into highly diverse structures

(Fig. 2), ranging from large two-dimensional sheet-like filaments (Fm7001) to low abundant small strings (Slr1301). Direct dialysis of Fm7001 from a high urea-containing buffer to a physiological buffer led to protein precipitation. However, upon slow stepwise renaturation (removing 0.5 M every 2 h), Fm7001 polymerized into a flat two-dimensional sheet floating on top of the dialysate in 4,5 M urea (Supplementary Fig. 3A). We addressed the eventuality that these structures could be the product of crystalized urea, but control experiments did not reveal filaments Self-polymerization of Fm7001 revealed two-dimensional filamentous sheets as well as single filamentous fibers (Fig. 2). Similar structures were observed for purified Fm7001-GFP and MBP-Fm7001-His_6 (Supplementary Fig 3B,C). A two-dimensional filamentation pattern was observed also for Slr7083, which formed single, long and straight filamentous strings that were interconnected by two-dimensional sheets, thereby producing a honeycomb-like structure (Fig. 2). All4981 assembled into an interconnected filamentous net with thin single filaments (Fig. 2). The heterologous expression of Syc2039-His_6 in *E. coli* failed, but we successfully purified Syc2039-GFP-His_6 from *Synechococcus* instead. The polymerization pattern of Syc2039 revealed sphere or cell-shape-like three-dimensional sheets (Fig. 2). However, we note that most of the protein precipitated upon renaturation. The polymerization of Syc1139 revealed similar cell-shape-like three-dimensional sheets but without detectable aggregates (Fig. 2). The resemblance between Syc2039 and Syc1139 sheets raised the possibility that the sheet-like structures observed in the Syc2039-GFP-His_6 sample represents co-precipitated and polymerized Syc1139. Supporting this, we identified direct interactions of Syc1139 and Syc2039 using the bacterial adenylate cyclase two-hybrid (BACTH) assays (Supplementary Fig. 4). For Slr1301, only minor, if at all filamentous-like structures were observed (Fig. 2). Nonetheless, we included this protein in further analyses since its homolog in *Anabaena* (CypS) has been recently reported as a filament-forming protein (Springstein *et al.*, 2019). Notably, crescentin, which we used as a positive control, polymerized into smooth and filigree filaments only in the presence of monovalent ions (i.e. NaCl; Supplementary Fig. 2A,B). The maltose binding protein (MBP), which served as a negative control, did not assemble into filamentous structures *in vitro* (Supplementary Fig. 2A). This observation

202 highlights the importance of suitable buffer conditions for polymerization assays of filament-
203 forming proteins.

204 To further inspect the self-assembly capacity of the six CCRPs, we evaluated the self-
205 association properties of the CCRPs using the BACTH assay (Supplementary Fig. 5). Despite
206 its unclear *in vitro* polymerization, Syc2039 and Slr1301 were able to self-interact in the BACTH
207 system, thus we cannot rule out that optimal buffer conditions for *in vitro* polymerization are
208 yet to be found. The identified self-binding properties of the cyanobacterial CCRPs provide
209 further support for the *in vitro* polymerization results, thereby demonstrating a major hallmark
210 of filament-forming proteins: their ability to polymerize *in vitro*.

211 **Putative filament-forming proteins form filaments *in vivo***

212 To investigate whether the genetic background influences the filamentation properties of the
213 candidate proteins, we expressed GFP or YFP translational fusion constructs of the putative
214 filament-forming CCRPs in multiple hosts: 1) *E. coli*, 2) their native cyanobacterium and 3) in
215 cyanobacteria of a different morphotype or subsection. Gene expression was driven by
216 inducible or constitutive promoters commonly used in cyanobacteria. These included P_{cpc560}
217 (for *Synechocystis*) (Zhou *et al.*, 2014), P_{trc} (for *E. coli*, *Synechocystis* and *Synechococcus*)
218 (Huang *et al.*, 2010) or P_{petE} (for *Anabaena* and *Fischerella*) (Buikema and Haselkorn, 2001).
219 As a positive control for the validation of *in vivo* filamentation, we expressed crescentin-GFP
220 in *Anabaena*, which formed round and helical filaments that seemingly traversed through cell-
221 cell connections of neighboring cells (Fig. 3A). However, we note that we cannot exclude that
222 neighboring cells have not yet fully segregated due to the limited resolution of fluorescence
223 microscopy.

Fm7001 forms filaments *in vivo* independent of the heterologous host

The *in vivo* localization of Fm7001 was inevitably linked to the tag orientation. Only N-terminal YFP fusions of Fm7001 resulted in filamentous structures (Fig. 3 and Supplementary Fig. 6). In *Synechocystis*, YFP-Fm7001 formed filaments throughout the cell (Fig. 3B) while in *Anabaena* we observed abundant single filamentous strings (Fig. 3C). In *Fischerella*, YFP-Fm7001 only rarely assembled into short filamentous strings (Fig. 3D inlay). Despite of the low abundance of filaments, heterologous expression of YFP-Fm7001 induced a swollen phenotype and the formation of *Fischerella* cell filaments that seemingly divided in more than one plane (resembling the multiseriate *Chlorogloeopsis fritschii* PCC 6912 phenotype). This effect suggests a contribution of Fm7001 in cell-size control in the true-branching phenotype of *Fischerella*, reminiscent of crescentin or CtpS, (Woldemeskel and Goley, 2017). Attempts to generate a Δ*fm7001* mutant strain remained unsuccessful. We note that we cannot rule out the possibility that Fm7001 is indispensable for cell growth since *fm7001* is expressed in young (about 1 week old) *Fischerella* cultures, independent of the availability of fixed nitrogen sources in the growth medium (Supplementary Fig. 7). Additionally, *fm7001* is constantly highly expressed (Koch *et al.*, 2017), suggesting that it has an essential function. Taken together, Fm7001 has the capacity to form filaments *in vitro* and *in vivo* and displays morphogenic properties.

Slr7083 and Slr1301 are involved in twitching motility in *Synechocystis*

To test for a role of Slr7083 and Slr1301 in cellular integrity, we first examined the expression pattern of both genes in *Synechocystis* cultures at different growth phases. Reverse transcription PCR showed that the transcription of *slr7083* was restricted to cultures growing in mid-exponential phase whereas *slr1301* was absent from early phase exponential cultures but readily expressed at later exponential stages (Supplementary Fig. 8). The expression of Slr7083-GFP in *Synechocystis* was localized to the cell periphery as well as rare focal spots and S-shaped filaments (Fig. 4A). Our attempts to express Slr7083-GFP in the motile

Synechocystis PCC-M substrain (hereafter PCC-M) failed to yield exconjugants, raising the possibility that Slr7083 may be involved in *Synechocystis* twitching motility.

The expression of Slr1301-YFP in the motile and non-motile *Synechocystis* strains revealed peripheral plug formation at indistinct sites, assembly into crescent shapes and rarely the formation of S-shaped filaments (Fig. 4A and Supplementary Fig. 9B). Similar structures have been previously reported for the pilus ATPase PilB (Schuergers *et al.*, 2015). Slr7083-GFP and YFP-Slr7083 localized to the cell periphery in *Anabaena* (Supplementary Fig. 10). In *E. coli*, Slr7083-GFP localized next to the cell poles (Supplementary Fig. 9A). Consequently, we conclude that the membrane circumvention of Slr7083 observed in *Anabaena* and *Synechocystis* might be the result of cyanobacterial-specific mechanisms that recruit Slr7083 to the cell periphery. When expressed in *E. coli*, Slr1301-GFP revealed similar polar plugs (Supplementary Fig. 9A). Additionally, reminiscent of Slr7083, Slr1301-YFP influenced *Anabaena* cell-shape where it formed plugs but also single filaments or thick filamentous bundles that seemingly traversed through several cells (Supplementary Fig. 9B). To further assess the role of Slr1301 and Slr7083 in *Synechocystis* motility, we generated *Synechocystis* and PCC-M Δ*slr7083* and Δ*slr1301* mutant strains. The *Synechocystis* Δ*slr7083* and Δ*slr1301* mutants revealed no phenotypic defects compared to the WT (Fig. 4B, Supplementary Fig. 12). In contrast, the PCC-M Δ*slr7083* mutant is characterized by a decrease in twitching motility and a defect in cytokinesis (Fig. 4B). Similarly, the PCC-M Δ*slr1301* mutant entirely lost its twitching motility (Fig. 4B; confirming previous results from Bhaya, Takahashi, Shahi, & Arthur (2001)). Attempts to complement the motility defect in the PCC-M Δ*slr1301* mutant by expressing Slr1301-YFP from the conjugation plasmid pRL153 failed, possibly as a result of the comparably high expression from the P_{trc}. Likewise, complementation attempts of the PCC-M Δ*slr7083* mutant never resulted in exconjugants, while control experiments with a plasmid carrying only the sites for double homologous recombination lead to numerous exconjugants. In order to further explore how Slr1301 affects motility, we further analyzed co-precipitated proteins of Slr1301-YFP expressed in *Synechocystis* by mass spectrometry (Supplementary

277 Fig. 11B). This revealed multiple putative interaction partners involved in motility, including a
278 twitching motility protein (Slr0161), two methyl-accepting chemotaxis proteins (McpA and PilJ)
279 and the type IV pilus assembly ATPase PilB (Fig. 4C). The interaction of Slr1301 with PilB,
280 together with their similar *in vivo* localization, prompted us to characterize the interaction of
281 both proteins. For this purpose, we attempted to express PilB-GFP in *Synechocystis* WT, and
282 in the Δ*slr1301* and Δ*slr7083* mutants. In *Synechocystis* WT, PilB-GFP localized to the cell
283 periphery and often formed crescent-like formations (reminiscent of Slr1301-YFP and Slr7083-
284 GFP; Fig. 4A), confirming previous results by Schuergers *et al.* (2015). However, we never
285 observed any PilB-GFP expression in the Δ*slr7083* and Δ*slr1301* mutants. The similarity
286 between our observations so far for Slr1301 and Slr7083 prompted us to test for an interaction
287 between these two proteins. Indeed, a bacterial two-hybrid assay confirmed a direct interaction
288 between Slr7083 and Slr1301 (Fig. 4D). Taken together, our investigation identified two
289 *Synechocystis* CCRPs that are involved in cell motility. Slr7083 is a cell envelope-localized
290 protein involved in cytokinesis and motility. It polymerized into filaments *in vitro* but only few
291 filaments were identified *in vivo*, thus it is possible that Slr7083 is a novel cyanobacterial
292 filament-forming CCRP. Slr1301, although failing to assemble into filaments *in vitro*,
293 occasionally polymerized into filaments *in vivo* and was shown to be a direct interaction partner
294 of proteins that function in twitching motility.

295 **All4981 is a *Anabaena* TPR protein that forms septal-arising filaments**

296 The expression of All4981-GFP in *Anabaena* revealed numerous filaments that traversed the
297 cell while in other cells, All4981-GFP was associated with the cell septa (Fig. 5A). The filaments
298 also occasionally spread in a star-like pattern into the cytosol. Additionally, in freshly ruptured
299 All4981-GFP-expressing cells, filamentous *ex vivo* structures assembled in the medium into a
300 higher order and strongly interconnected network (Supplementary Fig. 13A), resembling the *in*
301 *vitro* polymerization pattern of All4981 (Fig 2). We confirmed the *in vivo* polymerization capacity
302 of All4981 by expressing All4981-GFP in *Synechocystis*, which lacks homologs to that protein
303 (Fig. 5B). Intrigued by the septal localization, we tested for an interaction with SepJ, a septal

304 junction protein in *Anabaena* (Flores *et al.*, 2007) and found weak, albeit significant physical
305 interactions (Supplementary Fig. 13B). In addition, bacterial two-hybrid assays revealed that
306 All4981 interacted with two other *Anabaena* filament-forming CCRPs, namely LfiA and LfiB
307 (Springstein *et al.*, 2019), and strongly interacts with MreB (Supplementary Fig. 13B). Notably,
308 MreB has previously been shown to form similar filamentous structures in *Anabaena* (Hu *et*
309 *al.*, 2007). However, in contrast to genes in the *mreBCD* operon, whose overexpression
310 induces cell abnormalities (Hu *et al.*, 2007), no direct morphogenic influence was detected for
311 All4981 in *Anabaena*. Noteworthy, it is likely that All4981 is an essential protein in *Anabaena*
312 as we were not able to generate an *all4981* deletion strain. Initially, we created a YFP-All4981
313 fusion construct with a deletion of 240 bp between nt 735 and nt 975 of the *all4981* CDS,
314 resulting in a deletion of the third and fourth TPR (YFP-All4981$^{\Delta TPR3-4}$) leaving the remaining
315 ORF intact. Remarkably, this fusion protein, like All4981-GFP, formed cell-traversing filaments
316 in *Anabaena* and sometimes assembled into a filamentous structure within the cells
317 (Supplementary Fig. 13C). In contrast, YFP-All4981 localized to the septa between two
318 neighboring cells but also revealed indistinct cytosolic localization (Supplementary Fig. 13C).
319 Co-immunoprecipitation experiments following LC-MS/MS analytics from *Anabaena* WT
320 expressing YFP-All4981$^{\Delta TPR3-4}$ revealed an association of YFP-All4981$^{\Delta TPR3-4}$ with ParB, MinD
321 and MreB (Fig. 5C). Thus, All4981 might be involved in ParA/B/S-driven plasmid or
322 chromosome segregation. The interaction with MreB agrees with the *in vivo* localization of
323 YFP- All4981$^{\Delta TPR3-4}$ in *Anabaena* (Supplementary Fig.13C) and the results from the bacterial
324 two-hybrid assay (Supplementary Fig. 13B). Further significant interactions were found with a
325 variety of putative S-layer and prohibitin-like proteins and with DevH, an essential protein for
326 heterocyst glycolipid layer synthesis. Notably, we never observed any All4981 localization
327 within heterocysts, regardless of the fluorescence tag. All4981 also interacted with All4982, a
328 protein encoded directly upstream of *all4981*, but not with All4983, which is encoded directly
329 upstream of *all4982* (Supplementary Fig. 14). To further examine the association between
330 All4981, All4982 and All4983, we tested for a common transcript (i.e. an operon structure) and
331 identified operon structures of *all4981* with *all4982* and likely also with *all4983* (Supplementary

Fig. 15). Inspired by the interaction with All4982, we expressed All4982-eCFP in *Anabaena* WT but could not observe any coherent structures. Overall, our results demonstrate that All4981 is connected to other *Anabaena* filament-forming CCRPs, the MreB cytoskeleton, the septal junctions and the protective S-layer. Additionally, All4981 polymerizes *in vitro*, *in vivo* and *ex vivo*, is likely essential for *Anabaena* and is thus accordingly classified as a cyanobacterial filament-forming TPR-repeat protein.

***Synechococcus* CCRPs are involved in cytokinesis and colony integrity**

To test for a role of *syc2039* and *syc1139* in cellular integrity, we examined the expression pattern of both proteins in *Synechococcus* during cell growth. RT-PCR showed that *syc2039* and *syc1139* are primarily transcribed in late exponential phase but not in early exponential phase (Supplementary Fig. 16). *In vivo* localization of a functional Syc2039-GFP fusion protein (Supplementary Fig. 17E,F) contrasted the ambiguous *in vitro* polymerization pattern (Fig. 2). Filaments were readily observed in different cyanobacterial hosts, indicating that in Syc2039 self-polymerization is independent of the host (Fig. 6A). Notably, however, Syc2039 formed different structures in each host. In *Anabaena*, filaments were long, curved and intertwined; in *Synechocystis* filaments appeared as spindle-like structures, and in *Synechococcus* filaments were long, sometimes helical and often aligned with or in close proximity to the cell periphery (Fig. 6A). A similar helical or cell periphery-aligned localization pattern was also observed in *E. coli* (Supplementary Fig. 18). In *Synechocystis* and *Synechococcus* Syc1139-GFP localized as spots in close proximity to the cytoplasmic membrane while being localized to the cell periphery in *E. coli* (Fig. 6A, Supplementary Fig. 18). Notably, Syc1139 failed to be expressed in *Anabaena*, suggesting that overexpression of this protein has a negative impact on that organism. Using double homologous gene replacement, we generated a Δ*syc2039* *Synechococcus* mutant strain and a non-segregated Δ*syc1139* *Synechococcus* mutant strain (Supplementary Fig. 17A,B,C). The non-segregated nature of the Δ*syc1139* mutant suggests that this gene performs an essential cellular function. Colony integrity of the Δ*syc2039* mutant was unaltered while the Δ*syc1139* mutant was characterized by apparent changes in colony

359 morphology (Fig. 6B), which were lost upon growth on non-selective plates (Supplementary
360 Fig. 17D). Additionally, both mutants presented an impairment in liquid culture growth: the
361 Δ*syc2039* mutant grew in standard BG11 medium but failed to grow upon addition of several
362 osmotic stressors, whereas the Δ*syc1139* mutant failed to grow in liquid culture entirely (Fig.
363 6C). Spot assays confirmed a decreased viability of the Δ*syc1139* mutant and showed that it
364 is highly sensitive to Proteinase K but unaffected by lysozyme (Supplementary Fig. 19A).
365 These cell wall defects together with the *in vitro* cell-shape-like filamentation pattern suggest
366 that Syc1139 might form a protective and protease-resistant proteinaceous layer below the
367 cytoplasmic membrane. This would also be in concert with the distorted colony morphology of
368 the non-segregated Δ*syc1139* mutant strain. The Δ*syc2039* mutant was unaffected by cell wall
369 and membrane destabilizers (Supplementary Fig. 19B). To investigate the role of these
370 proteins in cell division, the mutants were stained with DAPI and FtsZ was detected by
371 immunofluorescence. A proportion of Δ*syc2039* mutant cells exhibited a segregated DNA
372 distribution either to both cell poles or to just one pole (Fig. 6D). Furthermore, some cells of
373 both mutants lacked any discernible intracellular DNA or perceptible chlorophyll signal and
374 were elongated compared to the WT (Fig. 6D,E). The WT phenotype of the Δ*syc2039* mutant
375 could be rescued by insertion of P_{trc}::*syc2039-gfp* or $P_{syc2039}$::*syc2039* into the neutral NS1
376 locus (Bustos and Golden, 1992) (Supplementary Fig. 18E,F). Although mutant cells were
377 elongated compared to the WT cells (Fig. 6E), the intracellular localization of FtsZ was
378 unaffected (Supplementary Fig.19C). Despite the defect in cytokinesis, the Δ*syc2039* mutant
379 strain grew similarly as the *Synechococcus* WT in liquid culture (Supplementary Fig. 19D).
380 Taken together, Syc2039 forms abundant filamentous networks *in vivo* and is involved in
381 cytokinesis or cell cycle control. We could further show that *syc1139* is an essential gene
382 important for cytokinesis, cellular integrity and colony formation, implicating structural
383 functions.

Discussion

Earlier studies suggested that there is likely a broad spectrum of coiled-coil rich and rod-domain containing proteins with IF-like function in prokaryotes (Bagchi *et al.*, 2008). And indeed, reports on such proteins followed with the discovery of Scy (in *Streptomyces coelicolor*) and several CCRPs from *Helicobacter pylori* (Waidner *et al.*, 2009; Walshaw, Gillespie and Kelemen, 2010; Specht *et al.*, 2011; Holmes *et al.*, 2013). Here we investigate further the presence and function of CCRPs with IF-like properties in prokaryotes, by predicting and evaluating CCPRs in cyanobacteria.

Our results show that Fm7001 assembles into polymers *in vitro* upon renaturation from urea as well as *in vivo,* and that this protein has an impact on cellular morphology, thereby fulfilling major IF criteria (Köster *et al.*, 2015; Kelemen, 2017). Consequently, we propose that Fm7001 constitutes a novel IF-like cytoskeletal protein specific to multicellular, cell-differentiating and branching cyanobacteria. The floating Fm7001 polymer sheet in high molar urea indicates an exceptionally high self-association capacity of Fm7001. In comparison, the eukaryotic vimentin exists only as tetramers in 5 M urea (Herrmann *et al.*, 1996). *In vivo* localization experiments revealed an essential role of the Fm7001 C-terminus for filamentation, which is a common observation for known prokaryotic cytoskeletal proteins, including MreB (Swulius and Jensen, 2012), crescentin (Ausmees, Kuhn and Jacobs-Wagner, 2003) as well as eukaryotic IF proteins (Geisler and Weber, 1982; Weber and Geisler, 1982; Traub and Vorgias, 1983; Nakamura *et al.*, 1993; Herrmann *et al.*, 1996). The assigned structural similarities of Fm7001 with acetyl-CoA-carboxylase provide further support for the theory that cytoskeletal proteins originated from metabolic enzymes that obtained polymerization features (Ingerson-Mahar and Gitai, 2012). Notwithstanding, the metabolic activity of Fm7001 was not evaluated in our study hence its presumed enzymatic activity remains unknown.

Several prokaryotic tubulin-like and actin-like cytoskeletal proteins, such as ParM and TubZ, are known to be encoded on plasmids or on bacteriophages (Hurme *et al.*, 1994; Wagstaff and Löwe, 2018). Slr7083 is encoded on the large toxin-antitoxin defense plasmid

411 (pSYSA) in *Synechocystis* (Kopfmann and Hess, 2013), thus it adds another protein to the list
412 of those IF-like CCRP carried by an autonomously replicating genetic element. Preliminarily
413 we suspected that Slr7083 has a role in plasmid-segregation similarly to ParM. However,
414 Slr7083 showed no indications of dynamic properties, which would be indispensable for a
415 plasmid segregation mechanism. Furthermore, unlike ParM (Carballido-Lopez, 2006), Slr7083
416 did not localize in a spindle-like pattern *in vivo* and was only expressed at later growth phases,
417 which is contradictory to a possible involvement in the cell cycle. In contrast, the polymers
418 formed by Slr7083 *in vitro* and *in vivo* rather suggest that it could form a (protective)
419 proteinaceous layer below the cytoplasmic membrane. Notably, Slr7083 *in vitro* structures
420 resemble the nuclear lamina formed by nuclear lamins and FilP lace-like filaments (Stuurman,
421 Heins and Aebi, 1998; Bagchi *et al.*, 2008; Fuchino *et al.*, 2013). It is thus conceivable that
422 Slr7083 has a role in cellular stiffness as well as rigidity and mediates mechanical cell
423 stabilization. Although, transcription data for *slr7083* suggests that it is not constantly
424 expressed, challenging the idea of a cell-stabilizing function for Slr7083. In contrast, cell motility
425 in *Synechocystis* seems to be partially regulated by Slr7083, reminiscent of the role of the actin
426 cytoskeleton in eukaryotes.

427 The role of Slr7083 in cell motility is possibly mediated by means of its interaction with
428 Slr1301, which has already previously been shown to be essential for twitching motility in
429 *Synechocystis* (Bhaya *et al.*, 2001). So far it is unknown how photoreceptors transduce the
430 perceived light stimuli to the motility apparatus in *Synechocystis* ultimately resulting in
431 phototactic movements (Schuergers, Mullineaux and Wilde, 2017). It is tenable to hypothesize
432 that Slr1301 might constitute the missing link between the two systems, possibly in
433 combination with Slr7083. This hypothesis is supported by the physical interaction of Slr1301
434 with PilB and the *in vivo* localization of Slr1301 that is similar to that observed for PilB
435 (Schuergers *et al.*, 2015). A comparable complex was observed in *Pseudomonas aeruginosa*,
436 where FimL (a proposed scaffolding protein) was shown to connect the chemosensory
437 receptor system to the type IV pili apparatus, regulating the chemotactic and virulence
438 pathways (Inclan *et al.*, 2016). Cellular motility of eukaryotic cells is strongly dependent on

cytoskeletal proteins (Cappuccinelli, 1980), thus it is likely that the cytoskeleton is a key factor for cell movements in prokaryotes as well. Although IFs do not directly participate in cell motility in eukaryotes (Lodish *et al.*, 2000), an adaptation of CCRPs in prokaryotes for this task is imaginable. Bactofilins constitute a separate class of prokaryotic-specific cytoskeletal proteins and were proposed to be involved in social motility in *C. crescentus* (Kühn *et al.*, 2010). Additionally, the filament-forming CCRP AglZ from *Myxococcus xanthus* was previously shown to govern gliding motility together with a multi-protein complex that also involves the MreB cytoskeleton (Yang *et al.*, 2004; Nan *et al.*, 2010). The interaction of Slr1301 with twitching motility proteins was apparent in the non-motile *Synechocystis* strain, hinting for additional beneficial functions of this interaction besides motility. Notably, we previously reported IF-like properties for Alr0931 (CypS), which is a homolog of Slr1301 in *Anabaena* (Springstein *et al.*, 2019). While CypS polymerizes into filaments *in vitro*, Slr1301 does not, which could indicate a specific adaptation of CypS to filament formation in multicellular cyanobacteria. Despite their different cellular functions and *in vitro* polymerization properties, the homologous proteins Slr1301, Syc1139 and CypS retained the ability to cross-interact (Supplementary Fig. 20A). Further studies will focus on identifying the amino acid sequences that mediate this prevailed interaction, likely residing within the highly conserved amino acid sequence domains in this homologous group (Supplementary Fig. 20B). Consequently, it is conceivable that the functional diversification of the three proteins relies on the non-conserved amino acid sequences. These regions are putatively employed by other species-specific proteins, ultimately dictating their cellular functions.

TPR proteins are known to mediate protein-protein interactions and can assemble into multimers, but their ability to polymerize into filaments has not been described so far (Blatch and Lässle, 1999). Nonetheless, All4981 polymerizes *in vitro* and *in vivo* in all tested hosts. Additionally, it forms extracellular filaments and is presumably an essential protein. These observations suggest that All4981 is a *bona fide* prokaryotic IF-like protein consisting of TPRs. The association of All4981 with MreB, FtsZ-regulators, the S-layer and SepJ indicates that it might function as a bridge that connects the shape-determinants outside of the cell wall and

467 inside of the cytoplasmic membrane to the sites of cell-cell connection. A function of All4981
468 in *Anabaena* cell and filament shape is also supported by its interaction with the *Anabaena*
469 filament and cell shape stabilizing proteins LfiA and LfiB (Springstein et al., 2019).

470 Considering the presence of an N-terminal transmembrane domain and the lack of
471 clear *in vitro* filaments, it is unlikely that Syc2039 constitutes a genuine IF-like protein.
472 Nonetheless, the highly abundant filamentous network it formed in all tested bacterial hosts
473 suggests that Syc2039 is associated with cytoskeletal structures in *Synechococcus*.
474 Specifically, the elongated phenotype and the disturbed cytokinesis in the Δ*syc2039* and the
475 non-segregated Δ*syc1139* mutant strains suggest an association with the FtsZ-driven
476 elongasome. Direct interaction with FtsZ or MreB could not be shown, as such, future studies
477 will attempt to unravel the presumed connection of the *Synechococcus* CCRPs to those two
478 major cytoskeletal systems. Surprisingly, besides its cytokinetic defect, the Δ*syc2039* mutant
479 showed growth characteristics similar to *Synechococcus* WT, suggesting that feedback
480 mechanisms between cytokinesis and cell division are disturbed in the Δ*syc2039* mutant.

481 Our results reveal two novel filament-forming CCRPs from different cyanobacterial
482 subsections and morphotypes (Fig. 7). Our study thus extends the spectrum of known CCRPs
483 of IF-like function in prokaryotes and expands the set of functional properties associated with
484 IF-like proteins in prokaryotes. Notably, as indicated by Bagchi *et al*. (2008), we demonstrate
485 that the sole observation of coiled-coil-rich regions within a protein is not equal to IF-like
486 function and evaluation of novel filament-forming proteins requires several *in vitro* and *in vivo*
487 assays for validation. The cyanobacterial CCRPs we report here, like other bacterial CCRPs
488 (Ausmees, Kuhn and Jacobs-Wagner, 2003; Bagchi *et al.*, 2008; Waidner *et al.*, 2009; Fiuza
489 *et al.*, 2010; Specht *et al.*, 2011; Holmes *et al.*, 2013) and eukaryotic IFs (Alberts *et al.*, 2014),
490 are important for cell shape determination (Fm7001, Syc1139 and Syc2039), mediate cellular
491 motility (Slr7083 and Slr1301), DNA segregation (Syc1139 and Syc2039) and colony integrity
492 (Syc1139). Therefore, our study strengthens the perception that, like eukaryotes, prokaryotes
493 require organized internal complexes and even microcompartments to maintain cell shape,

494 size and proper cell function and highlights the usefulness of polymerized proteinaceous
495 structures for cellular processes. Remarkably, some of the identified CCRPs were highly
496 conserved among all cyanobacterial morphotypes, suggesting that their functions would also
497 be conserved. Future studies are required in order to evaluate the functional conservation of
498 homologous proteins in different cyanobacterial species. On the other hand, Syc2039 and
499 Slr7083 are highly strain specific, possibly performing functions adapted to the very needs of
500 their hosts. Similarly to the eukaryotic cytolinker proteins (Leung, Green and Liem, 2002;
501 Wiche, Osmanagic-Myers and Castañón, 2015), cyanobacterial CCRPs were often associated
502 with other cytoskeletal systems (MreB, FtsZ and other filament-forming CCRPs) and sites of
503 cell-cell connections (i.e., SepJ), which demonstrates the necessity for those structures to be
504 in a constant interplay even in comparably small cells. The discovery of IF-like filament-forming
505 CCRPs with different levels of conservation in various cyanobacterial morphotypes thus opens
506 up a new avenue of research on the cyanobacterial morphological diversity.

Material and Methods

Data and CCRP prediction

The cyanobacteria protein families were constructed from completely sequenced genomes available in RefSeq database (O'Leary *et al.*, 2015) (ver. May 2016; Supplementary File 2). For the construction of protein families, at the first stage, all protein sequences annotated in the genomes were blasted all-against-all using stand-alone BLAST (Altschul *et al.*, 1990) (V. 2.2.26). Protein sequence pairs that were found as reciprocal best BLAST hits (rBBHs; Tatusov, Koonin and Lipman, 1997) with a threshold of E-value ≤ $1x10^{-5}$ were further compared by global alignment using needle (EMBOSS package, V. 6.6.0.0; (Rice, Longden and Bleasby, 2000). Sequence pairs having ≥30% identical amino acids were clustered into protein families using the Markov clustering algorithm (MCL) (Enright, Van Dongen and Ouzounis, 2002) (ver. 12-135) with the default parameters. For the CCRPs prediction, 1,535 protein sequences containing non-standard amino acids were discarded. Coiled coil regions in protein sequences were predicted using PEPCOIL (EMBOSS package, V. 6.6.0.0; (Rice, Longden and Bleasby, 2000). The algorithm was executed with a window size of 21 and the threshold for amino acids in coiled-coil conformation was set to ≥ 80 amino acid residues similarly as described by Bagchi *et al.* (2008). Statistical tests were performed with MatLab©. For the comparison of CCRPs proportion, the compared groups included: 1) SynProCya group, 2) unicellular cyanobacteria, 3) unicellular cyanobacteria that divide in more than one plane, and 4) filamentous cyanobacteria. Identification of conserved amino acid domains within cyanobacterial CCRP homologs (CypS (Alr0931), Slr1301 and Syc1139) was done using MULTALIGN (Corpet, 1988).

Protein candidates were further manually examined with online available bioinformatic tools (NCBI Conserved Domain (CD) Search (Marchler-Bauer *et al.*, 2016), TMHMM Server (Krogh *et al.*, 2001) (V. 2.0), PSIPRED (McGuffin, Bryson and Jones, 2000), PSORTb (Yu *et al.*, 2010) (ver. 3.0), I-TASSER (Zhang, 2009). CCRPs exhibiting similar predictions to known IF and IF-like proteins like CreS, FilP, vimentin, desmin or keratin were selected, and proteins predicted to be involved in other cellular processes were excluded.

Bacterial strains and growth conditions

Fischerella, *Anabaena* and *Synechocystis* were obtained from the Pasteur Culture Collection (PCC) of cyanobacteria (France). *Synechococcus* was a gift from Martin Hagemann (University Rostock). Glucose-tolerant motile *Synechocystis* PCC-M substrain was a gift from Annegret Wilde (University Freiburg). Cells were grown photoautotropically in BG11 or without combined nitrogen ($BG11_0$) at a 16h/8h light/dark regime (*Fischerella*) or at constant light (*Anabaena*, *Synechococcus* and *Synechocystis*) with a light intensity of 20 µmol m^{-2} s^{-1}. When

appropriate, 50 µg ml^{-1} kanamycin (Km), 2.5 µg ml^{-1} spectinomycin (Sp), 2.5 µg ml^{-1} streptomycin (Sm) or 30 µg ml^{-1} neomycin (Nm) was added. Non-segregated Δ*syc1139* cells were always grown in the presence of Km. *E. coli* strains DH5α, DH5αMCR, XL1-blue and HB101 were used for cloning and conjugation by triparental mating. BTH101 was used for BACTH assays and BL21 (DE3) was used for expression of His- and GFP-tagged proteins in *E. coli*. All *E. coli* strains (Supplementary Table 2) were grown in LB medium containing the appropriate antibiotics at standard concentrations.

Plasmid and strain construction

All plasmids employed in this study were either generated by using standard restriction enzyme-base cloning procedures or using Gibson assembly (Gibson *et al.*, 2009). A detailed description of the cloning strategies for the respective plasmids is available upon request from the authors. All primers, plasmids and strains employed or generated in this study are listed in Supplementary Tables 2-5. GFP, YFP and eCFP protein tags were used as reporter proteins and His_6 tag was used for protein affinity purification. For gene replacement mutants, homologous flanks for double homologous recombination comprised 1000 bp upstream and downstream of the gene of interest. Mutant strains harboring gene replacements with antibiotic resistance cassettes (*nptII* or *CS.3*; Beck *et al.*, 1982; Sandvang, 1999) were verified by colony PCR testing for absence of gene of interest using primers #129/#130 for Δ*slr7083*, primers #168/#169 for Δ*slr1301*, primers #146/#147 for Δ*syc2039* or primers #161/#162 for Δ*syc1139*. We also attempted to generate gene replacement mutants for *all4981* and *fm7001* but remained unsuccessful.

Transformation of cyanobacteria

Transformation of *Synechococcus* was achieved by natural transformation as described by Ivleva *et al.* (2005) and transformation of *Synechocystis* was accomplished by natural transformation as described by Vermaas *et al.* (2002) or by conjugation as described by Ungerer and Pakrasi (2016). *Anabaena* and *Fischerella* were transformed by conjugation as described by Ungerer and Pakrasi (2016) or Stucken *et al.* (2012), respectively. Ex-conjugant colonies from *Synechococcus* and *Synechocystis* carrying gene replacements were re-streaked three to four times and absence of genes of interest was verified by colony PCR. Transformation of sonicated (fragmented) and NaCl-treated *Fischerella* cells followed by the conjugational method described by Ungerer and Pakrasi (2016) was also feasible for *Fischerella*, albeit with a lower transformation frequency.

574 Phenotypic characterization of the mutant strains

575 Defects in cell viability were evaluated by spot assays adapted from Dörrich *et al.* (2014). Wild
576 type and mutant strains from liquid cultures or BG11 plates were adjusted to an OD_{750} of about
577 0.4 in liquid BG11 liquid. Next, 5 µl of cells were spotted in triplicates onto BG11 plates or
578 BG11 plates supplemented with Proteinase K or lysozyme at indicated concentrations in 10-
579 fold serial dilutions and incubated under standard growth conditions until no further colonies
580 arose in the highest dilution.

581 Growth defects were assessed with growth curves. For this, cells were grown in liquid BG11
582 medium, washed three times by centrifugation (6500 x *g*, RT, 3 min) in BG11, adjusted to an
583 OD_{750} of 0.1 and then grown in triplicates or quadruples at standard growth conditions in 15 ml
584 culture volumes. OD_{750} values were recorded every 24 h.

585 Cell length of *Synechococcus* WT, mutant strains and mutant complementation strains was
586 measured using the line tool from the imaging software Fiji.

587 Cell wall integrity defects were evaluated by testing the influence of osmotic factors on cell
588 growth. *Synechococcus* WT and mutant strains were grown on BG11 agar plates, transferred
589 to BG11 liquid medium and grown under standard growth conditions with or without 5 mM
590 glucose, 200 mM glucose, 2 mM NH_4Cl, 200 mM maltose or 500 mM NaCl.

591 To evaluate the motility of *Synechocystis* and PCC-M WT and mutant strains, three single
592 colonies of the respective strain were streaked on a line on a BG11 growth plate. Growth plates
593 were then placed into the standard culture incubator for 10 d with with illumination limited from
594 one direction.

595 Protein purification and *in vitro* filamentation assays

596 C-terminally His_6-tagged proteins were expressed and subsequently purified under denaturing
597 conditions using Ni-NTA affinity columns as previously described by Springstein *et al.* (2019).
598 For expression of MBP-Fm7001-His_6, DH5α cells carrying pMAL-c2x-Fm7001-His_6 were
599 grown and induced accordingly but in the presence of 0.2% glucose. Purified proteins were
600 dialyzed overnight against polymerization buffer (PLB: 50 mM PIPES, 100 mM KCl, pH 7.0;
601 HLB: 25 mM HEPES, 150 mM NaCl, pH 7.4) at 18 °C and 180 rpm with three bath changes
602 using a Slide-A-Lyzer™ MINI Dialysis Device (10K MWCO, 0.5 ml or 2 ml; Thermo Fischer
603 Scientific). Purified proteins were stained with 0.005 mg NHS-Fluorescein (Thermo Fischer
604 Scientific) per 1 ml protein dialysate and *in vitro* filamentation was analyzed by epifluorescence
605 microscopy.

606 For Fm7001-His_6, proteins were slowly dialyzed against 2 mM Tris-HCl, 4.5 M urea, pH 7.5
607 (18°C, 200 rpm) decreasing 0.5 M urea every 2 h (from 6 M to 4.5 M urea). The resulting
608 floating filamentous web was then analyzed by bright field microscopy.

609 Syc2039-His_6 failed to be expressed in *E. coli* BL21 (DE3). To bypass this, Syc2039-GFP-His,
610 under the control of an IPTG-inducible P_{trc}, was inserted into a neutral locus of *Synechococcus*.
611 Cells were grown to an OD_{750} of 0.8 and protein expression was induced with 0.05 mM IPTG
612 for 3 d. Induced cells were harvested and washed with PBS by centrifugation (4800 x *g*, 4 °C,
613 10 min) and stored at -80 °C. Protein purification, dialysis and labeling was then performed as
614 described above with the exception that BG11 growth medium was used as dialysate.

615 Co-immunoprecipitation

616 For co-immunoprecipitations of fluorescently tagged CCRP candidates, cyanobacterial strains
617 expressing YFP-All4981 or Slr1301-YFP were grown in BG11 or $BG11_0$ liquid medium. Co-
618 immunoprecipitation was performed using the µMACS GFP isolation kit (Miltenyl Biotec) as
619 previously described by Springstein *et al.* (2019) using PBS-N (PBS supplemented with 1%
620 NP-40) or HSLB (50 mM NaH_2PO_4, 500 mM NaCl, 1% NP-40, pH 7.4) lysis buffers
621 supplemented with a protease inhibitor cocktail (cOmplete™, EDTA-free Protease Inhibitor
622 Cocktail, Sigma-Aldrich). Proteins were identified by mass spectrometry as previously
623 described by Springstein *et al.* (2019) for YFP-All4981 or by Kahnt *et al.* (2007) for Slr1301-
624 YFP.

625 Immunofluorescence

626 The localization of FtsZ in *Synechococcus* WT and mutant strains was evaluated by
627 immunofluorescence using a modified protocol from Heinz *et al.* (2016). In contrast, cells were
628 lysed in 50 mM Tris-HCl pH 7.4, 10 mM EDTA and 0.2 mg ml^{-1} lysozyme for 30 min at 37 °C
629 and samples were blocked in 1x Roti®-ImmunoBlock (Carl Roth) in PBS supplemented with
630 0.05% Tween 20. Samples were incubated with rabbit anti-FtsZ primary antibody (Agrisera;
631 raised against *Anabaena* FtsZ; 1:250 diluted) in blocking buffer followed by incubation with 7.5
632 µg ml^{-1} Alexa Fluor 488-conjugated goat anti-rabbit IgG (H+L) secondary antibody (Thermo
633 Fischer Scientific) in blocking buffer. Before microscopy, cells were stained with 10 µg ml^{-1}
634 DAPI (final concentration) in PBS.

635 Brightfield and fluorescence microscopy analysis

636 Bacterial strains grown in liquid culture were either directly applied to a microscope slide or
637 previously immobilized on a 2% low-melting agarose in PBS agarose pad and air dried before
638 microscopic analysis. Epifluorescence microscopy was performed using an Axio Imager.M2
639 light microscope (Carl Zeiss) equipped with Plan-Apochromat 63x/1.40 Oil M27 objective and

the AxioCam MR R3 imaging device (Carl Zeiss). GFP, Alexa Fluor 488, eCFP and YFP fluorescence was visualized using filter set 38 (Carl Zeiss; excitation: 470/40 nm band pass (BP) filter; emission: 525/50 nm BP). Chlorophyll auto-fluorescence was recorded using filter set 15 (Carl Zeiss; excitation: 546/12 nm BP; emission: 590 nm long pass). When applicable, cells were previously incubated in the dark at RT for about 5 min with 10 µg ml^{-1} DAPI in PBS to stain intracellular DNA. For visualization of DAPI fluorescence filter set 49 (Carl Zeiss; excitation: G 365 nm; emission: 455/50 nm) was employed. *E. coli* BL21 (DE3) cells expressing C-terminally GFP-tagged protein candidates were grown over night in LB and then diluted 1:40 in the same medium the following day. Cells were grown for 2 h at 37 °C, briefly acclimated to 20 °C for 10 min and induced with 0.05 mM IPTG at 20 °C. Protein localization of GFP/YFP-tagged proteins was then observed after indicated time points of cells immobilized on an agarose pad.

Statistical analysis

Beta-galactosidase values were measured in triplicates from three independent colonies and significant differences compared to WT were determined by a one-way ANOVA using Dunnett's multiple comparison test. For statistical evaluation of *Synechococcus* WT and mutant cell length, a one-way ANOVA using Turkey's multiple comparison test was used. Significance levels are the same as for the beta-galactosidase assay. Statistical tests were performed with the GraphPad Prims 8.0.0 software. Significance levels are indicated by stars (*) and correspond to: *: $P < 0.05$, **: $P < 0.01$, ***: $P < 0.001$, ****: $P < 0.0001$.

RNA isolation and RT-PCR

Total RNA was isolated from 10 ml culture using either the Direct-zol™ RNA MiniPrep Kit (Zymo Research; *Synechocystis*, *Synechococcus* and *Anabaena*) according to the manufacturer's instructions or the Plant RNA Reagent (Thermo Fischer Scientific; *Anabaena*, *Fischerella* and *Synechocystis*). For RNA isolation using the Plant RNA Reagent, a modified protocol was employed. To this end, cells were pelleted by centrifugation (4800 x *g*, 10 min, 4 °C) and the supernatant was discarded. The pellet was resuspended in 0.5 ml of Plant RNA Reagent und lysed in a Precellys® 24 homogenizer (Bertin) with 3 strokes at 6500 rpm for 30 s in 2 ml soil grinding (SK38) or tough microorganism (VK05) lysis tubes (Bertin). RNA was then isolated according to the manufacturer's instructions. Isolated RNA was treated with DNA-free™ Kit (2 units rDNAs/reaction; Thermo Fischer Scientific) and 1 µg (*Fischerella*, *Synechocystis* and *Synechococcus*) or 200 ng (*Anabaena*) RNA was reverse transcribed using the Maxima™ H Minus cDNA Synthesis Master Mix (with dsDNase; Thermo Fischer Scientific, for *Fischerella*, *Synechocystis* and *Synechococcus*) or the qScript™ cDNA Synthesis Kit (Quanta Biosciences, for *Anabaena*). RT-PCR of cDNA samples for *fm7001*, *ftsZ*, *slr7083*,

675 *rnpB*, *slr1301*, *syc2039*, *syc1139*, *all4981*, *all4981+all4982* and *all4981+all4983* was done
676 using primer pairs #1/#2, #3/#4, #5/#6, #7/#8, #9/#10, #11/#12, #13/#14, #15/#16, #17/#15
677 and #18/#15, respectively.

678 Bacterial two hybrid assays

679 In this study, the BACTH system (Euromedex) was employed. Gene candidates were cloned
680 into the expression vectors pKNT25, pKT25, pUT18 and pUT18C by GIBSON assembly,
681 thereby generating C and N-terminal translational fusions to the T25 or T18 subunit.
682 Chemically competent *E. coli* BTH101 (Δ*cya*) cells were co-transformed with 5 ng of the
683 indicated plasmids, plated onto LB plates supplemented with 200 µg ml^{-1} X-gal, 0.5 mM IPTG,
684 Amp, Km and grown at 30 °C for 24-36 h. Interactions were quantified by beta-galactosidase
685 assays from three colonies for each combination according to the protocol described by
686 Euromedex or in a 96 well format according to Karimova, Davi and Ladant (2012). For this aim,
687 cultures were either grown over night at 30 °C or for 2 d at 20 °C in LB Amp, Km, 0.5 mM IPTG
688 and interaction strength of the investigated proteins was by quantified by beta-galactosidase-
689 mediated hydrolyzation of ONPG (ortho-Nitrophenyl-β-galactoside), which is then recorded in
690 Miller units (Miller, 1992).

691

692 **Acknowledgements**

693 We thank Katrin Schumann, Myriam Barz, Lisa Stuckenschneider, Lisa-Marie Philipp and
694 Marius Lasse Theune for their assistance in the experimental work. Furthermore, we thank
695 Martin Thanbichler and Daniela Kiekebusch (both from Philipps University, Marburg, Germany)
696 for their support with mass spectrometry analysis. The study was supported by the German
697 science foundation (DFG) (Grant No. STU513/2-1 awarded to KS).

698 **Author contribution**

699 BLS and KS designed the study. BLS established and performed the experimental work with
700 contributions from JW. CW and TD performed the comparative genomics analysis. AOH
701 analyzed protein samples by mass spectrometry. BLS, TD and KS drafted the manuscript with
702 contributions from all coauthors.

References

Alberts, B. *et al.* (2014) *Molecular Biology of the Cell*. 6th editio. Garland Science.

Altschul, S. F. *et al.* (1990) 'Basic local alignment search tool', *Journal of Molecular Biology*. Academic Press, 215(3), pp. 403–410. doi: 10.1016/S0022-2836(05)80360-2.

Ausmees, N., Kuhn, J. R. and Jacobs-Wagner, C. (2003) 'The bacterial cytoskeleton: An intermediate filament-like function in cell shape', *Cell*, pp. 705–713. doi: 10.1016/S0092-8674(03)00935-8.

Bagchi, S. *et al.* (2008) 'Intermediate filament-like proteins in bacteria and a cytoskeletal function in Streptomyces', *Molecular Microbiology*, 70(4), pp. 1037–1050. doi: 10.1111/j.1365-2958.2008.06473.x.

Beck, E. *et al.* (1982) 'Nucleotide sequence and exact localization of the neomycin phosphotransferase gene from transposon Tn5', *Gene*, 19(3), pp. 327–336. doi: 10.1016/0378-1119(82)90023-3.

Bharat, T. A. M. *et al.* (2015) 'Structures of actin-like ParM filaments show architecture of plasmid-segregating spindles', *Nature*. Nature Publishing Group, a division of Macmillan Publishers Limited. All Rights Reserved., 523, p. 106. Available at: https://doi.org/10.1038/nature14356.

Bhaya, D. *et al.* (2001) 'Novel Motility Mutants of Synechocystis Strain PCC 6803 Generated by In Vitro Transposon Mutagenesis Novel Motility Mutants of Synechocystis Strain PCC 6803 Generated by In Vitro Transposon Mutagenesis †', *Journal of Bacteriology*, 183(20), pp. 1–5. doi: 10.1128/JB.183.20.6140.

Bi, E. and Lutkenhaus, J. (1991) 'FtsZ ring structure associated with division in Escherichia coli', *Nature*, 354(6349), pp. 161–164. doi: 10.1038/354161a0.

Blatch, G. L. and Lässle, M. (1999) 'The tetratricopeptide repeat: A structural motif mediating protein-protein interactions', *BioEssays*, 21(11), pp. 932–939. doi: 10.1002/(SICI)1521-1878(199911)21:11<932::AID-BIES5>3.0.CO;2-N.

Boyer, H. and Roulland-Dessoix, D. (1969) 'A complementation analysis of the restrcition and modification of DNA in Escherichia coli.', *J. Mol. Biol.*, 41, pp. 459–472.

Buikema, W. J. and Haselkorn, R. (2001) 'Expression of the Anabaena hetR gene from a copper-regulated promoter leads to heterocyst differentiation under repressing conditions', *Proceedings of the National Academy of Sciences*, 98(5), pp. 2729–2734. doi:

734 10.1073/pnas.051624898.

735 Bustos, S. A. and Golden, S. S. (1992) 'Light-regulated expression of the psbD gene family in
736 Synecbococcus sp. strain PCC 7942: evidence for the role of duplicated psbD genes in
737 cyanobacteria', *Molecular and General Genetics MGG*, 232(2), pp. 221–230. doi:
738 10.1007/BF00280000.

739 Cabeen, M. T. *et al.* (2009) 'Bacterial cell curvature through mechanical control of cell growth',
740 *The EMBO Journal*, pp. 1208–1219. doi: 10.1038/emboj.2009.61.

741 Cai, Y. and Wolk, C. P. (1990) 'Use of a conditionally lethal gene in Anabaena sp. strain PCC
742 7120 to select for double recombinats and to entrap insertion sequnces', *Journal of*
743 *Bacteriology*, 172(6), pp. 3138–3145.

744 Cappuccinelli, P. (1980) 'The movement of eukaryotic cells', in *Motility of Living Cells*.
745 Dordrecht: Springer Netherlands, pp. 59–74. doi: 10.1007/978-94-009-5812-8_4.

746 Carballido-Lopez, R. (2006) 'The Bacterial Actin-Like Cytoskeleton', *Microbiology and*
747 *Molecular Biology Reviews*, 70(4), pp. 888–909. doi: 10.1128/MMBR.00014-06.

748 Charbon, G., Cabeen, M. T. and Jacobs-Wagner, C. (2009) 'Bacterial intermediate filaments:
749 In vivo assembly, organization, and dynamics of crescentin', *Genes and Development*, pp.
750 1131–1144. doi: 10.1101/gad.1795509.

751 Corpet, F. (1988) 'Multiple sequence alignment with hierarchical clustering.', *Nucleic acids*
752 *research*, 16(22), pp. 10881–90. doi: 10.1093/nar/16.22.10881.

753 Dörrich, A. K. *et al.* (2014) 'Deletion of the Synechocystis sp. PCC 6803 kaiAB1C1 gene cluster
754 causes impaired cell growth under light???dark conditions', *Microbiology (United Kingdom)*,
755 160(2014), pp. 2538–2550. doi: 10.1099/mic.0.081695-0.

756 Enright, A. J., Van Dongen, S. and Ouzounis, C. A. (2002) 'An efficient algorithm for large-
757 scale detection of protein families', *Nucleic acids research*. Oxford University Press, 30(7), pp.
758 1575–1584.

759 Fiuza, M. *et al.* (2010) 'Phosphorylation of a novel cytoskeletal protein (RsmP) regulates rod-
760 shaped morphology in Corynebacterium glutamicum', *Journal of Biological Chemistry*, pp.
761 29387–29397. doi: 10.1074/jbc.M110.154427.

762 Flärdh, K. *et al.* (2012) 'Regulation of apical growth and hyphal branching in Streptomyces',
763 *Current Opinion in Microbiology*, 15(6), pp. 737–743. doi:
764 https://doi.org/10.1016/j.mib.2012.10.012.

765 Flores, E. *et al.* (2007) 'Septum-localized protein required for filament integrity and diazotrophy
766 in the heterocyst-forming cyanobacterium Anabaena sp. strain PCC 7120', *Journal of*
767 *Bacteriology*, 189(10), pp. 3884–3890. doi: 10.1128/JB.00085-07.

768 Fuchino, K. *et al.* (2013) 'Dynamic gradients of an intermediate filament-like cytoskeleton are
769 recruited by a polarity landmark during apical growth', *Proceedings of the National Academy*
770 *of Sciences*, pp. E1889–E1897. doi: 10.1073/pnas.1305358110.

771 Fuchs, E. and Weber, K. (1994) 'INTERMEDIATE FILAMENTS: Structure, Dynamics, Function
772 and Disease', *Annual Review of Biochemistry*, 63, pp. 345–382.

773 Geisler, N. and Weber, K. (1982) 'The amino acid sequence of chicken muscle desmin
774 provides a common structural model for intermediate filament proteins', *The EMBO journal*,
775 1(12), pp. 1649–1656. Available at: https://www.ncbi.nlm.nih.gov/pubmed/6202512.

776 Gibson, D. G. *et al.* (2009) 'Enzymatic assembly of DNA molecules up to several hundred
777 kilobases', *Nature Methods*, 6(5), pp. 343–345. doi: 10.1038/nmeth.1318.

778 Grant, S. G. *et al.* (1990) 'Differential plasmid rescue from transgenic mouse DNAs into
779 Escherichia coli methylation-restriction mutants.', *Proceedings of the National Academy of*
780 *Sciences*, 87(12), pp. 4645–4649. doi: 10.1073/pnas.87.12.4645.

781 Heinz, S. *et al.* (2016) 'Thylakoid Membrane Architecture in *Synechocystis* Depends on CurT,
782 a Homolog of the Granal CURVATURE THYLAKOID1 Proteins', *The Plant Cell*, 28(9), pp.
783 2238–2260. doi: 10.1105/tpc.16.00491.

784 Hempel, A. M. *et al.* (2012) 'The Ser/Thr protein kinase AfsK regulates polar growth and hyphal
785 branching in the filamentous bacteria Streptomyces', *Proceedings of the National Academy of*
786 *Sciences of the United States of America*. 2012/08/06. National Academy of Sciences,
787 109(35), pp. E2371–E2379. doi: 10.1073/pnas.1207409109.

788 Herrero, A., Stavans, J. and Flores, E. (2016) 'The multicellular nature of filamentous
789 heterocyst-forming cyanobacteria', *FEMS Microbiology Reviews*, 40(6), pp. 831–854. doi:
790 10.1093/femsre/fuw029.

791 Herrmann, H. *et al.* (1996) 'Structure and assembly properties of the intermediate filament
792 protein vimentin: The role of its head, rod and tail domains', *Journal of Molecular Biology*,
793 264(5), pp. 933–953. doi: 10.1006/jmbi.1996.0688.

794 Herrmann, H. and Aebi, U. (2000) 'Intermediate filaments and their associates: Multi-talented
795 structural elements specifying cytoarchitecture and cytodynamics', *Current Opinion in Cell*
796 *Biology*, 12(1), pp. 79–90. doi: 10.1016/S0955-0674(99)00060-5.

797 Herrmann, H. and Aebi, U. (2004) 'Intermediate Filaments: Molecular Structure, Assembly
798 Mechanism, and Integration Into Functionally Distinct Intracellular Scaffolds', *Annual Review*
799 *of Biochemistry*, 73(1), pp. 749–789. doi: 10.1146/annurev.biochem.73.011303.073823.

800 Holmes, N. A. *et al.* (2013) 'Coiled-coil protein Scy is a key component of a multiprotein
801 assembly controlling polarized growth in Streptomyces', *Proceedings of the National Academy*
802 *of Sciences*, pp. E397–E406. doi: 10.1073/pnas.1210657110.

803 Hu, B. *et al.* (2007) 'MreB is important for cell shape but not for chromosome segregation of
804 the filamentous cyanobacterium Anabaena sp. PCC 7120', *Molecular Microbiology*, 63(6), pp.
805 1640–1652. doi: 10.1111/j.1365-2958.2007.05618.x.

806 Huang, H.-H. *et al.* (2010) 'Design and characterization of molecular tools for a Synthetic
807 Biology approach towards developing cyanobacterial biotechnology', *Nucleic acids research*.
808 2010/03/17. Oxford University Press, 38(8), pp. 2577–2593. doi: 10.1093/nar/gkq164.

809 Hurme, R. *et al.* (1994) 'Intermediate filament-like network formed in vitro by a bacterial coiled
810 coil protein', *Journal of Biological Chemistry*, pp. 10675–10682.

811 Inclan, Y. F. *et al.* (2016) 'A scaffold protein connects type IV pili with the Chp chemosensory
812 system to mediate activation of virulence signaling in Pseudomonas aeruginosa', *Molecular*
813 *Microbiology*, 101(4), pp. 590–605. doi: 10.1111/mmi.13410.

814 Ingerson-Mahar, M. and Gitai, Z. (2012) 'A growing family: the expanding universe of the
815 bacterial cytoskeleton', *FEMS Microbiol Rev*, 36(1), pp. 256–266. doi: 10.1111/j.1574-
816 6976.2011.00316.x.

817 Ivleva, N. B. *et al.* (2005) 'LdpA: A component of the circadian clock senses redox state of the
818 cell', *EMBO Journal*, 24(6), pp. 1202–1210. doi: 10.1038/sj.emboj.7600606.

819 Jain, I. H., Vijayan, V. and O'Shea, E. K. (2012) 'Spatial ordering of chromosomes enhances
820 the fidelity of chromosome partitioning in cyanobacteria.', *Proceedings of the National*
821 *Academy of Sciences of the United States of America*, 109(34), pp. 13638–43. doi:
822 10.1073/pnas.1211144109.

823 Jones, L. J. F., Carballido-López, R. and Errington, J. (2001) 'Control of cell shape in bacteria:
824 Helical, actin-like filaments in Bacillus subtilis', *Cell*, 104(6), pp. 913–922. doi: 10.1016/S0092-
825 8674(01)00287-2.

826 Kahnt, J. *et al.* (2007) 'Post-translational modifications in the active site region of methyl-
827 coenzyme M reductase from methanogenic and methanotrophic archaea', *The FEBS journal*.
828 Wiley Online Library, 274(18), pp. 4913–4921.

829 Kalliomaa-Sanford, A. K. *et al.* (2012) 'Chromosome segregation in Archaea mediated by a
830 hybrid DNA partition machine', *Proceedings of the National Academy of Sciences*, 109(10),
831 pp. 3754–3759. doi: 10.1073/pnas.1113384109.

832 Karimova, G., Davi, M. and Ladant, D. (2012) 'The β-lactam resistance protein Blr, a small
833 membrane polypeptide, is a component of the Escherichia coli cell division machinery', *Journal*
834 *of Bacteriology*, 194(20), pp. 5576–5588. doi: 10.1128/JB.00774-12.

835 Kelemen, G. H. (2017) 'Intermediate Filaments Supporting Cell Shape and Growth in Bacteria
836 BT - Prokaryotic Cytoskeletons: Filamentous Protein Polymers Active in the Cytoplasm of
837 Bacterial and Archaeal Cells', in Löwe, J. and Amos, L. A. (eds). Cham: Springer International
838 Publishing, pp. 161–211. doi: 10.1007/978-3-319-53047-5_6.

839 Koch, R. *et al.* (2017) 'Plasticity first: Molecular signatures of a complex morphological trait in
840 filamentous cyanobacteria', *BMC Evolutionary Biology*. BMC Evolutionary Biology, 17(1), pp.
841 1–11. doi: 10.1186/s12862-017-1053-5.

842 Kopfmann, S. and Hess, W. R. (2013) 'Toxin-antitoxin systems on the large defense plasmid
843 pSYSA of synechocystis sp. pCC 6803', *Journal of Biological Chemistry*, 288(10), pp. 7399–
844 7409. doi: 10.1074/jbc.M112.434100.

845 Köster, S. *et al.* (2015) 'Intermediate filament mechanics in vitro and in the cell: From coiled
846 coils to filaments, fibers and networks', *Current Opinion in Cell Biology*, 32, pp. 82–91. doi:
847 10.1016/j.ceb.2015.01.001.

848 Krogh, A. *et al.* (2001) 'Predicting transmembrane protein topology with a hidden Markov
849 model: application to complete genomes', *Journal of molecular biology*. Elsevier, 305(3), pp.
850 567–580.

851 Kruse, T., Bork-Jensen, J. and Gerdes, K. (2005) 'The morphogenetic MreBCD proteins of
852 Escherichia coli form an essential membrane-bound complex', *Molecular Microbiology*, 55(1),
853 pp. 78–89. doi: 10.1111/j.1365-2958.2004.04367.x.

854 Kühn, J. *et al.* (2010) 'Bactofilins, a ubiquitous class of cytoskeletal proteins mediating polar
855 localization of a cell wall synthase in Caulobacter crescentus', *EMBO Journal*, pp. 327–339.
856 doi: 10.1038/emboj.2009.358.

857 Kunert, A., Hagemann, M. and Erdmann, N. (2000) 'Construction of promoter probe vectors
858 for Synechocystis sp. PCC 6803 using the light-emitting reporter systems Gfp and LuxAB',
859 *Journal of Microbiological Methods*, 41(3), pp. 185–194. doi: 10.1016/S0167-7012(00)00162-
860 7.

Larsen, R. A. *et al.* (2007) 'Treadmilling of a prokaryotic tubulin-like protein, TubZ, required for plasmid stability in Bacillus thuringiensis', *Genes and Development*, 21(11), pp. 1340–1352. doi: 10.1101/gad.1546107.

Leipe, D. D. *et al.* (2002) 'Classification and evolution of P-loop GTPases and related ATPases', *Journal of Molecular Biology*. Academic Press, 317(1), pp. 41–72. doi: 10.1006/JMBI.2001.5378.

Leung, C. L., Green, K. J. and Liem, R. K. H. (2002) 'Plakins: A family of versatile cytolinker proteins', *Trends in Cell Biology*, 12(1), pp. 37–45. doi: 10.1016/S0962-8924(01)02180-8.

Lin, L. and Thanbichler, M. (2013) 'Nucleotide-independent cytoskeletal scaffolds in bacteria', *Cytoskeleton*, 70(8), pp. 409–423. doi: 10.1002/cm.21126.

Lodish, H. *et al.* (2000) *Molecular Cell Biology*. 4th edn. New York: W. H. Freeman. Available at: https://www.ncbi.nlm.nih.gov/books/NBK21560/ (Accessed: 27 February 2018).

Lopes Pinto, F. *et al.* (2011) 'FtsZ degradation in the cyanobacterium Anabaena sp. strain PCC 7120', *Journal of Plant Physiology*. Elsevier GmbH., 168(16), pp. 1934–1942. doi: 10.1016/j.jplph.2011.05.023.

Löwe, J. and Amos, L. A. (2009) 'Evolution of cytomotive filaments: The cytoskeleton from prokaryotes to eukaryotes', *International Journal of Biochemistry and Cell Biology*, 41(2), pp. 323–329. doi: 10.1016/j.biocel.2008.08.010.

Lupas, A., Van Dyke, M. and Stock, J. (1991) 'Predicting coiled coils from protein sequences', *Science*, pp. 1162–1164. doi: 10.1126/science.252.5009.1162.

Marchler-Bauer, A. *et al.* (2016) 'CDD/SPARCLE: functional classification of proteins via subfamily domain architectures', *Nucleic acids research*. Oxford University Press, 45(D1), pp. D200–D203.

McGuffin, L. J., Bryson, K. and Jones, D. T. (2000) 'The PSIPRED protein structure prediction server', *Bioinformatics*. Oxford University Press, 16(4), pp. 404–405.

Meselson, M. and Yuan, R. (1968) 'DNA restriction enzyme from E. coli.', *Nature*, 217(5134), pp. 1110–4. Available at: http://www.ncbi.nlm.nih.gov/pubmed/4868368 (Accessed: 22 February 2018).

Miller, J. H. (1992) *A Short Course in Bacterial Genetics – A Laboratory Manual and Handbook for Escherichia coli and Related Bacteria*, *Cold Spring Harbor Laboratory Press*. Cold Spring Harbor. doi: 10.1002/jobm.3620330412.

892 Nakamura, Y. *et al.* (1993) 'Acceleration of bovine neurofilament L assembly by deprivation of
893 acidic tail domain', *European Journal of Biochemistry*, 212(2), pp. 565–571. doi:
894 10.1111/j.1432-1033.1993.tb17694.x.

895 Nan, B. *et al.* (2010) 'A multi-protein complex from Myxococcus xanthus required for bacterial
896 gliding motility', *Molecular Microbiology*, 76(6), pp. 1539–1554. doi: 10.1111/j.1365-
897 2958.2010.07184.x.

898 Nayar, A. S. *et al.* (2007) 'FraG is necessary for filament integrity and heterocyst maturation in
899 the cyanobacterium Anabaena sp. strain PCC 7120', *Microbiology*, 153(2), pp. 601–607. doi:
900 10.1099/mic.0.2006/002535-0.

901 O'Leary, N. A. *et al.* (2015) 'Reference sequence (RefSeq) database at NCBI: current status,
902 taxonomic expansion, and functional annotation', *Nucleic acids research*. Oxford University
903 Press, 44(D1), pp. D733–D745.

904 Ormö, M. *et al.* (1996) 'Crystal Structure of the Aequorea victoria Green Fluorescent Protein',
905 *Science*, 273(5280), pp. 1392 LP – 1395. Available at:
906 http://science.sciencemag.org/content/273/5280/1392.abstract.

907 Ramos-León, F. *et al.* (2015) 'Divisome-dependent subcellular localization of cell-cell joining
908 protein SepJ in the filamentous cyanobacterium Anabaena', *Molecular Microbiology*, 96(3), pp.
909 566–580. doi: 10.1111/mmi.12956.

910 Rice, P., Longden, I. and Bleasby, A. (2000) 'EMBOSS: the European Molecular Biology Open
911 Software Suite.', *Trends in genetics : TIG*. Elsevier, 16(6), pp. 276–7. doi: 10.1016/S0168-
912 9525(00)02024-2.

913 Rippka, R. *et al.* (1979) 'Generic Assignments, Strain Histories and Properties of Pure Cultures
914 of Cyanobacteria', *Microbiology*, 111(1), pp. 1–61. doi: 10.1099/00221287-111-1-1.

915 Sandvang, D. (1999) 'Novel streptomycin and spectinomycin resistance gene as a gene
916 cassette within a class 1 integron isolated from Escherichia coli', *Antimicrobial Agents and
917 Chemotherapy*, 43(12), pp. 3036–3038. doi: 10.1128/AAC.44.2.475-475.2000.

918 Schuergers, N. *et al.* (2015) 'PilB localization correlates with the direction of twitching motility
919 in the cyanobacterium Synechocystis sp. PCC 6803', *Microbiology (Reading, England)*,
920 161(2015), pp. 960–966. doi: 10.1099/mic.0.000064.

921 Schuergers, N., Mullineaux, C. W. and Wilde, A. (2017) 'Cyanobacteria in motion', *Current
922 Opinion in Plant Biology*. Elsevier Ltd, 37, pp. 109–115. doi: 10.1016/j.pbi.2017.03.018.

923 Shoeman, R. L. and Traub, P. (1993) 'Assembly of Intermediate Filaments', *Bioessays*, 15(9),
924 pp. 605–611. doi: 10.1002/bies.950150906.

925 Specht, M. *et al.* (2011) 'Helicobacter pylori Possesses Four Coiled-Coil-Rich Proteins That
926 Form Extended Filamentous Structures and Control Cell Shape and Motility', *Journal of*
927 *Bacteriology*, 193(17), pp. 4523–4530. doi: 10.1128/JB.00231-11.

928 Springstein, B. L. *et al.* (2019) 'A cytoskeletal network maintains filament shape in the
929 multicellular cyanobacterium Anabaena sp. PCC 7120', *bioRxiv*, p. 553073. doi:
930 10.1101/553073.

931 Stucken, K. *et al.* (2012) 'Transformation and conjugal transfer of foreign genes into the
932 filamentous multicellular cyanobacteria (subsection V) Fischerella and Chlorogloeopsis',
933 *Current Microbiology*, 65(5), pp. 552–560. doi: 10.1007/s00284-012-0193-5.

934 Studier, F. W. and Moffatt, B. A. (1986) 'Use of bacteriophage T7 RNA polymerase to direct
935 selective high-level expression of cloned genes', *Journal of Molecular Biology*, 189(1), pp.
936 113–130. doi: 10.1016/0022-2836(86)90385-2.

937 Stuurman, N., Heins, S. and Aebi, U. (1998) 'Nuclear lamins: Their structure, assembly, and
938 interactions', *Journal of Structural Biology*, 122(1–2), pp. 42–66. doi: 10.1006/jsbi.1998.3987.

939 Swulius, M. T. and Jensen, G. J. (2012) 'The helical mreb cytoskeleton in Escherichia coli
940 MC1000/pLE7 is an artifact of the N-terminal yellow fluorescent protein tag', *Journal of*
941 *Bacteriology*, 194(23), pp. 6382–6386. doi: 10.1128/JB.00505-12.

942 Tatusov, R. L., Koonin, E. V and Lipman, D. J. (1997) 'A genomic perspective on protein
943 families', *Science*. American Association for the Advancement of Science, 278(5338), pp. 631–
944 637.

945 Tolonen, A. C., Liszt, G. B. and Hess, W. R. (2006) 'Genetic manipulation of Prochlorococcus
946 strain MIT9313: green fluorescent protein expression from an RSF1010 plasmid and Tn5
947 transposition', *Applied and environmental microbiology*. 2006/10/13. American Society for
948 Microbiology, 72(12), pp. 7607–7613. doi: 10.1128/AEM.02034-06.

949 Traub, P. and Vorgias, C. E. (1983) 'Involvement of the N-terminal polypeptide of vimentin in
950 the formation of intermediate filaments', *Journal of Cell Science*, 63(1), pp. 43 LP – 67.
951 Available at: http://jcs.biologists.org/content/63/1/43.abstract.

952 Ungerer, J. and Pakrasi, H. B. (2016) 'Cpf1 Is A Versatile Tool for CRISPR Genome Editing
953 Across Diverse Species of Cyanobacteria', *Scientific Reports*. Nature Publishing Group, 6, pp.
954 1–9. doi: 10.1038/srep39681.

955 Vermaas, W. F. J. *et al.* (2002) 'Transformation of the cyanobacterium Synechocystis sp. PCC
956 6803 as a tool for genetic mapping: optimization of efficiency', *FEMS Microbiology Letters*,
957 206(2), pp. 215–219. doi: 10.1111/j.1574-6968.2002.tb11012.x.

958 Wagstaff, J. and Löwe, J. (2018) 'Prokaryotic cytoskeletons: protein filaments organizing small
959 cells', *Nature Reviews Microbiology*. Nature Publishing Group. doi: 10.1038/nrmicro.2017.153.

960 Waidner, B. *et al.* (2009) 'A novel system of cytoskeletal elements in the human pathogen
961 Helicobacter pylori', *PLoS Pathogens*. doi: 10.1371/journal.ppat.1000669.

962 Walshaw, J., Gillespie, M. D. and Kelemen, G. H. (2010) 'A novel coiled-coil repeat variant in
963 a class of bacterial cytoskeletal proteins', *Journal of Structural Biology*, pp. 202–215. doi:
964 10.1016/j.jsb.2010.02.008.

965 Weber, K. and Geisler, N. (1982) 'The structural relation between intermediate filament
966 proteins in living cells and the alpha-keratins of sheep wool', *The EMBO journal*, 1(10), pp.
967 1155–1160. Available at: https://www.ncbi.nlm.nih.gov/pubmed/6202505.

968 Wiche, G., Osmanagic-Myers, S. and Castañón, M. J. (2015) 'Networking and anchoring
969 through plectin: A key to IF functionality and mechanotransduction', *Current Opinion in Cell*
970 *Biology*, 32, pp. 21–29. doi: 10.1016/j.ceb.2014.10.002.

971 Wickstead, B. and Gull, K. (2011) 'The evolution of the cytoskeleton', *Journal of Cell Biology*,
972 194(4), pp. 513–525. doi: 10.1083/jcb.201102065.

973 Wilk, L. *et al.* (2011) 'Outer membrane continuity and septosome formation between vegetative
974 cells in the filaments of Anabaena sp. PCC 7120', *Cellular Microbiology*, 13(11), pp. 1744–
975 1754. doi: 10.1111/j.1462-5822.2011.01655.x.

976 Woldemeskel, S. A. and Goley, E. D. (2017) 'Shapeshifting to Survive: Shape Determination
977 and Regulation in Caulobacter crescentus', *Trends in Microbiology*, pp. 673–687. doi:
978 10.1016/j.tim.2017.03.006.

979 Wolk, C. P. *et al.* (1988) 'Isolation and complementation of mutants of Anabaena sp. strain
980 PCC 7120 unable to grow aerobically on dinitrogen.', *Journal of bacteriology*, 170(3), pp. 1239–
981 1244. doi: 10.1128/jb.170.3.1239-1244.1988.

982 Yang, J. and Zhang, Y. (2015) 'I-TASSER server: New development for protein structure and
983 function predictions', *Nucleic Acids Research*, 43(W1), pp. W174–W181. doi:
984 10.1093/nar/gkv342.

985 Yang, R. *et al.* (2004) 'AglZ Is a Filament-Forming Coiled-Coil Protein Required for

Adventurous Gliding Motility of Myxococcus xanthus', *Journal of bacteriology*, 186(18), pp. 6168–6178. doi: 10.1128/JB.186.18.6168.

Yu, N. Y. *et al.* (2010) 'PSORTb 3.0: Improved protein subcellular localization prediction with refined localization subcategories and predictive capabilities for all prokaryotes', *Bioinformatics*, 26(13), pp. 1608–1615. doi: 10.1093/bioinformatics/btq249.

Zhang, C.-C. C. *et al.* (1995) 'Analysis of genes encoding the cell division protein FtsZ and a glutathione synthetase homologue in the cyanobacterium Anabaena sp. PCC 7120', *Research in Microbiology*, 146(6), pp. 445–455. doi: 10.1016/0923-2508(96)80290-7.

Zhang, Y. (2009) 'I-TASSER: Fully automated protein structure prediction in CASP8', *Proteins: Structure, Function and Bioinformatics*, 77(SUPPL. 9), pp. 100–113. doi: 10.1002/prot.22588.

Zhou, J. *et al.* (2014) 'Discovery of a super-strong promoter enables efficient production of heterologous proteins in cyanobacteria', *Scientific Reports*, 4, pp. 1–6. doi: 10.1038/srep04500.

Figures

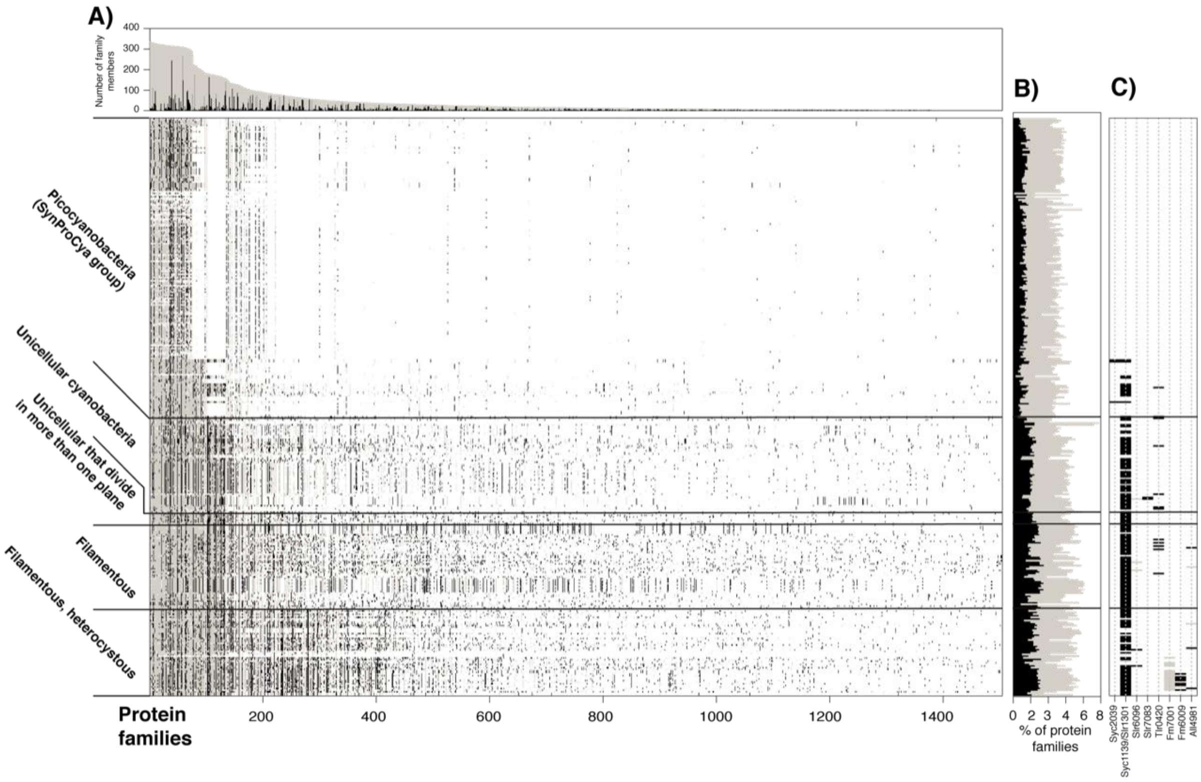

Fig. 1: Distribution of CCRP protein families within cyanobacteria

(**A**) Lines in the presence/absence matrix designate cyanobacterial genomes; each column shows a protein family. Gray dots designate any homologous protein in the same protein family and black dots represent CCRP members. Protein families are sorted according to the number of members. Protein family size and the number of CCRP members are presented in a bar graph above. (**B**) The proportion of protein families containing CCRPs (gray) and CCRP proteins (black) in each genome. (**C**) Presence/absence pattern of CCRP candidate protein families. Only protein families with at least three members predicted to be CCRPs are shown.

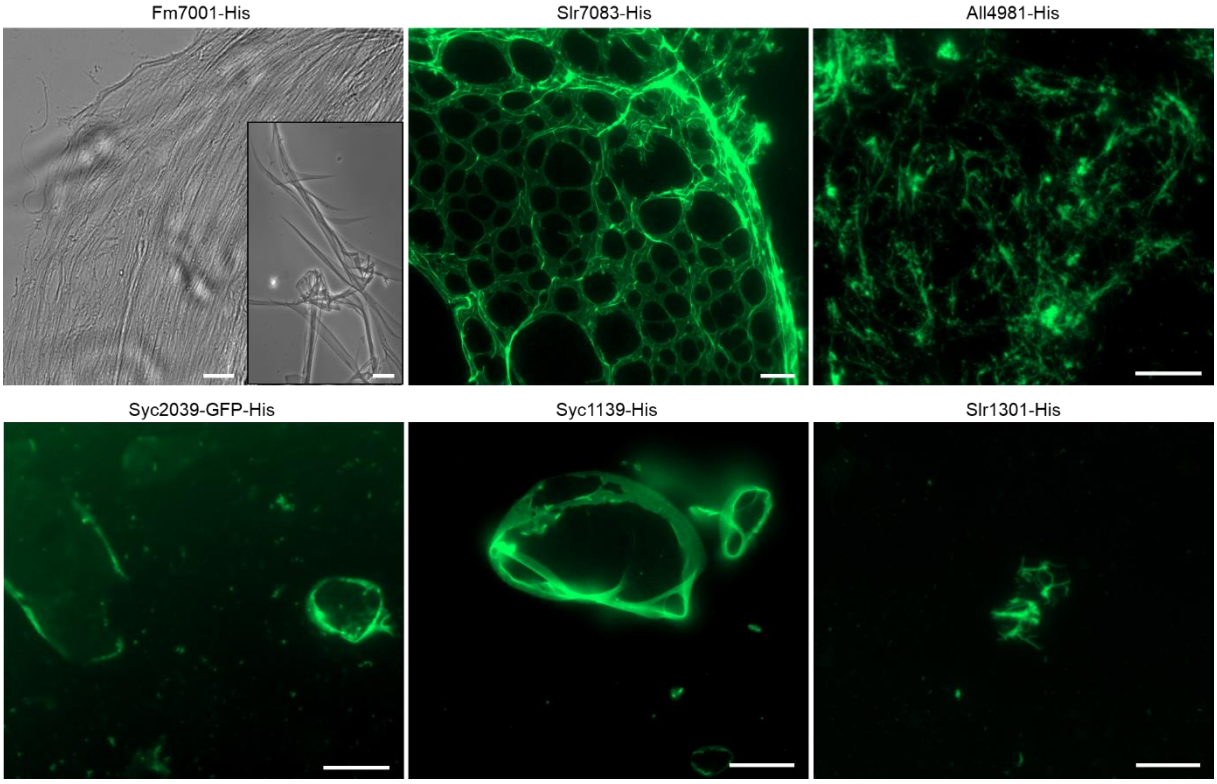

Fig. 2: Cyanobacterial CCRPs assemble into diverse filamentous structures *in vitro*

Bright field and epifluorescence micrographs of filamentous structures formed by purified and renatured Fm7001-His_6 (0.7 mg ml^{-1}), Slr7083-His_6 (1 mg ml^{-1}), All4981-His_6 (0.5 mg ml^{-1}), Syc2039-GFP-His_6 (0.3 mg ml^{-1}), Syc1139-His_6 (0.5 mg ml^{-1}) and Slr1301-His_6 (0.5 mg ml^{-1}). Proteins were dialyzed into 2 mM Tris-HCl, 4.5 M urea pH 7.5 (Fm7001), HLB (Slr7083), PLB (All4981, Syc1139, Slr1301) or BG11 (Syc2039). Renatured proteins were either directly analyzed by bright field microscopy (Fm7001) or stained with an excess of NHS-Fluorescein and analyzed by epifluorescence microscopy. The NHS-Fluorescein dye binds primary amines and is thus incompatible with urea, which is why Fm7001 filaments were visualized by bright field microscopy. Scale bars: 10 µm or (Fm7001 inlay and Slr7083) 20 µm.

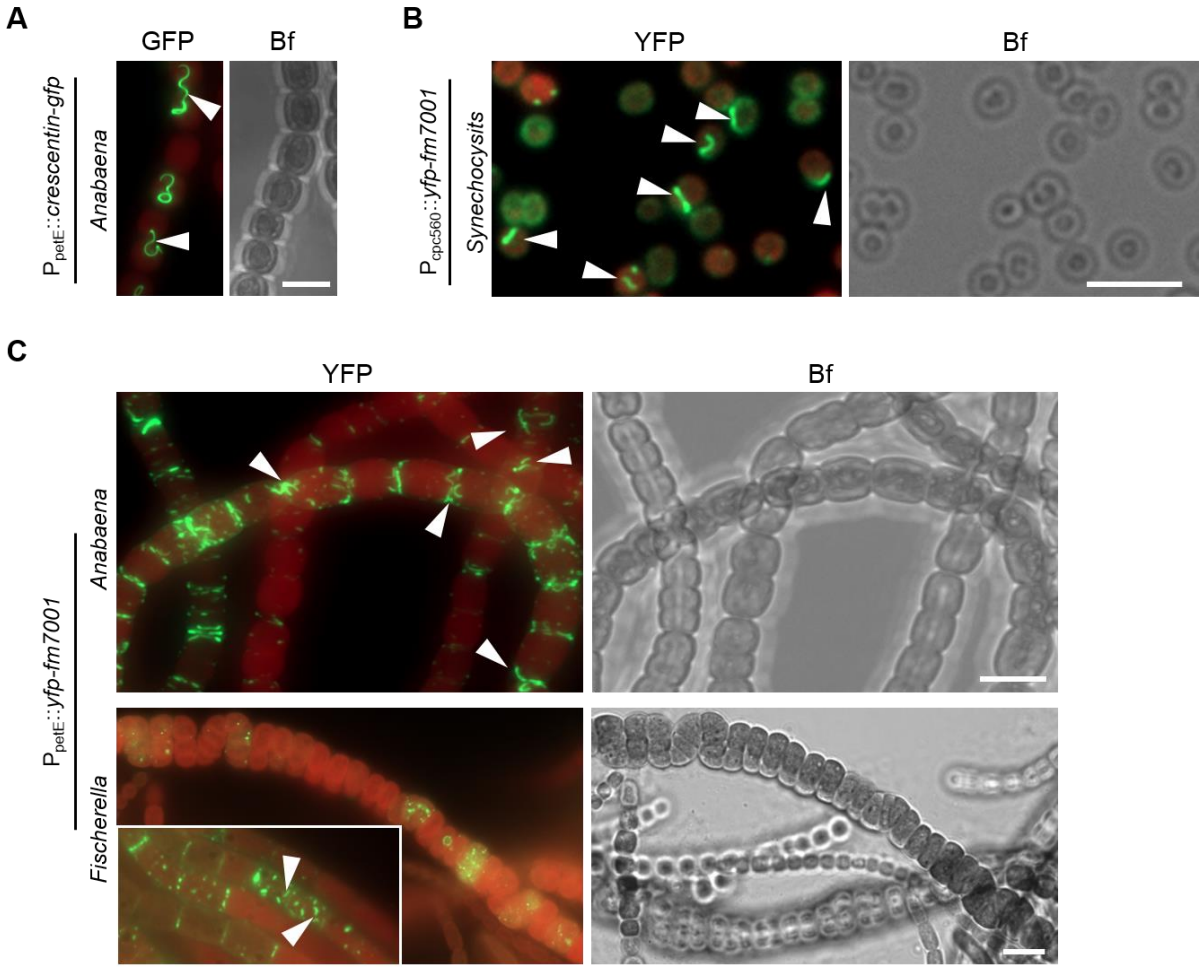

Fig. 3: Host-independency for Fm7001 *in vivo* filamentation

Merged GFP fluorescence and chlorophyll autofluorescence (red) and bright field micrographs of *Anabaena*, *Synechocystis* or *Fischerella* cells expressing (**A**) crescentin-GFP or (**B**,**C**) YFP-Fm7001. Cells were either grown in (**A**,**B**,**C** upper image) liquid BG11 or (**D** lower image) liquid BG11 without copper supplemented with 0.5 µM $CuSO_4$. Notably, YFP-Fm7001-expressing *Fischerella* cells failed to grow upon transfer to BG11 liquid medium and protein expression had to be induced with the addition of $CuSO_4$ later on. This indicates that Fm7001 must be strictly regulated for proper culture development. White triangles point to (**A**) seemingly cell-cell traversing crescentin-GFP filaments or (**B**,**C**) selected YFP-Fm7001 filamentous strings within the cell. Notably, unlike in *Anabaena* and *Fischerella*, Fm7001-GFP induced a swollen morphotype in *E. coli* and a subpopulation of *Synechocystis* cells (Supplementary Fig. 6). (**A**) Crescentin forms filaments with a diameter of 10 nm (Ausmees, Kuhn and Jacobs-Wagner, 2003) while the diameter of the GFP protein is approximately 2.4 nm (Ormö *et al.*, 1996). As such, crescentin-GFP could traverse through the septal junctions, which are predicted to be between 5-14 nm in diameter (Herrero, Stavans and Flores, 2016). (**A**,**C** top image): maximum intensity projection of a Z-stack. Scale bars: **(A**,**B**, **C** top image) 5 µm, (C lower image) 10 µm.

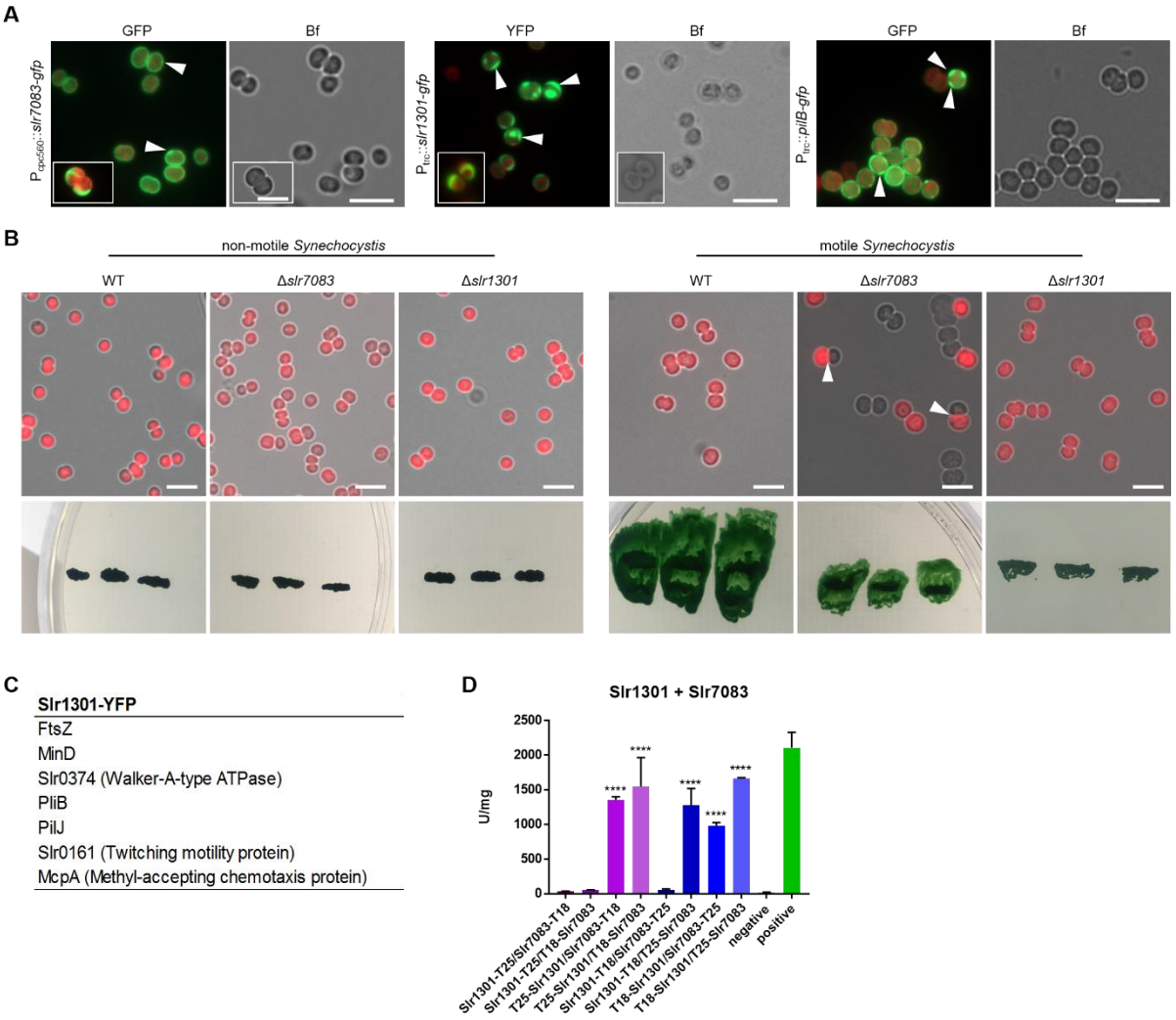

Fig. 4: Slr7083 and Slr1301 are involved in twitching motility in *Synechocystis*

(**A**) Merged GFP fluorescence and chlorophyll autofluorescence (red) and bright field micrographs of *Synechocystis* cells expressing, Slr7083-GFP, Slr1301-YFP or PilB-GFP from P_{cpc560} (Slr7083) or P_{trc} (Slr1301, PilB). Expression of PilB-GFP in PCC-M resulted in the same localization pattern (data not shown). White triangles indicate focal spots and crescent-like formations. (**B**) Merged bright field and chlorophyll autofluorescence micrographs of motile and non-motile *Synechocystis* WT, Δ*slr7083* and Δ*slr1301* mutant cells. Below, motility tests of three single colonies from indicated cells streaked on BG11 plates and illuminated from only one direction are shown. (**C**) Excerpt of interacting proteins of interest from mass spectrometry analysis of anti-GFP co-immunoprecipitations of *Synechocystis* cells expressing Slr1301-YFP from P_{trc} grown in BG11 (Supplementary Fig. 11B). (**D**) Beta-galactosidase assays of *E. coli* cells co-expressing indicated translational fusion constructs of all possible pair-wise combinations of Slr7083 with Slr1301 grown for 1 d at 30 °C. Quantity values are given in Miller Units per milligram LacZ of the mean results from three independent colonies. Error bars indicate standard deviations. Neg: pKNT25 plasmid carrying *slr1301* co-transformed with empty pUT18C. Pos: Zip/Zip control.*: $P < 0.05$, **: $P < 0.01$, ***: $P < 0.001$, ****: $P < 0.0001$ (Dunnett's multiple comparison test and one-way ANOVA). Scale bars: 5 µm.

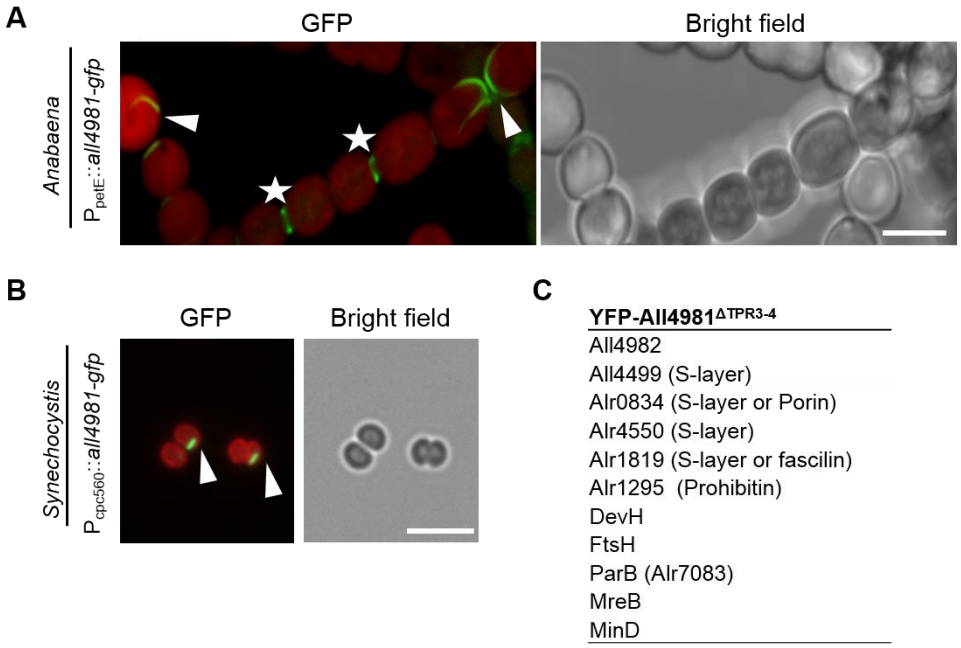

Fig. 5: All4981 forms cell-traversing filaments in cyanobacteria

(**A**,**B**) GFP fluorescence and merged GFP fluorescence and chlorophyll autofluorescence (red) and bright field micrographs of (**A**) *Anabaena* and (**B**) *Synechocystis* cells expressing All4981-GFP. *Anabaena* cells were grown in $BG11_0$ and *Synechocystis* cells were grown in BG11. (**A**): Maximum intensity projections of a Z-stack. White triangles indicate selected filaments traversing through the cells. White arrows point to spindle-like YFP-All4981 filaments. White stars mark septal formations between two neighboring cells. Scale bars: 5 µm. (**C**) Excerpt of interacting proteins of interest from mass spectrometry analysis of anti-GFP co-immunoprecipitations of *Anabaena* cells expressing YFP-All4981$^{\Delta TPR3-4}$ from P_{petE} (Supplementary Fig. 11A).

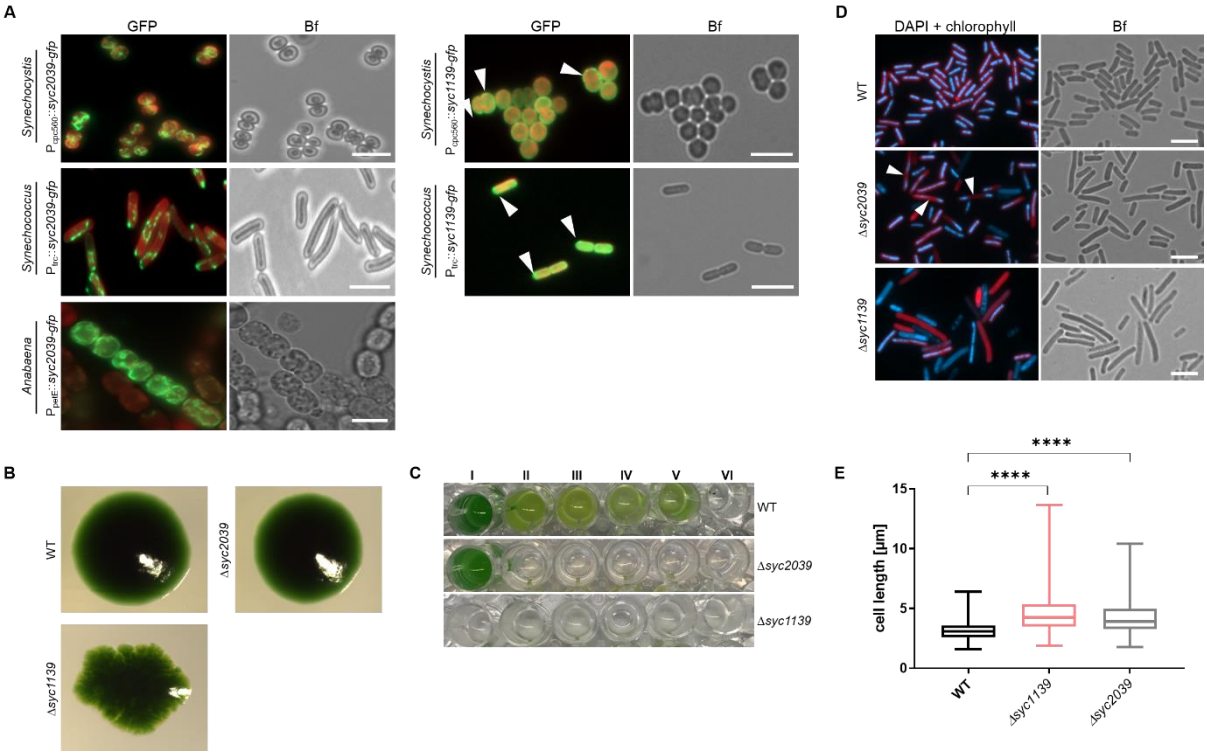

Fig. 6: *Synechococcus* CCRPs affect cytokinesis and cellular integrity

(**A**) Merged GFP fluorescence and chlorophyll autofluorescence (red) and bright field micrographs of *Synechocystis*, *Synechococcus* and *Anabaena* cells expressing Syc2039-GFP or Syc1139-GFP from P_{trc}. *Synechocystis* cells were grown in BG11, *Anabaena* cells were grown in $BG11_0$ supplemented with 0.25 µM $CuSO_4$ for 1 day, and *Synechococcus* cells were grown on BG11 plates supplemented with 0.01 mM (Syc2039) or 1 mM (Syc1139) IPTG. Micrographs of *Synechococcus* and *Anabaena* cells expressing Syc2039-GFP are maximum intensity projections of a Z-stack. White triangles indicate Syc1139-GFP spots. Attempts to translationally fuse a YFP-tag to the N-terminus of Syc2039 were unsuccessful, possibly due to the transmembrane domain predicted to the Syc2039 N-terminus (Supplementary Table 1). (**B**) Colony formation of *Synechococcus* WT and mutant strains on BG11 plates. (**C**) Cell viability of *Synechococcus* WT and mutant strains grown in (I) BG11 or BG11 supplemented with (II) 5 mM glucose, (III) 200 mM glucose, (IV) 2 mM NH_4Cl, (V) 200 mM maltose or (VI) 500 mM NaCl. (**D**) Merged DAPI fluorescence and chlorophyll autofluorescence (red) and bright field micrographs of *Synechococcus* WT and mutant strains grown on BG11 plates and stained with 10 µg ml^{-1} DAPI. White triangles indicate non-dividing cells revealing inhomogeneous DNA placement. (**E**) Cell length of *Synechococcus* WT (n = 648), non-segregated Δ*syc1139* (n = 417) and Δ*syc2039* mutant (n = 711) cells. Values indicated with * are significantly different from the WT. ****: P < 0.0001 (one-way ANOVA, using Turkey's multiple comparison test: P < 0.0001 for WT vs. each mutant). Scale bars: 5 µm.

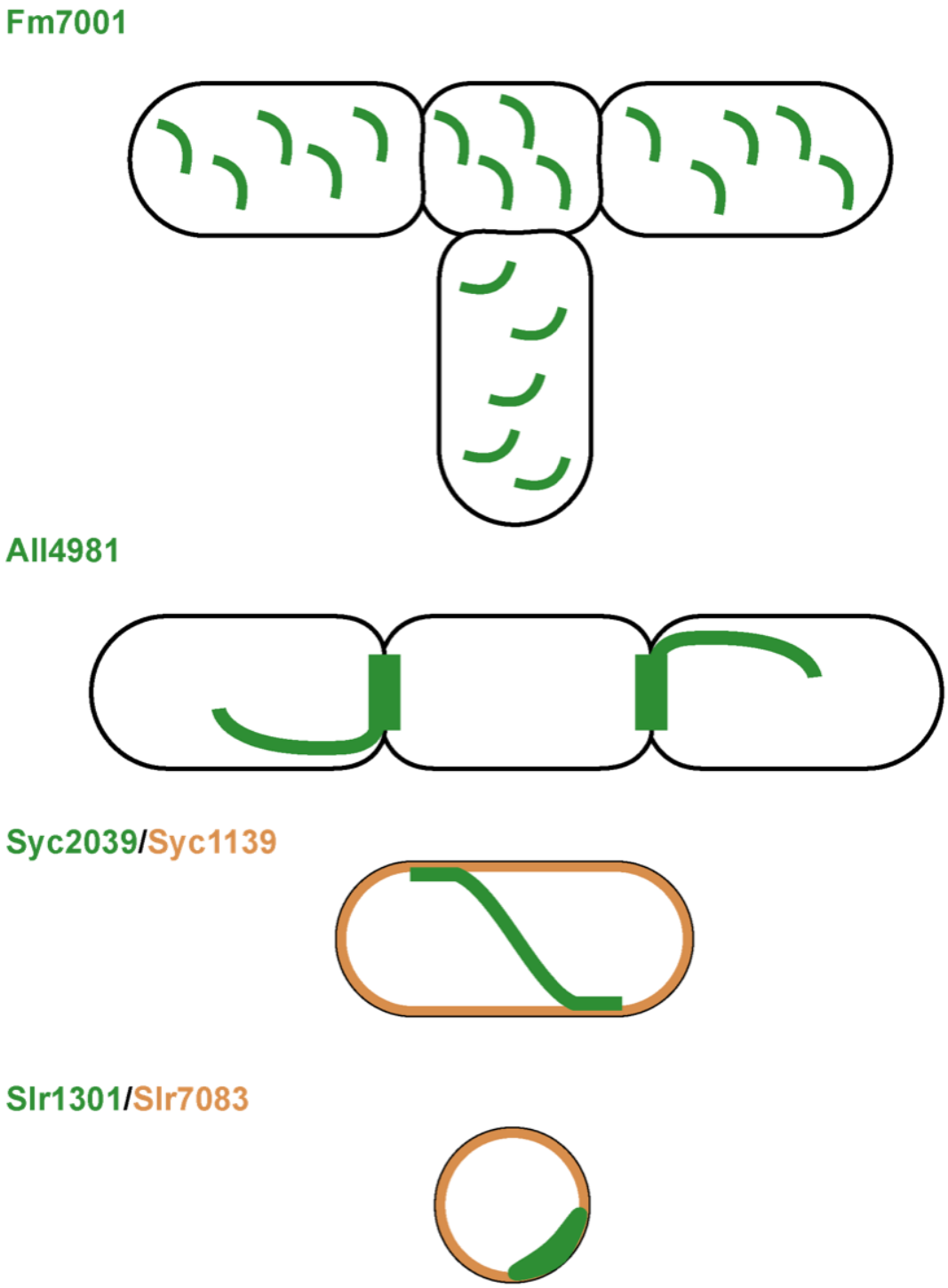

Fig. 7: Cyanobacterial CCRP systems

Schematic models for the *in vivo* localization of cyanobacterial CCRPs in their respective hosts. Fm7001 forms filamentous strings in *Fischerella*. In *Anabaena*, All4981 assembles into pole-arising filaments that traverse through the cell or forms septal-localized bridge-like formations. Syc2039, either independently of other *Synechococcus* proteins, or in direct cooperation with other filamentous proteins, forms long and sometimes helical strings that are often aligned with or in close proximity to the cell periphery. In *Synechococcus*, Syc1139 likely forms a protective proteinaceous layer below the cytoplasmic membrane. In *Synechocystis*, Slr1301 forms crescent-like structures while Slr7083 seemingly underlies the cytoplasmic membrane. Both localization types were also observed for PilB, suggesting a cooperative function.

Supplementary information

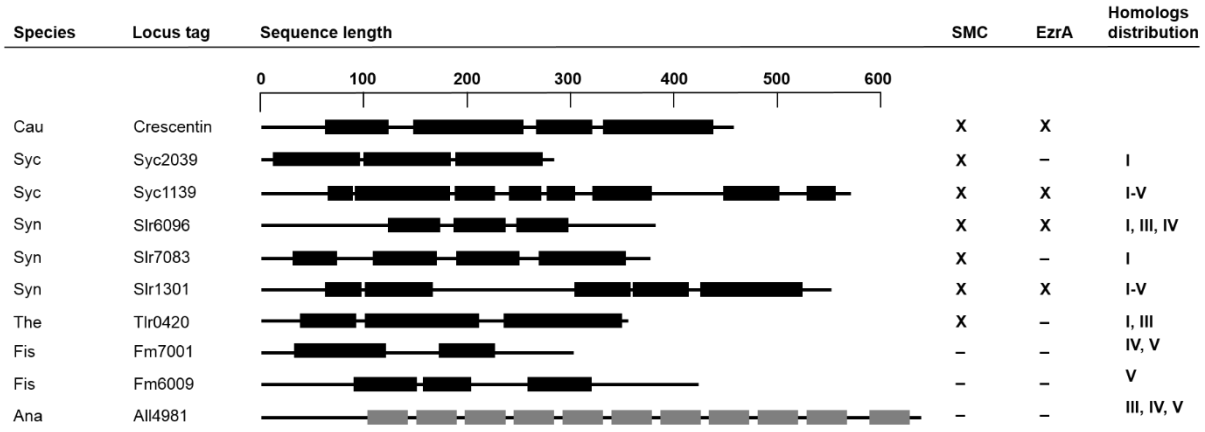

Supplementary Fig. 1:Distribution of coiled-coil domains in CCRPs selected for experimental validation

Depiction of cyanobacterial CCRP candidates selected for experimental evaluation. Scale on top is given in amino acid residues. Amino acid sequences in coiled-coil conformation are depicted by black bars with non-coiled-coil sequences represented by black lines. Tetratricopeptide repeats (TPR), also predicted by the COILS algorithm, are shown as grey bars. Proteins are given as cyanobase locus tags. Fm7001 and Fm6009 correspond to NCBI accession numbers WP_016868005.1 and WP_020476706, respectively. Abbreviations: Cau: *Caulobacter crescentus*; Syc: *Synechococcus*, Syn: *Synechocystis*; Ana: *Anabaena*; The: *Thermosynechococcus elongatus* BP-1; Fis: *Fischerella*. Cyanobacterial CCRPs revealed conserved domains present in other prokaryotic IF-like and eukaryotic IF proteins (Supplementary Table 1). Presence of a structural maintenance of chromosomes (SMC) domain or structural similarities to the cell division protein EzrA are marked with "**X**", absence are indicated with "**-**". Full list of domain and structural similarities are given in Supplementary Table 1. Notably, Fm7001 reveals domain similarities to the metabolic enzyme acetyl-CoA carboxylase. Last column indicates presence of homologs in indicated subsections (I, II, III, IV, V). Note: *Anabaena* CCRPs have been described elsewhere before: *Springstein et al*., bioRxiv, doi: 10.1101/553073.

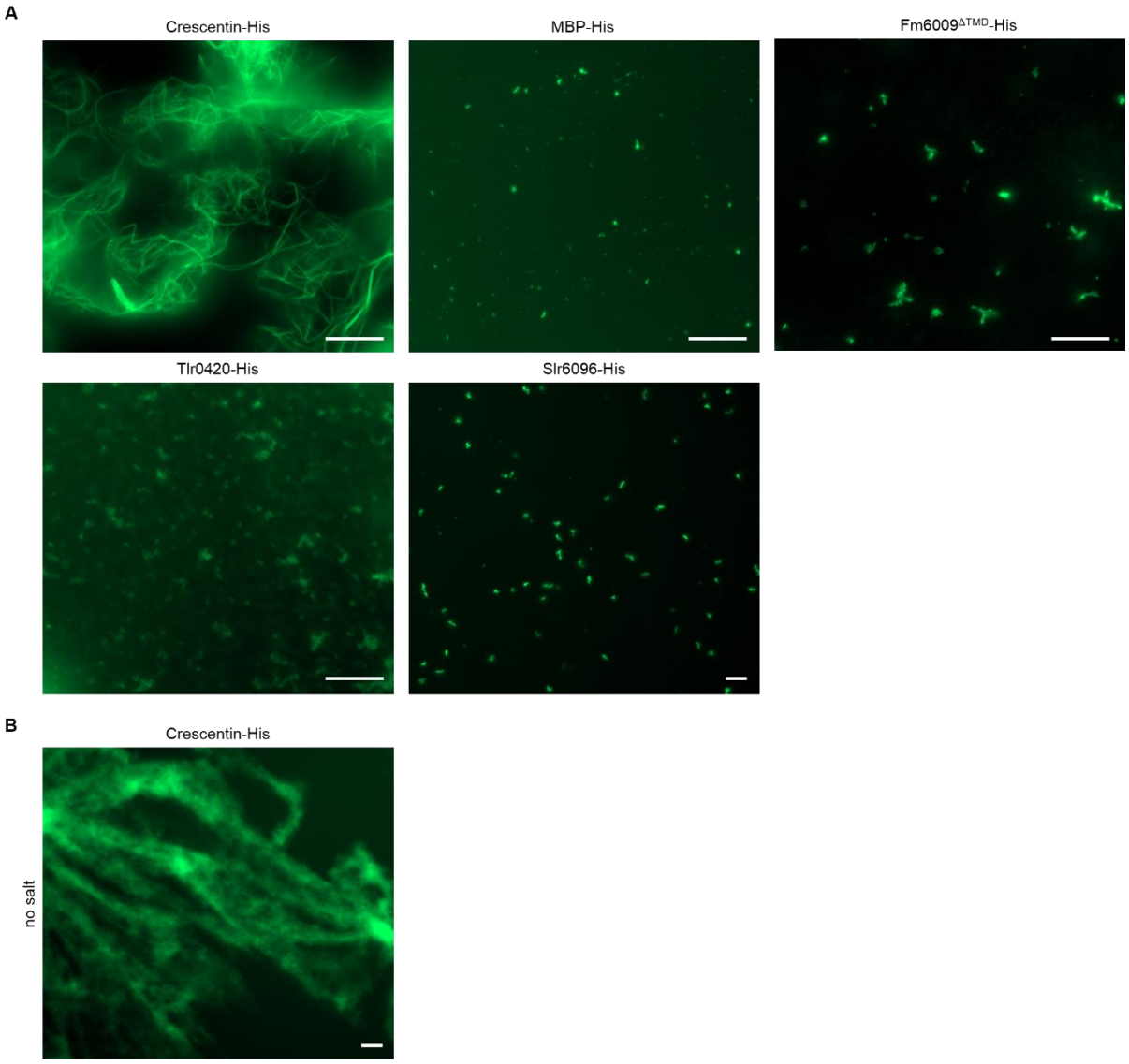

Supplementary Fig. 2: Crescentin *in vitro* polymerization is dependent on monovalent ions

(**A**) NHS-fluorescein fluorescence micrographs of *in vitro* structures formed by purified and renatured Crescentin-His_6 (0.7 mg ml^{-1}), $Fm6009^{\Delta TMD}$-His_6 (lacking the first 91 aa), MBP-His_6, Tlr0420-His_6 or Slr6096-His_6 (1 mg ml^{-1} each) in HLB or (**B**) Crescentin-His_6 (0.7 mg ml^{-1}) renatured in 25 mM Hepes, pH 7.4. Crescentin-His *in vitro* polymerization into smooth filaments is strictly dependent of the presence of salt in the renaturation buffer as Crescentin-His without salt assembles only into filamentous aggregates. Proteins were dialyzed in a step-wise urea-decreasing manner and stained with an excess of NHS-Fluorescein. Scale bars: 10 µm.

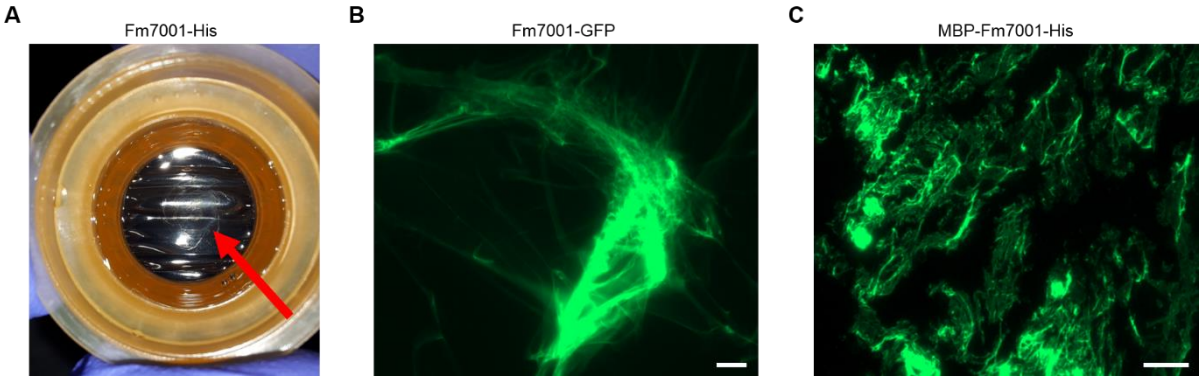

Supplementary Fig. 3: Fm7001 polymerizes in vitro in the presence of high-molar urea

(**A**) Bright field micrograph of a sheet-like and flat object floating on top of the dialysate (red arrow) formed upon dialysis of Fm7001-His_6 (0.7 mg ml^{-1}) into 2 mM Tris-HCl, 4.5 M urea, pH 7.5. (**B**,**C**) Epifluorescence micrographs of filamentous structures formed by (**B**) whole cell-free extract of *E. coli* BL21 (DE3) expressing Fm7001-GFP (0.7 mg ml^{-1} whole protein) dialyzed into 2 mM Tris-HCl, 3 M urea, pH 7.5 and by (**C**) natively purified MBP-Fm7001-His_6 (0.8 mg ml^{-1}) dialyzed into HLB. Scale bars: (**B**) 20 µm and (**C**) 10 µm.

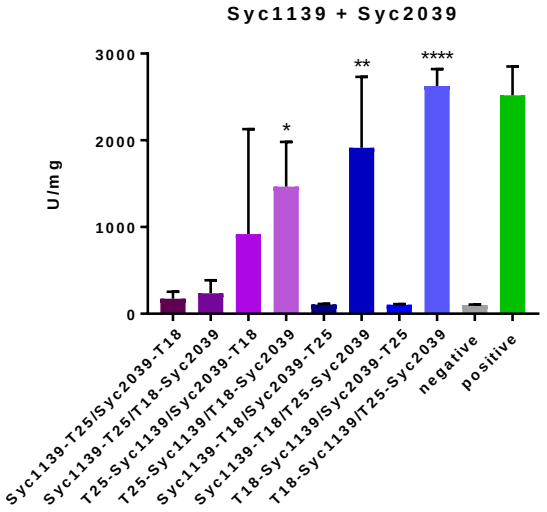

Supplementary Fig. 4: *Synechococcus* CCRPs interact with each other

Beta-galactosidase assays (BACTH) of E. coli BTH101 cells co-expressing indicated T25 and T18 translational fusions of all possible pair-wise combinations of Syc1139 and Syc2039. E. coli cells carrying the respective plasmids were subjected to the beta-galactosidase assay as described by (Karimova, Davi and Ladant, 2012) in triplicates from three independent colonies grown for 2 d at 20 °C. Quantity values are given in Miller Units per milligram LacZ of the mean results from three independent colonies. Negative: N-terminal T25 fusion construct of the respective protein co-transformed with empty pUT18C. Positive: Zip/Zip control. Error bars indicate standard deviations. *: $P < 0.05$, **: $P < 0.01$, ****: $P < 0.0001$ (Dunnett's multiple comparison test and one-way ANOVA).

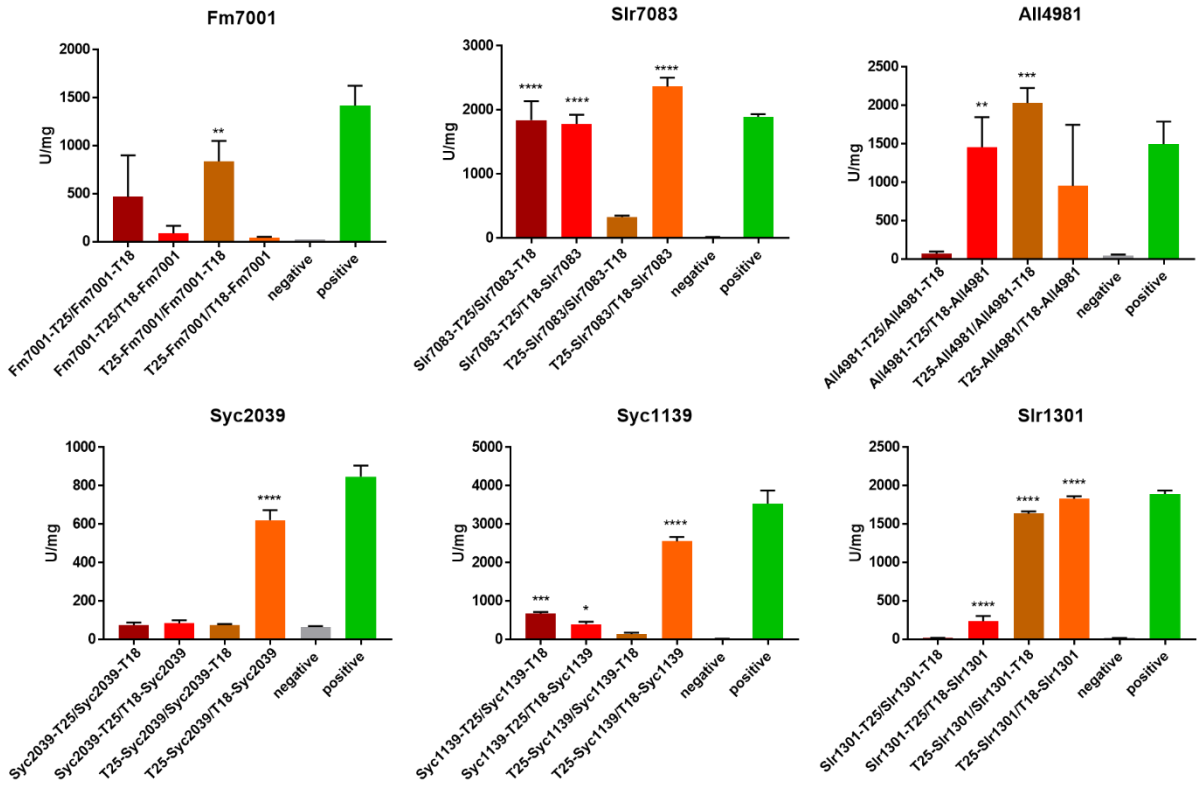

Supplementary Fig. 5: Cyanobacterial CCRPs interact with themselves

Beta-galactosidase assays (BACTH) of E. coli BTH101 cells co-expressing indicated T25 and T18 translational fusions of all possible pair-wise combinations. E. coli cells carrying the respective plasmids were subjected to beta-galactosidase assay described by (Karimova, Davi and Ladant, 2012) in triplicates from three independent colonies grown for 1 d at 30 °C. Quantity values are given in Miller Units per milligram LacZ of the mean results from three independent colonies. Negative: N-terminal T25 fusion construct of the respective protein co-transformed with empty pUT18C. Positive: Zip/Zip control. Error bars indicate standard deviations. *: $P < 0.05$, **: $P < 0.01$, ***: $P < 0.001$, ****: $P < 0.0001$ (Dunnett's multiple comparison test and one-way ANOVA).

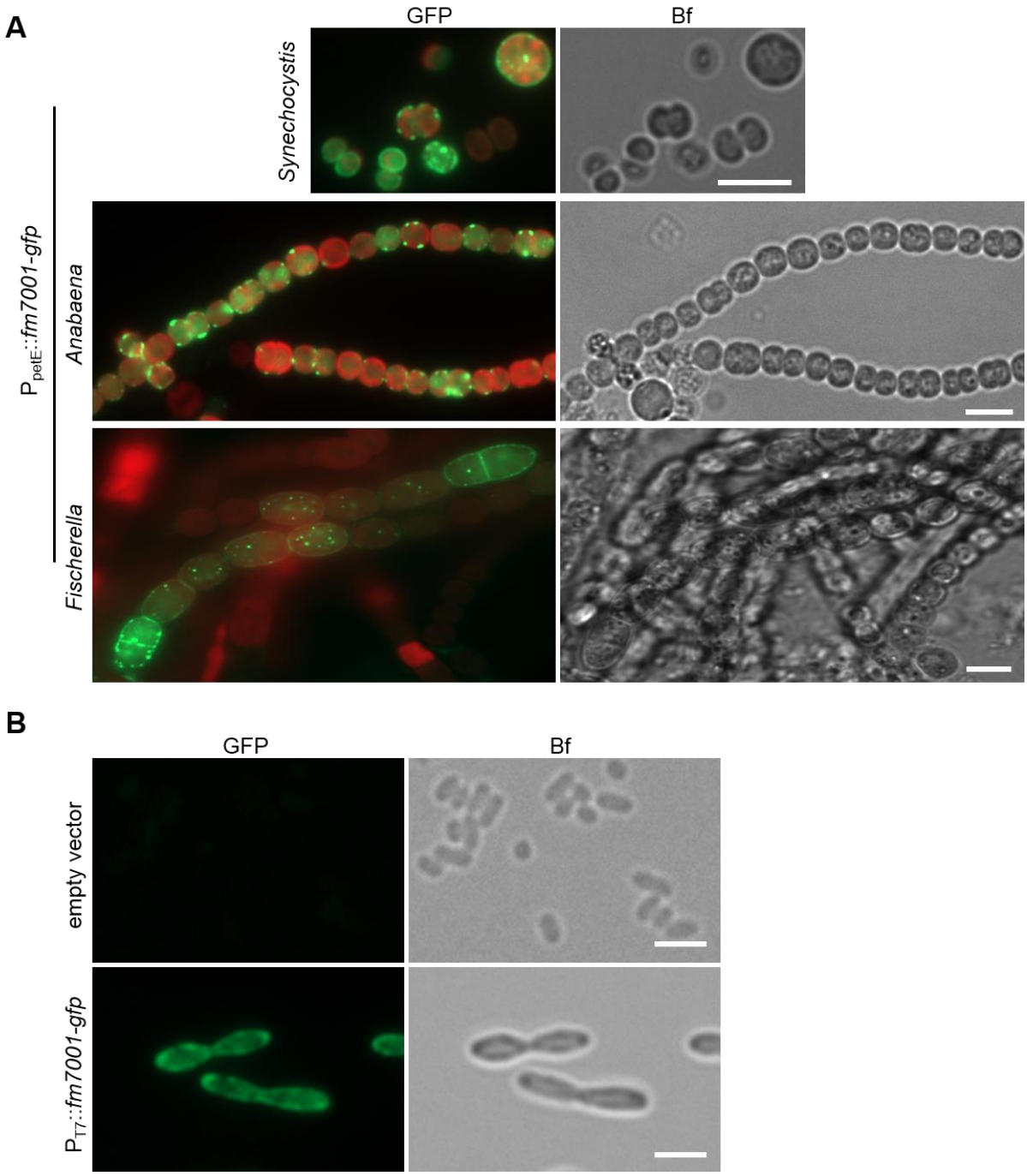

Supplementary Fig. 6: Overexpression of Fm7001-GFP affects *E. coli* and *Synechocystis* cell shape

(**A**) Merged GFP fluorescence and chlorophyll autofluorescence (red) and bright field micrographs or (**B**) GFP fluorescence and bright field micrographs Synechocystis, Anabaena, Fischerella and E. coli BL21 (DE3) cells expressing Fm7001-GFP. No in vivo filaments can be observed upon C-terminal fusion of Fm7001 with a GFP-tag (**B**) E. coli cells were grown at 16 °C and protein expression was induced with 0.05 mM IPTG for 24 h. Scale bars: (**A**) 5 µm or (**B**) 2.5 µm.

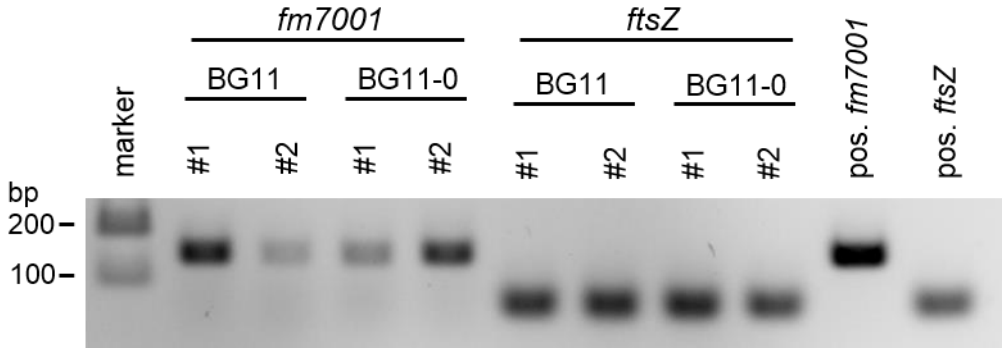

Supplementary Fig. 7: *fm7001* is expressed in early growth stages

RT-PCR of reverse transcribed whole RNA from young *Fischerella* WT cultures grown in BG11 or $BG11_0$ at standard growth conditions from two independent biological replicates. Gene transcripts were verified using internal *fm7001* gene primers (#1/#2) or internal *ftsZ* gene primers (#3/#4), as a control. *Fischerella* genomic DNA was included as positive control. PCR fragments were resolved on a 1% agarose gel in TAE buffer.

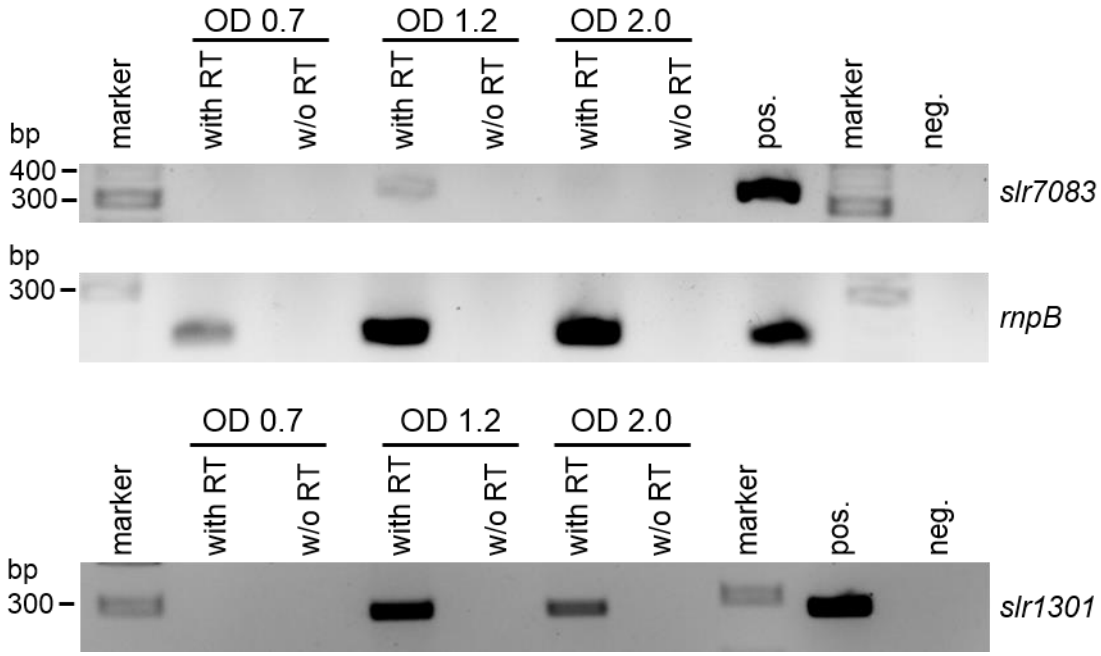

Supplementary Fig. 8: Expression of *slr7083* and *slr1301*

RT-PCR of reverse transcribed whole RNA from *Synechocystis* WT (OD_{750} 0.7, 1.2 or 2.0) grown in BG11 at standard growth conditions using internal *slr7083* gene primers (#5/#6) or internal *slr1301* gene primers (#9/#10). Internal *rnpB* gene primers (#7/#8) were included as a positive control. RNA was either reverse transcribed in the reaction buffer containing reverse transcriptase (with RT) or without reverse transcriptase (w/o RT) as a control for residual genomic DNA contamination. *Synechocystis* genomic DNA was included as positive control. PCR fragments were resolved on a 2% agarose gel in TAE buffer.

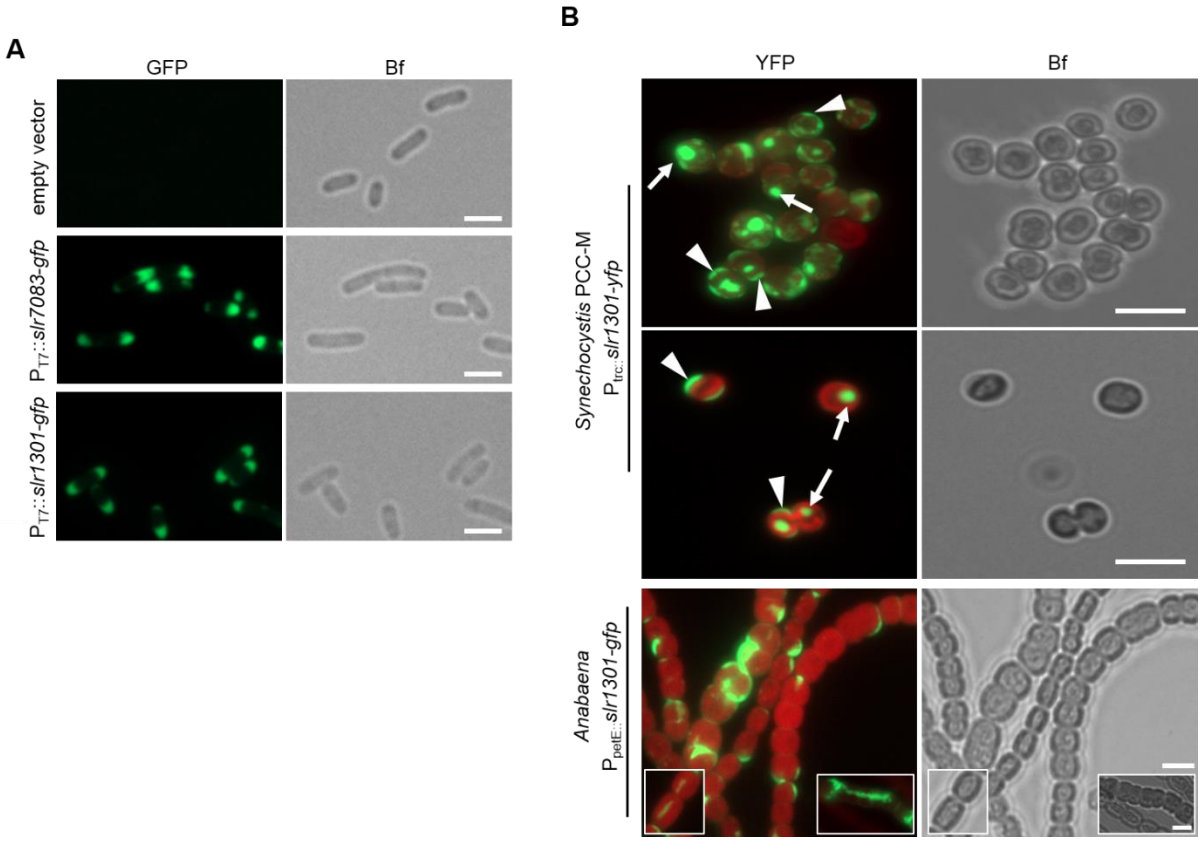

Supplementary Fig. 9: *In vivo* localization of Slr7083 and Slr1301

(**A**) GFP fluorescence and bright field micrographs of *E. coli* BL21 (DE3) WT cells or *E. coli* BL21 (DE3) cells expressing Slr7083-GFP or Slr1301-GFP from P_{T7}. Cells were induced with 0.05 mM IPTG and grown at 20 °C for 5 h. (**B**) Merged GFP fluorescence and chlorophyll autofluorescence (red) and bright field micrographs of *Synechocystis* cells expressing Slr1301-YFP from P_{trc} or *Anabaena* cells expressing Slr1301-GFP from P_{petE} grown on BG11 plates. Besides intracellular filaments (figure inlays), Slr1303 formed large plugs or sheets within the cells and induced a partial swollen cell phenotype. White triangles mark crescent-like localizations. White arrows show Slr1301-YFP plugs. Scale bars: (**A**) 2.5 µm or (**B**) 5 µm.

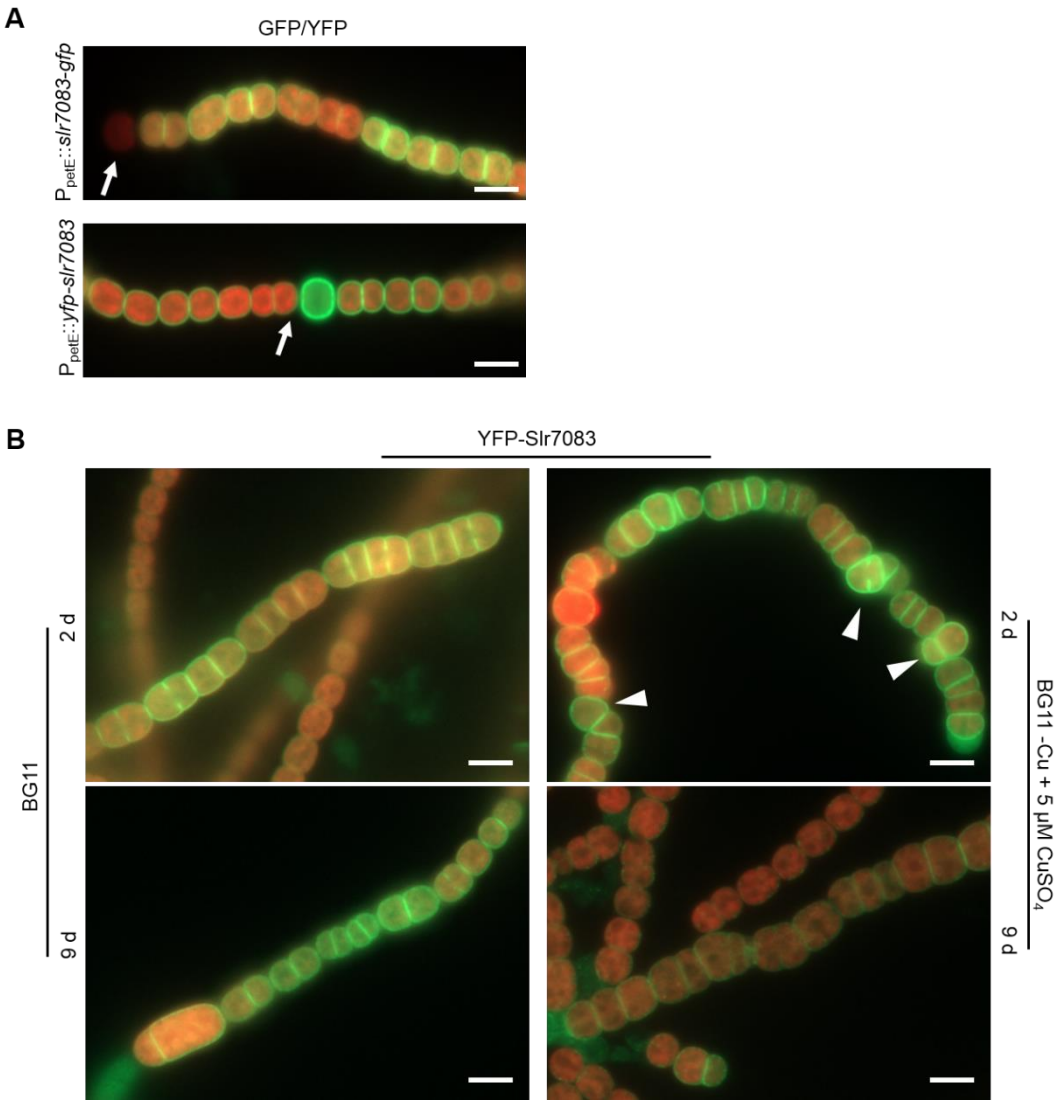

Supplementary Fig. 10: Slr7083 affects cell morphology and linear growth in *Anabaena*

(**A**,**B**) Merged GFP fluorescence and chlorophyll auto-fluorescence (red) micrographs of *Anabaena* cells expressing (**A**) Slr7083-GFP or YFP-Slr7083 from P_{petE} and grown on BG11-0 plates. (**B**) *Anabaena* cells expressing YFP-Slr7083 from P_{petE} in liquid BG11 or liquid BG11 without copper and induced with 5 µM $CuSO_4$ for 2 and 9 d. White arrows indicate heterocysts. White triangles point to multiseriate *Anabaena* filament growth. Scale bars: 5 µm

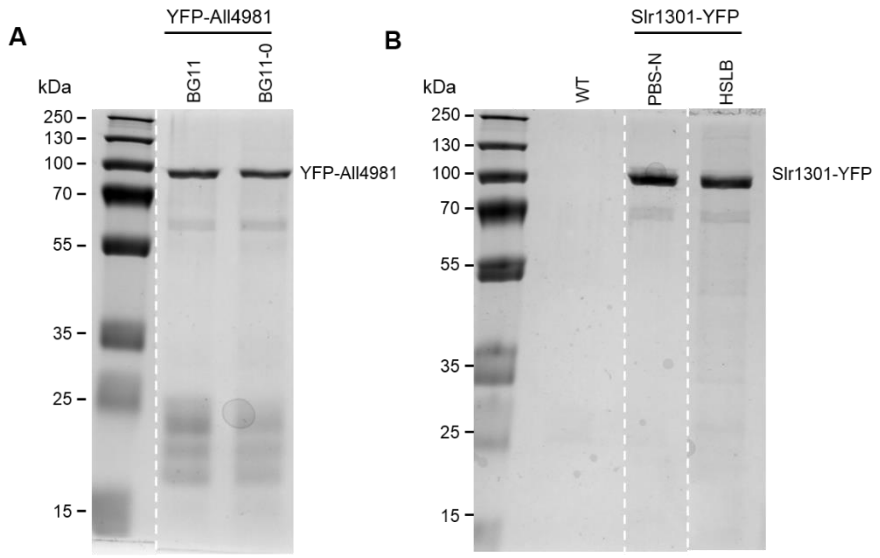

Supplementary Fig. 11: Co-immunoprecipitation of CCRP candidates

Cell-free lysates of (**A**) *Anabaena* cells expressing YFP-All4981 from P_{petE} grown in BG11 or BG11-0 supplemented with 0.5 µM $CuSO_4$ for two days and (**B**) *Synechocystis* WT and *Synechocystis* cells expressing Slr1301-YFP from P_{trc} were subjected to co-immunoprecipitation using anti-GFP magnetic beads (µMACS GFP isolation Kit, Miltenyi Biotec). Pooled duplicates of precipitated proteins of two independent experiments were analyzed by mass spectrometry and 25 µl of the precipitate were resolved in a 10% SDS-polyacrylamide gel and detected by Quick Coomassie stain (Serva). *Anabaena* WT control samples grown in BG11 and $BG11_0$ were provided to the mass spectrometry facility and not resolved on an SDS-polyacrylamide gel.

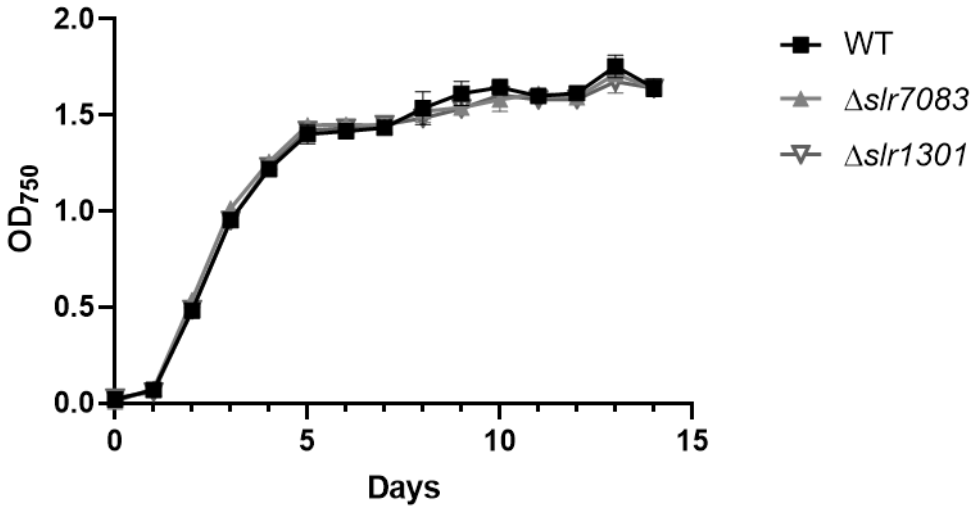

Supplementary Fig. 12: Deletion of *slr7083* and *slr1301* do not affect *Synechocystis* viability

Synechocystis WT, Δ*slr7083 and* Δ*slr1301* mutant strains were grown in BG11, adjusted to an OD_{750} of 0.1 and then grown in quadruples at standard growth conditions. OD_{750} values were recorded once a day for 15 d. Error bars show the standard deviation.

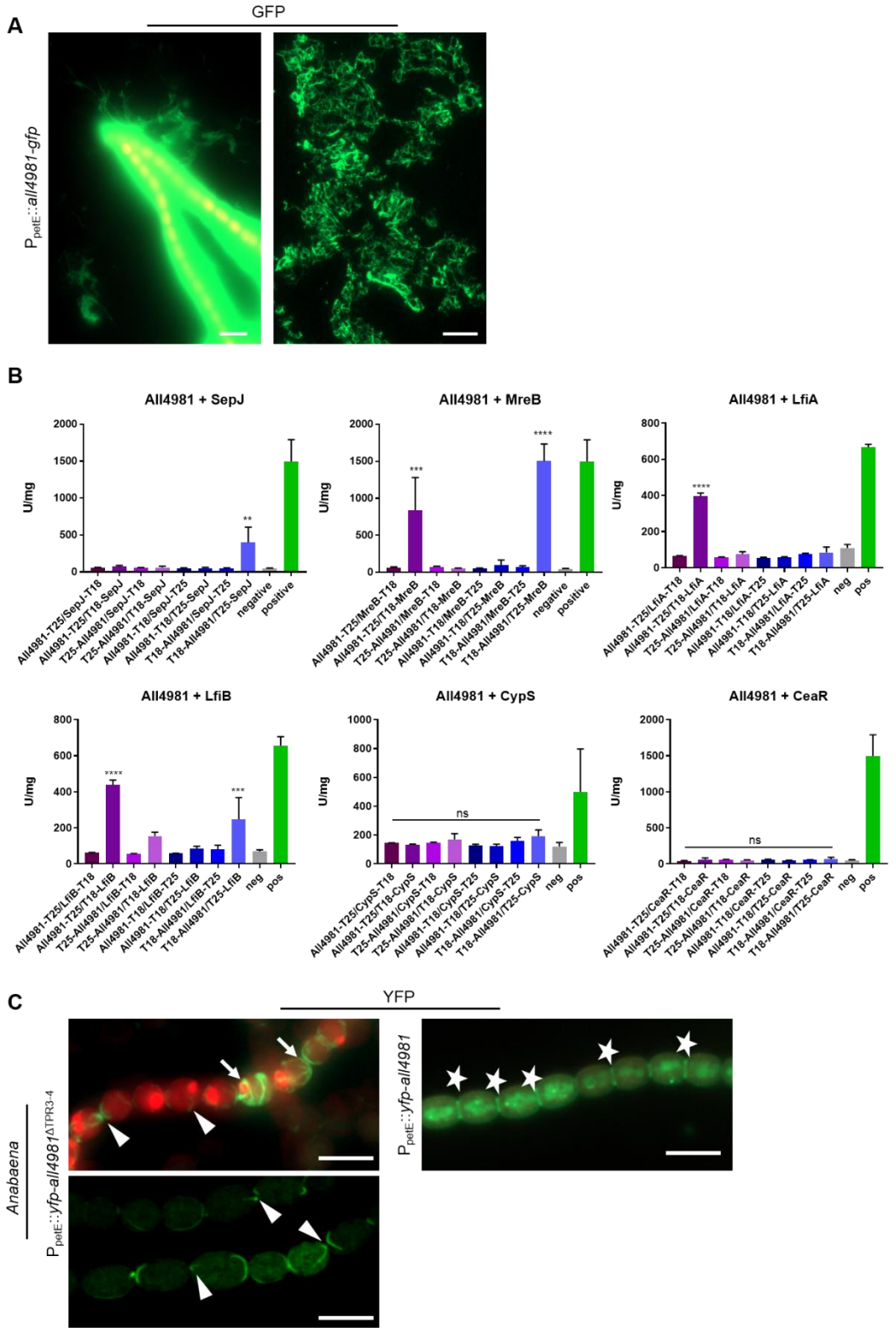

Supplementary Fig. 13: All4981 assembles into extracellular filaments and interacts with SepJ, MreB and *Anabaena* CCRPs

(**A**) GFP fluorescence and bright field micrographs of *Anabaena* cells expressing All4981-GFP from P_{petE} grown in BG11 supplemented with 0.5 µM $CuSO_4$ for 2 d. Extended period of overexpression of this construct then leads to cell lysis/rupture of a subpopulation of *Anabaena* filaments, releasing their internal components into the growth medium. Protein filaments released from the *Anabaena* filament are shown in the left image while the right GFP fluorescence image shows extracellular filaments observed in the growth medium. Notably, overexpression of YFP-All4981$^{\Delta TPR3-4}$ also induced cell lysis and extracellular filament formation but to a lesser degree. Scale bars: (left)

10 µm or (right) 20 µm. (**B**) Beta-galactosidase assays (BACTH) of *E. coli* BTH101 cells co-expressing indicated T25 and T18 translational fusions of all possible pair-wise combinations of All4981 with SepJ, MreB, LfiA, LfiB, CypS and CeaR. *E. coli* cells carrying the respective plasmids were subjected to beta-galactosidase assay described by Karimova et al. (2012) in triplicates from three independent colonies grown for 2 d at 20 °C. Quantity values are given in Miller Units per milligram LacZ of the mean results from three independent colonies. Negative: N-terminal T25 fusion construct of the respective protein co-transformed with empty pUT18C. Positive: Zip/Zip control. Error bars indicate standard deviations. *: $P < 0.05$, **: $P < 0.01$, ***: $P < 0.001$, ****: $P < 0.0001$ (Dunnett's multiple comparison test and one-way ANOVA). (**C**) Merged GFP fluorescence and chlorophyll autofluorescence (red) micrographs of *Anabaena* cells expressing YFP-All4981$^{\Delta TPR3-4}$ or YFP-All4981 from P_{petE}. *Anabaena* cells were grown in BG11-0 supplemented with 0.5 µM $CuSO_4$. White triangles indicate selected filaments traversing through the cells. White arrows point to spindle-like YFP- All4981$^{\Delta TPR3-4}$ filaments. White stars mark septal localization. Scale bars: 5 µm

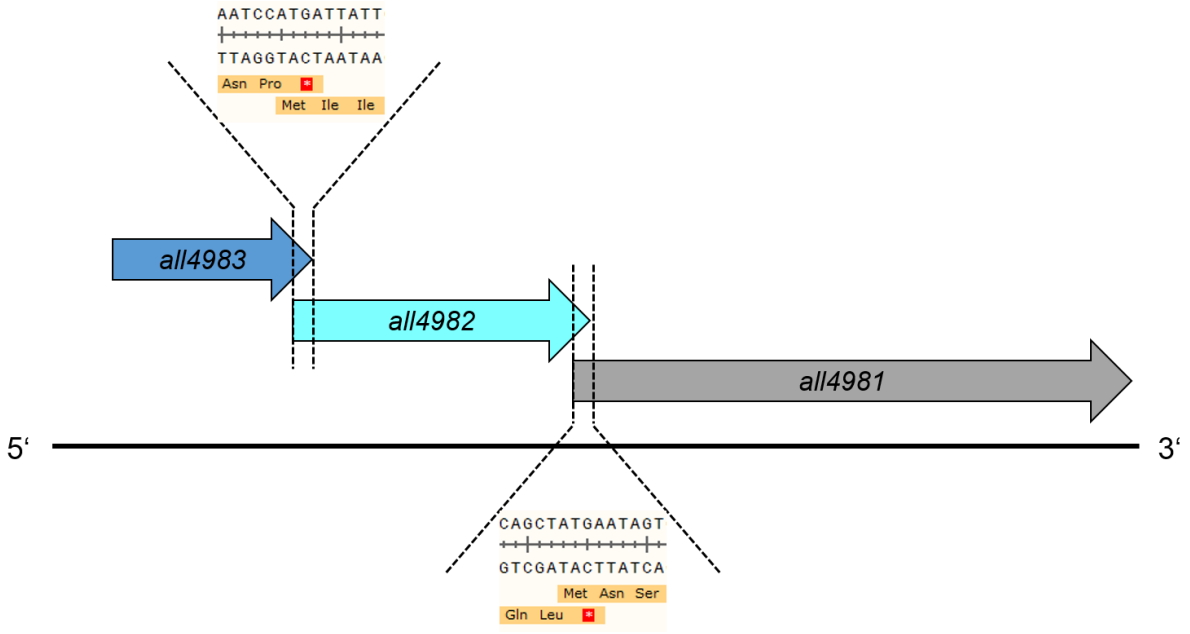

Supplementary Fig. 14: *all4981* genomic environment

Schematic representation of the genomic context of All4981. The 3’ end of *all4983* displays a 4 bp overlap to the 5’ region of *all4982*, which in turn has an overlap of 4 bp at its 3’ end with the 5’ end of *all4981*. In both cases, the overlapping sequence is comprised of the same four nucleotides (ATGA), reminiscent of *segA* and *segB* from *Sulfolobus solfataricus* (Kalliomaa-Sanford *et al.*, 2012). Notably, All4982 is predicted to belong to the large family of P-loop NTPases that also comprises the bacterial-specific cytoskeletal class of Walker A Cytoskeletal ATPases (Leipe *et al.*, 2002; Ingerson-Mahar and Gitai, 2012). Based on this buildup, it is conceivable that All4981, All4982 and All4983 share similar cellular functions.

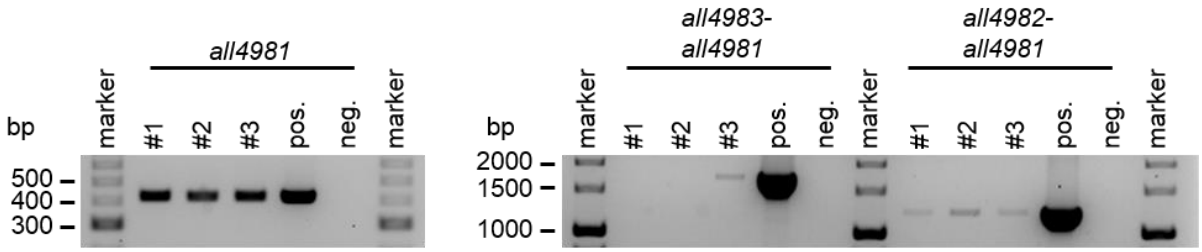

Supplementary Fig. 15: *all4981* is transcribed in an operon with *all4982* and *all4983*

RT-PCR of reverse transcribed whole RNA from Anabaena WT cultures grown in BG11 (OD_{750} 1.8) at standard growth conditions from three independent biological replicates. Gene and operon transcripts were verified using internal all4981 gene primers (#15/#16), internal all4983 forward and internal all4981 reverse gene primers (#17/#16) as well as internal all4982 forward and internal all4981 reverse gene primers (#18/#16). Only one of three replicates show a common transcript for all three genes, however, this likely is the result of the long fragment (about 1800 bp). The employed qScript cDNA SuperMix is optimized for fragments up to 1000 bp, thus making longer reverse transcriptions unlikely. As a positive control, *Anabaena* genomic DNA was included. PCR fragments were resolved on a 2% (left) or 0.7% (right) agarose gel in TAE buffer.

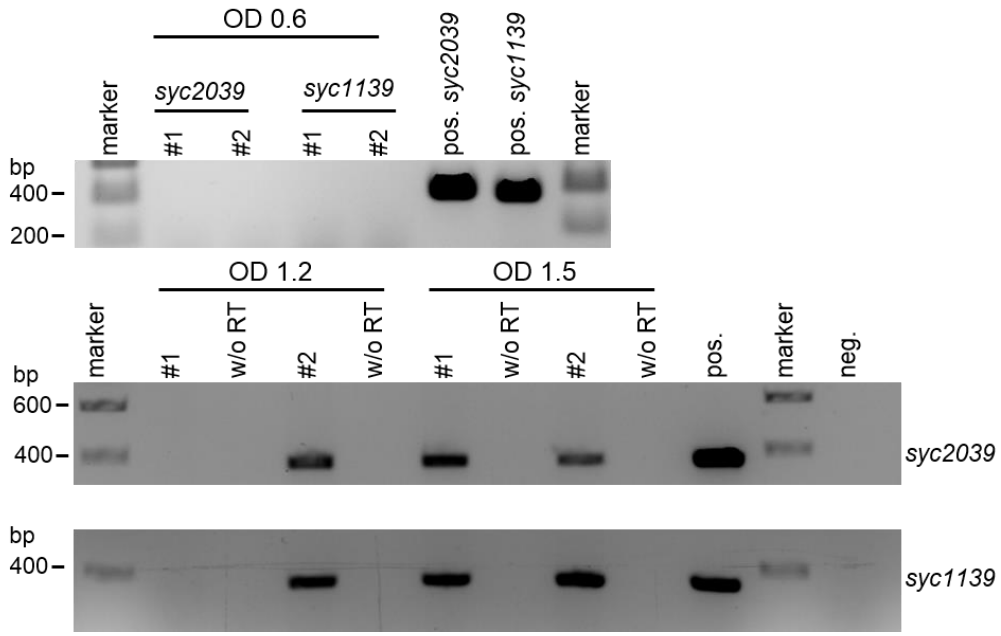

Supplementary Fig. 16: *Synechococcus* CCRPs are expressed at exponential growth phase

RT-PCR of reverse transcribed whole RNA from *Synechococcus* WT (OD_{750} 0.6, 1.2 or 1.5) grown in BG11 at standard growth conditions from two independent biological replicates (#1 and #2). Gene transcripts were verified using internal *syc2039* gene primers (#11/#12) and internal *syc1139* gene primers (#13/#14). RNA was either reverse transcribed in the reaction buffer containing reverse transcriptase (#1 and #2) or without reverse transcriptase (w/o RT) as a control for residual genomic DNA contamination. *Synechococcus* genomic DNA was included as positive control. PCR fragments were resolved on a 2% agarose gel in TAE buffer.

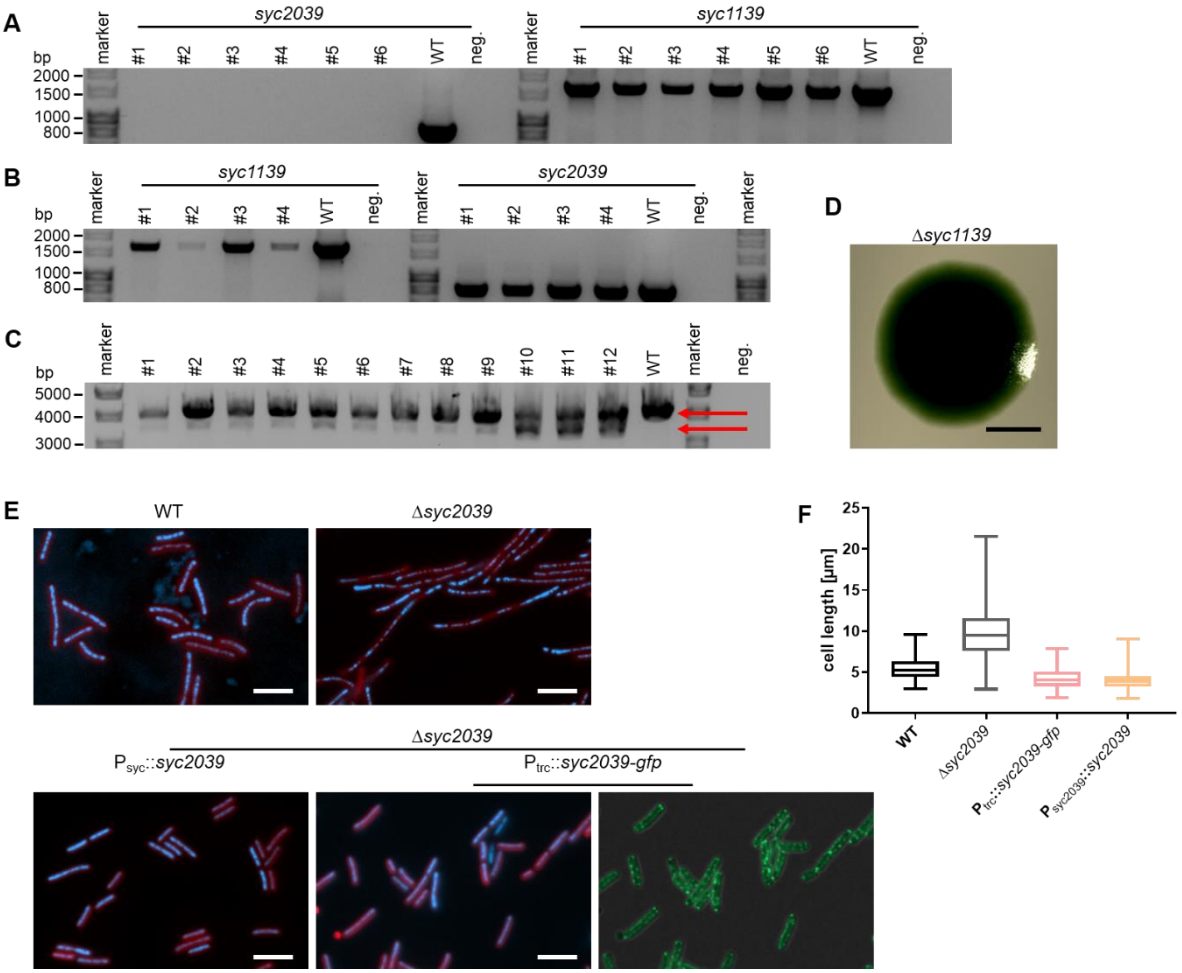

Supplementary Fig. 17: Verification of *Synechococcus* CCRP mutants

(**A**) Colony PCR of six Δ*syc2039* mutant clones using *syc2039* gene primers (#149/#147) and *syc1139* gene primers (#161/#162) as a control. (**B**) Colony PCRs of four non-segregated Δ*syc1139* mutant clones using *syc1139* gene primers (#174/#175) or *syc2039 gene* primers (#159/#160) as a control. (**C**) Colony PCR of twelve non-segregated Δ*syc1139* mutant clones using primers encompassing the homologous flanking regions used for homologous recombination (#238/#239). Upper red arrow indicates WT allele PCR product. Lower red arrow indicates Δ*syc1139* mutant PCR product. As a positive control, *Synechococcus* genomic DNA was included. (**D**) Growth of Δ*syc1139* on non-selective plates leads to a reversal to WT phenotype. (**E**) Merged DAPI fluorescence and chlorophyll autofluorescence (red) and merged GFP fluorescence and bright field micrographs of *Synechococcus* WT, Δ*syc2039* mutant strain and Δ*syc2039* mutant complemented with P_{syc}::*syc2039* or P_{trc}::*syc2039-gfp* inserted into the neutral NS1 locus. Cells were grown in BG11 or BG11 supplemented with 0.001 mM IPTG (for strain carrying P_{trc}::*syc2039-gfp*) and stained with 10 µg ml^{-1} DAPI. (**F**) Cell length of *Synechococcus* WT (n=505), Δ*syc2039* (n=517), Δ*syc2039* carrying P_{trc}::*syc2039-gfp* (n=547) and Δ*syc2039* carrying $P_{syc2039}$::*syc2039* (n=529) cells measured using Fiji software.

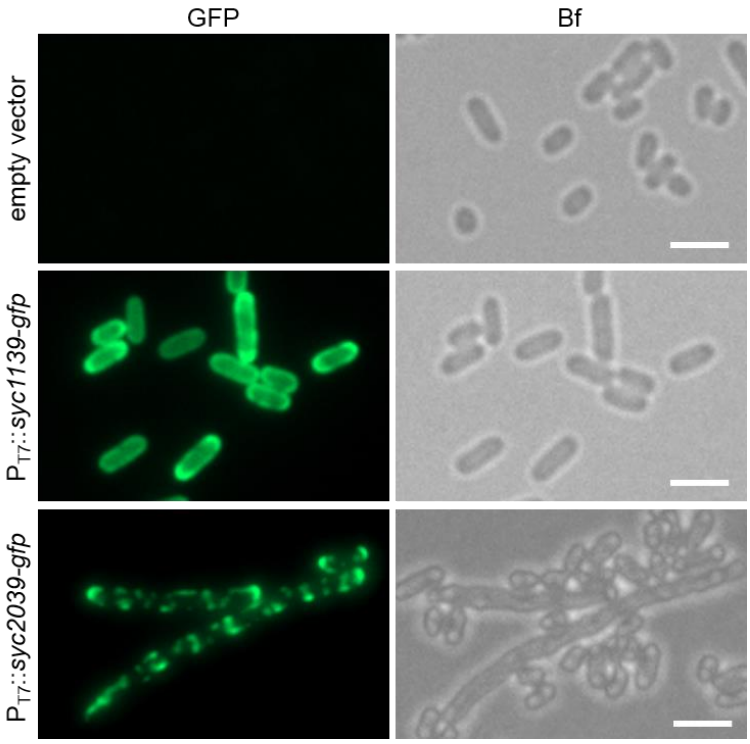

Supplementary Fig. 18: Localization of *Synechococcus* CCRPs in *E. coli*

GFP fluorescence and bright field micrographs of *E. coli* BL21 (DE) WT cells or *E. coli* BL21(DE3) cells expressing Syc1139-GFP or Syc2039-GFP. Proteins were expressed at 20 °C with 0.05 mM IPTG for 24 h. Micrograph showing Syc2039-GFP expression is a maximum intensity projection of a Z-stack. Scale bars: 2.5 µm.

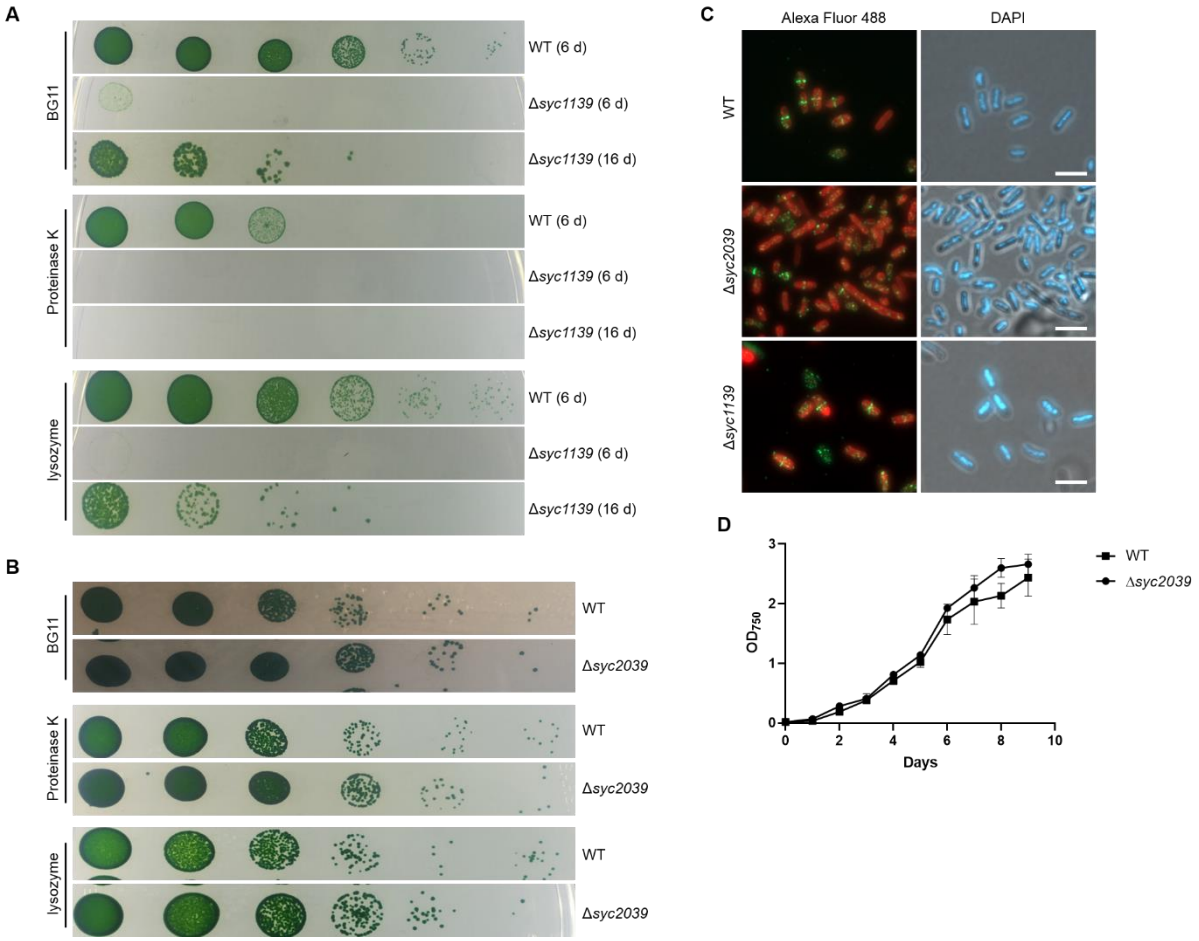

Supplementary Fig. 19: Phenotypic characterization of *Synechococcus* mutant strains

(**A**) *Synechococcus* WT (upper lane, after 6 days) and non-segregated Δ*syc1139* mutant (middle lane: after 6 days and lower lane after 16 days) strains were grown on BG11 plates or BG11 plates supplemented with 50 µg ml^{-1} Km. Cells were resuspended in BG11, adjusted to an OD_{750} of 0.4 and spotted in triplicates of serial 10-fold dilutions on BG11 plates or BG11 plates supplemented with 100 µg ml^{-1} Lysozyme or 50 µg ml^{-1} Proteinase K. Cells were grown until no further colonies arose in the highest dilution. (**B**) *Synechococcus* WT and Δ*syc2039* mutant strains were grown in liquid culture at standard growth conditions until an OD_{750} of about 2.0, diluted in BG11 to an OD_{750} of 0.4 and spotted in triplicates of serial 10-fold dilutions on BG11 plates or BG11 plates supplemented with 100 µg ml^{-1} Lysozyme or 30 µg ml^{-1} Proteinase K. Cells were grown until no further colonies arose in the highest dilution. (**C**) Merged Alexa Flour-488 fluorescence and chlorophyll autofluorescence (red) and merged bright field and DAPI fluorescence micrographs of *Synechococcus* WT, Δ*syc2039* or non-segregated Δ*syc1139* mutant strains grown on BG11 plates and subjected to immunofluorescence staining using an anti-FtsZ primary antibody (Agrisera, raised against *Anabaena* FtsZ) and an Alexa Fluor-488 coated secondary antibody. Cells were mounted in Prolong Diamond antifade mountant with DAPI (Thermo Fischer Scientific). (**D**) *Synechococcus* WT and Δ*syc2039* mutant strain were grown in BG11, adjusted to an OD_{750} of 0.1 and then grown in triplicates at standard growth conditions. OD_{750} values were recorded once a day for 10 d. Error bars show the standard deviation. Scale bars: 5 µm.

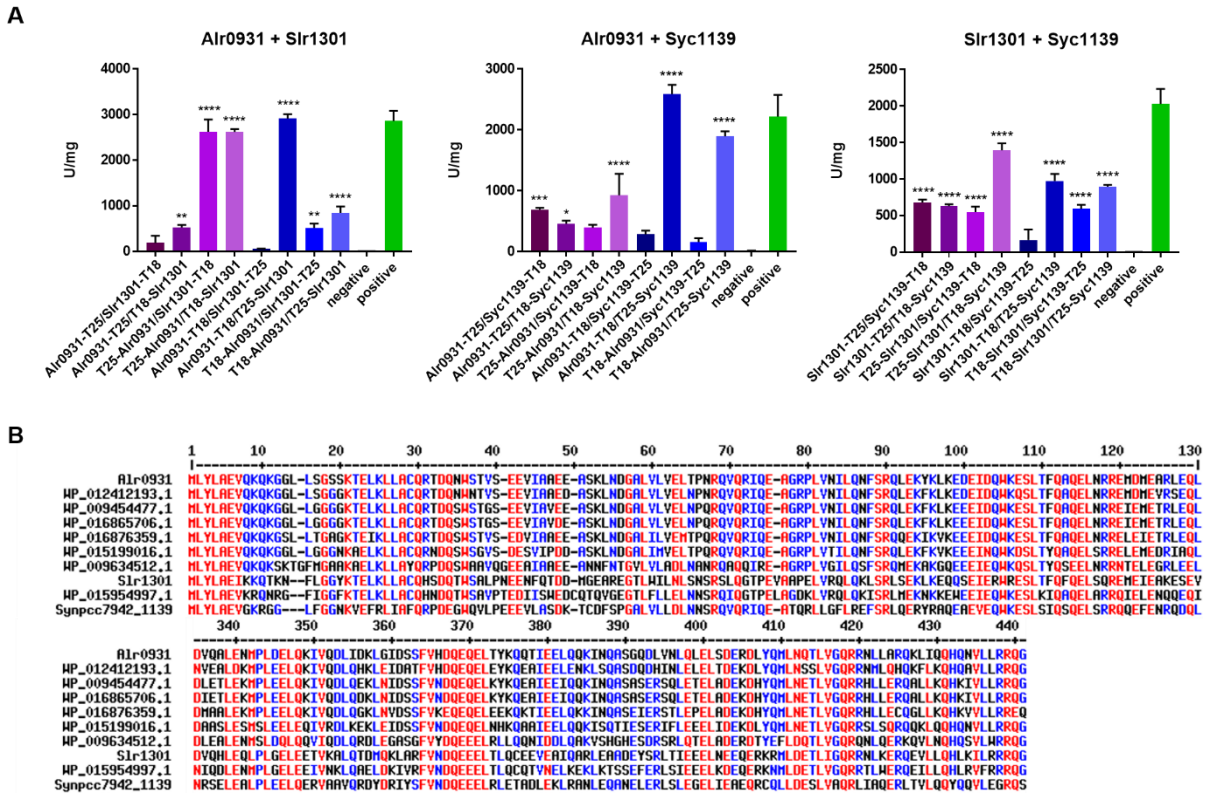

Supplementary Fig. 20: Interaction of cyanobacterial CCRP homologs

(**A**) Beta-galactosidase assays (BACTH) of *E. coli* BTH101 cells co-expressing indicated T25 and T18 translational fusions of all possible pair-wise combinations of Alr0931 (CypS), Slr1301 and Syc1139. *E. coli* cells carrying the respective plasmids were subjected to beta-galactosidase assay described by (Karimova, Davi and Ladant, 2012) in triplicates from three independent colonies grown for 1 d at 30 °C. Quantity values are given in Miller Units per milligram LacZ of the mean results from three independent colonies. Negative: N-terminal T25 fusion construct of the respective protein co-transformed with with empty pUT18C. Positive: Zip/Zip control. Error bars indicate standard deviations. *: P < 0.05, **: P < 0.01, ***: P < 0.001, ****: P < 0.0001 (Dunnett's multiple comparison test and one-way ANOVA). (**B**) Multiple sequence alignment of selected cyanobacterial homologous CCRPs using MULTALIGN (Corpet, 1988) with default settings and sorted according to relatedness. Alr0931 (termed CypS; *Anabaena*), Slr1301 (*Synechocystis*) and Synpcc7942_1139 (*Synechococcus*) are identified by their designated cyanobase locus tag. Other proteins are given as NCBI accession numbers. WP_012412193.1 (*Nostoc punctiforme* PCC 73102), WP_009454477.1 (*Fischerella thermalis* PCC 7521), WP_016865706.1 (*Fischerella*), WP_016876359.1 (*C. fritschii* PCC 9212), WP_015199016.1 (*Calothrix* sp. PCC 6303), WP_009634512.1 (*Synechocystis* sp. PCC 7509), and WP_015954997.1 (*Cyanothece* sp. PCC 7424). Amino acids from 1-130 and 334-441 are depicted. Red highlighted amino acid residues are conserved among all listed species while amino acid residues highlighted in blue are mostly conserved. Amino acids depicted in black are not conserved. Characteristic for this group of conserved cyanobacterial CCRPs is a highly conserved N-terminus with a M-L-Y-L-A-E-V sequence motif present in nearly all homologs, followed by a moderately conserved N-terminal region of the first 120 amino acids. Two other highly conserved domains are present in this group, one located around the centre of the proteins (between the 340th and 370th amino acid), and another one shortly thereafter between the 400th and 420th amino acid.

1293 **Supplementary Table 1: Properties of cyanobacterial CCRPs**

Gene /Locus tag	Genus	Subsection	Homologs distribution	Predicted proteins of similar structure (I-TASSER)	Homolog similarities	Conserved domains	Others
crescentin	*C. crescentus*	n/a	n/a	Cytoplasmic domain of bacterial cell division protein EzrA		SMC, CCDC158	Validated IF-like protein
filP	*Streptomyces coelicolor*	n/a	n/a	Dynein tail; α-Actinin; Tropomyosin		DUF3552, SMC, RNase_Y	Validated IF-like protein
desmin	*Homo sapiens*	n/a	n/a	PI4KIIIa lipid kinase		Filament (pfam00038), SMC, Spc7, MscS_TM	IF protein
vimentin	*Homo sapiens*	n/a	n/a	PI4KIIIa lipid kinase		Filament (pfam00038), SMC, Spc7	IF protein
syc2039	*Synechococcus*	I	I	Tropomyosin		SMC, MukB, CALCOCO1	N-terminal TMD; only in *Synechococcus* sp.
syc1139	*Synechococcus*	I	I, II, III, IV, V	Cytoplasmic domain of bacterial cell division protein EzrA	39%	SMC, MukB, Spc7	Homolog to *slr1301*
slr6096	*Synechocystis*	I	I, III, IV	Cytoplasmic domain of bacterial cell division protein EzrA		SMC	
slr7083	*Synechocystis*	I	I	Plectin		SMC, MscS_TM	Encoded on pSYSA plasmid, only in *Synechocystis* sp.
slr1301	*Synechocystis*	I	I, II, III, IV, V	Cytoplasmic domain of bacterial cell division protein EzrA	39%	SMC, SbcC, APG6, DUF3552	Homolog to *syc1139*
tlr0420	*BP-1*	I	I, III	Plectin		SMC, MscS_TM	
fm7001	*Fischerella*	V	IV, V	α-catenin or vinculin; similarity to acyl-CoA dehydrogenase	63%	Acetyl-CoA carboxylase carboxyl transferase (PLN0322)	Highly expressed; 3’ end 9 bp overlap to *fm7000*
fm6009	*Fischerella*	V	V	Structure of β-catenin and HTCF-4		COG0610	
all4981	*Anabaena*	IV	III, IV, V	TTC7B/Hyccin Complex, Clathrin	47%	TPR	5’ with a 4 bp overlap to *all4982*

The first column indicates the respective gene name or locus tags of each protein candidate. The second and third column indicate the respective subsection of the corresponding cyanobacterial genus. Column four lists the subsections that contain homologous proteins to the respective CCRP. Column five indicates structural similarities of the candidate to proteins in the Protein Data Bank (PDB) based on I-TASSER (Zhang, 2009; Yang and Zhang, 2015). The sixth column lists predicted sub-domains of protein candidates identified by BLAST Conserved Domain Search. Column seven names other features of interest. Abbreviations: (TMH) Transmembrane helix; (DUF) Domain of unknown function; (CCDC158) Coiled-coil domain-containing protein 158; (SMC) Structural maintenance of chromosomes; (MukB) The hinge domain of chromosome partition protein MukB; (APG6) Autophagy protein Apg6, (SbcC) DNA repair exonuclease SbcCD ATPase; (CALCOCO1) Calcium binding and coiled-coil domain; (Spc7) Spc7 kinetochore protein; (Filament) Intermediate filament protein; (TPR): Tetratricopeptide repeat; (PLN0322) Acetyl-CoA carboxylase carboxyl transferase; (COG0610) Type I site-specific restriction-modification system. *Anabaena* CCRPs CypS, LfiB, CeaR, Alr4393 and All4935 (Springstein *et al.*, 2019) also revealed structural similarities to EzrA. n/a: not applicable.

Supplementary Table 2: Employed E. coli strains

Strain	Genotype	Resistance	Reference
XL1 blue	*endA*1 *gyrA*96(nal^R) thi-1 *recA*1 *relA*1 *lac gln*V44 F'[::Tn10 *proAB*$^+$ *lacI*^{q} Δ(*lacZ*)M15] *hsd*R17(r_K^- m_K^+)	Tet	Stratagene
HB101	F$^-$ *mcrB mrr hsd*S20(r_B^- m_B^-) *recA*13 *leuB*6 *ara*-14 *proA*2 *lacY*1 *galK*2 *xyl-5 mtl*-1 *rpsL*20(Sm^R) *gln*V44 λ$^-$	Sm	Boyer and Roulland-Dessoix, 1969
DH5α	F– Φ80*lacZ*ΔM15 Δ(*lacZ*YA-*arg*F) U169 *recA*1 *endA*1 *hsdR17* (rK–, mK+) *phoA supE*44 λ– *thi*-1 *gyrA*96 *relA*1		(Meselson and Yuan, 1968)
DH5αMCR	F- *endA*1 *supE*44 *thi-1* λ$^-$ *recA1 gyrA*96 *relA*1 *deoR* Δ(*lacZYA-argF*)U169 Φ80d*lacZ*ΔM15 *mcrA* Δ(*mrr hsdRMS mcrBC*)		Grant *et al.*, 1990
BL21 (DE3)	F$^-$ *ompT gal dcm lon hsdS$_B$*($r_B^-m_B^-$) λ(DE3 [*lacI lacUV5-T7p07 ind1 sam7 nin5*]) [*malB*$^+$]$_{K-12}$(λ^S)		Studier and Moffatt, 1986
BTH101	F$^-$, *cya-99*, *araD139*, *galE15*, *galK16*, *rpsL1* (*Str$_r$*), *hsdR2, mcrA*, *mcrB1*	Sm	Euromedex

Supplementary Table 3: Cyanobacterial strains

Strain	Description	Resistance	Reference
Fischerella muscicola PCC 7414	WT		Pasteur culture collection of cyanobacteria (PCC), France
Synechocystis sp. PCC 6803	Glucose tolerant Kazusa substrain WT		PCC, France
BLS4	Δ*slr1301*::*nptII*	Km	This study
BLS5	Δ*slr7083*::*nptII*	Km	This study
Synechocystis sp. PCC-M 6803	Glucose tolerant and motile Moscow PCC-M substrain WT		A gift from Annegret Wilde (University of Freiburg)
BLS6	Δ*slr1301*::*CS.3*	Sm,Sp	
BLS7	Δ*slr7083*::*CS.3*	Km	This study
Synechococcus elongatus PCC 7942	WT		A gift from Martin Hagemann (University of Rostock)
BLS8	Non-segregated Δ*syc2039*::*nptII*	Km	This study
BLS9	Δ*syc2039*::*nptII*	Km	This study
Anabaena sp. PCC 7120	WT		PCC, France

1306 **Supplementary Table 4: Employed oligonucleotides**

#	Given name	Sequence 5' -> 3'	Purpose
1	Fm7001_intern_A	AGCGGGAAGATGGCTACTATC	RT-PCR
2	7001_northern	TCTGCGGCTTGACTTGATAC	RT-PCR
3	ftsZ 7414 primer fwd	TGGAACTAAAGCTGCCGAGG	RT-PCR
4	ftsZ 7414 primer rev	CTGTACCAGTTCCACCACCC	RT-PCR
5	Syn017_intern_A	TGCAACAGCAAACGGAACAG	RT-PCR
6	Syn017_intern_B	TTGGGAGCTAACTTGCCCAC	RT-PCR
7	rnpb 6803 primer fwd	GGAGTTGCGGATTCCTGTCA	RT-PCR
8	rnpb 6803 primer rev	AAGACCAACCTTTGCCCCTC	RT-PCR
9	Syn708_intern_A	TGGAGTGCCCTGCCTAACG	RT-PCR
10	Syn708_intern_B	CCCTTCTAACCTTTGTCGGGC	RT-PCR
11	Syc484_intern_A	CTACCATTCTTGGTGTGGCGG	RT-PCR
12	Syc484_intern_B	GAAATCCTGCGATCGCTGTTG	RT-PCR
13	Syc879_intern_A	CCTGTGACTTCTCTCCAGGG	RT-PCR
14	Syc879_intern_B	CTTTTAACTCGCGATCGCGGC	RT-PCR
15	Nos389_intern_A	ATCACCTGAATTAGCTGCGG	RT-PCR
16	Nos389_intern_B	CTAATAATGCCGCAATCAGCG	RT-PCR
17	All4982_intern_A	ATCAGATGGTGGAGGGAAGC	RT-PCR
18	All4983_intern_A	AGTAGCTGCATTTATCGGTGC	RT-PCR
19	pET19bmod-Fwd	GGAATTGTGAGCGGATAACAATT	Sequencing of pET21a(+) inserts
20	T7R	CTAATACGACTCACTATAGGGA	Sequencing of pET21a(+) inserts
21	pAM2991_Seq_A	GCGCCGACATCATAACGGTTC	Sequencing of pAM2991 inserts
22	pAM2991_Seq_B	GCTGAAAATCTTCTCTCATCCGCC	Sequencing of pAM2991 inserts
23	pRL153_Seq_Rev	AGGAGATTAACCCGCCCAAG	Sequencing of pRL153 inserts
24	CS3_Seq_Fwd	CGCGCAGATCAGTTGGAAG	Sequencing of gene replacement plasmids
25	CS3_Seq_Rev	AACGTCGGTTCGAGATGGC	Sequencing of gene replacement plasmids
26	GFP_Seq_Rev	TTGTGCCCATTAACATCACCATC	Sequencing of GFP containing plasmids
27	pJET1.2 forward sequencing primer	CGACTCACTATAGGGAGAGCGGC	Sequencing of pJET1.2 inserts
28	pJET1.2 reverse sequencing primer	AAGAACATCGATTTTCCATGGCAG	Sequencing of pJET1.2 inserts
29	pKO_Seq_Fwd	GCCTTTTTACGGTTCCTGGC	Sequencing pTHS121

30	pKO_Seq_Rev	TCTTTTCTACGGGGTCTGACG	Sequencing pTHS121
31	pIGA_Seq_Fwd	TGCGCATAGAAATTGCATCA	Sequencing of pIGA inserts
32	pIGA_Seq_Rev	GTCAGCAACACCTTCTTCA	Sequencing of pIGA inserts
33	pRL271_Seq_Fwd	GCCTGGTGCTACGCCTGAATA	Sequencing of pRL271 inserts
34	pRL271_Seq_Rev	CCAGTTAATAGTTTGCGCAACGTTG	Sequencing of pRL271 inserts
35	pRL278_Seq_Fwd	GGGGCGTAATTTTTTTAAGGCAGTTATTG	Sequencing of pRL278 inserts
36	pSL2680_Seq_A	CAAGAGGGCAAAAAACTCAATTTG	Sequencing of pSL2680 inserts
37	cpf1_1A	TTGGTCATGAGATTATCAAAAAGGATCCTGGAAAACGTTCTTCGGGGC	Amplification of *cpf1* for pTHS123
38	pRL25c_CRISPR_2B	AGGCCCTTTCGTCTTCAAGAATTCTTTACACTGATGAATGTTCCGTTGCG	Amplification of *cpf1* for pTHS123
39	cpf1-1	CTCCAGAAGCTATAAACTATGAAC	Sequencing of *cpf1*
40	cpf1-2	CTACTTCAAGCTAGTGCGGAA	Sequencing of *cpf1*
41	cpf1-3	GTTGAAAATCAAGGCTACAAACTAAC	Sequencing of *cpf1*
42	cpf1-4	CGTTTCAAGGTAGAGAAGCAGG	Sequencing of *cpf1*
43	pRL25c_Seq_Fwd	CTTTGATCTTTTCTACGGGGTCT	Sequencing of pRL25C inserts
44	pRL25c_Seq_Rev	TTGAGGTGAGGGATGAGCG	Sequencing of pRL25C inserts
45	pMAL_Seq_Fwd	AGAAAGGTGAAATCATGCCG	Sequencing of pMAL-c2x inserts
46	pMAL_Seq_Rev	CTGCAAGGCGATTAAGTTGG	Sequencing of pMAL-c2x inserts
47	MB_Seq_A	GGCTCGTATGTTGTGTGG	Sequencing of pKNT25, pKT25 and pUT18 inserts
48	MB_Seq_B	GGCTTAACTATGCGGCATC	Sequencing of pKNT25, pUT18 and pUT18C inserts
49	MB_Seq_C	TAACGCCAGGGTTTTCCCA	Sequencing of pKT25 inserts
50	pKNT25_Seq_Rev	CGTTTGCGTAACCAGCC	Sequencing of pKNT25 inserts
51	pKT25_Seq_Fwd	GATTCGGTGACCGATTACCTG	Sequencing of pKT25 inserts
52	pUT18_Seq_Rev	GATGCGTTCGCGATCCAG	Sequencing of pUT18 inserts

53	pUT18C_Seq_Fwd	TCGCCGGATGTACTGGAAAC	Sequencing of pUT18C inserts
54	N-term_1A	GAGGATCCCCGGGTACC	Amplification of pKNT25 and pUT18
55	N-term_1B	TAGAGTCGACCTGCAGGCA	Amplification of pKNT25 and pUT18
56	pKT25_1A	CCCCGGGTACCTAAGTAAGTAAG	Amplification of pKT25
57	pKT25_1B	ATCCTCTAGAGTCGACCCTGC	Amplification of pKT25
58	pUT18C_1A	CCGAGCTCGAATTCATCGAT	Amplification of pUT18C
59	pUT18C_1B	TACCCGGGGATCCTCTAGAGT	Amplification of pUT18C
60	pET21a_1A	CACCACCACCACCACCAC	Amplification of pET21a(+) for gfp fusions
61	pET21a_1B	ATGTATATCTCCTTCTTAAAGTTAAA CAAAATTATTTCTAGAGG	Amplification of pET21a(+) for gfp fusions
62	pRL271_Fwd	GAGCTCGCGAAAGCTTGCATG	Amplification of pRL271 and pRL278
63	pRL271_Rev	CTCGAGATCTAGATATCGAATTTCTG CCAT	Amplification of pRL271
64	pRL278_Rev	CCGCTTATTATCACTTATTCAGGCG	Amplification of pRL278
65	pETM22_Vec_R	ATGTTTTTCGTATTTTCCCTACCAGA AGAATGATGATGATGATGG	Amplificaiton of pETM22
66	pETM22_Vec_F	TGGATGAACTATACAAATAAATCCG GCTGCTAACAAAGC	Amplificaiton of pETM22
67	Vector.FOR	TGATGTTCAACTTCGACAGCGAATT CCTCGACCTGCAGGG	Amplification of pIGA
68	Vector.REV	AGGGACTCTTCTCTACAGGTGGTAC CCCGGGTTCGAAATCG	Amplification of pIGA
69	YFP_pcpc560_2A	CATAAAGTCAAGTAGGAGATTAATTC AATGCTGAGCAAGGGCGA	Amplification of YFP with overhang to P_{cpc560}
70	YFP_2A	TACAGGTTAGGAGAACGCCATGCTG AGCAAGGGCG	Amplification of YFP
71	YFP-Myc_2B	CAGATCCTCTTCAGAGATGAGTTTC TGCTCCTTGTACAGCTCGTCCATGC	Amplification of YFP with C-terminal *myc*
72	Myc+Linker_2B	TCCTGAACCCGATCCAGAGCCCAGA TCCTCTTCAGAGATGAGTTTC	Amplification of YFP with C-terminal *myc* and a GSGSGSG linker
73	XIII-GFP_1A	GCTAGCGACTCGACCGGTTC	Amplification of pRL153

74	XIII-GFP_1B	GCTTAATTTCTCCTCTTTAATTCTAG GTACCCG	Amplification of pRL153
75	eYFP_MYC_3A	GAGCAGAAACTCATCTCTGAAGAGG ATCTGATGCTGAGCAAGGGCGAG	*yfp* for pTHS82
76	eYFP_3B	AACCGGTCGAGTCGCTAGCTTACTT GTACAGCTCGTCCATGC	*yfp* for pTHS82
77	GFP_pAM2991_2B	GCCTGCAGGTCGACTCTAGATTATT TGTATAGTTCATCCATGCCATGTG	*syc1139-gfp* for pTHS74
78	His_pAM2991_2B	GCCTGCAGGTCGACTCTAGATCAGT GGTGGTGGTGGTG	*syc2039-gfp-his* for pTHS75
79	CS.3_Fwd	GATCCGTGCACAGCACCTTG	Amplification of CS.3 cassette
80	CS.3_Rev	TTATTTGCCGACTACCTTGGTGATCT	Amplification of CS.3 cassette
81	nptII_Fwd	ATGATTGAACAAGATGGATTGCACG	Amplification of nptII
82	nptII_Rev	TCAGAAGAACTCGTCAAGAAGGCG	Amplification of nptII
83	pUC_ori_Fwd	TTGAGATCCTTTTTTTCTGCGCGTAA TC	Amplification of pUC origin
84	pUC_ori_Rev	TTTCCATAGGCTCCGCCCC	Amplification of pUC origin
85	nptII_A	AAGCTTCACGCTGCCGCAA	Amplification of P_{nptII}::*nptII*
86	nptII_B	TCAGAAGAACTCGTCAAGAAGGCG	Amplification of P_{nptII}::*nptII*
87	GFP_pET21a_2B	AGTGGTGGTGGTGGTGGTGTTTGTA TAGTTCATCCATGCCATGTGTAATC	Amplification of *gfp*-fusions for insertion into pET21a(+)
88	7001_EcoRI_Fwd	GCATGAATTCAGGGAAAATACGAAA AACATTG	*fm7001* for pTHS73
89	7001_His_PstI_R	GCTACTGCAGTCAGTGGTGATGGTG ATGATGGACTAAGGCAGTCATTAAA TAGT	*fm7001* for pTHS73
90	Fragment 1.FOR	GATTTCGAACCCGGGGTACCACCTG TAGAGAAGAGTCCCTGAATATCAA	P_{cpc560} for pTHS60
91	Fragment 1.REV	TTTTTCGTATTTTCCCTCATTGAATTA ATCTCCTACTTGACTTTATGAGTTGG GA	P_{cpc560} for pTHS60
92	Fragment 2.FOR	TCAAGTAGGAGATTAATTCAATGAG GGAAAATACGAAAAACATTGGAGT	*fm7001* for pTHS60
93	Fragment 2.REV	GCACTAGCAGATGCACTAGCGACTA AGGCAGTCATTAAATAGTGAAGTAA GTAATTAAAGTAAC	*fm7001* for pTHS60
94	Fragment 3.FOR	ATTTAATGACTGCCTTAGTCGCTAGT GCATCTGCTAGTGCTAGT	*gfp*-tagged genes for pTHS60
95	Fragment 3.REV	CCGACAATCCAAACACCGGTTTATT TGTATAGTTCATCCATGCCATGTGTA ATCC	*gfp*-tagged genes for pTHS60
96	Fragment 4.FOR	TGGATGAACTATACAAATAAACCGG TGTTTGGATTGTCGG	T_{rbcL} for pTHS60
97	Fragment 4.REV	CCCTGCAGGTCGAGGAATTCGCTGT CGAAGTTGAACATCAGTAAGC	T_{rbcL} for pTHS60

98	TrbcL_A	ACCGGTGTTTGGATTGTCGG	Amplification of pIGA containing P_{cpc560} and T_{rbcL} for pTH76
99	pIGA_Pcpc560_1B	TGAATTAATCTCCTACTTGACTTTATGAGTTGGG	Amplification of pIGA containing P_{cpc560} and T_{rbcL} for pTH76
100	YFP_pcpc560_2A	CATAAAGTCAAGTAGGAGATTAATTCAATGCTGAGCAAGGGCGA	*yfp-fm7001* for pTHS76
101	7001_TrbcL_2B	CCGACAATCCAAACACCGGTTCAGACTAAGGCAGTCATTAAATAGTGAAG	*yfp-fm7001* for pTHS76
102	7001F_BamHI	ACTGGATCCAGGGAAAATACGAAAAACATTGGA	*fm7001* for pTHS63
103	7001R_NotI	AGCGGCCGCTCAGACTAAGGCAGTCATTAAATAGTG	*fm7001* for pTHS63
104	7001F_BamHI	GGATCCTATGAGGGAAAATACGAAAAAC	*fm7001* for pTHS95, pTHS96, pTHS97 and pTHS98
105	7001R_EcoRI	AGCGAATTCTCAGACTAAGGCAGTCAT	*fm7001* for pTHS96 and pTHS98
106	7001R_SacI	GAGCTCCTGACTAAGGCAGTCATTA	*fm7001* for pTHS95 and pTHS97
107	7120petER_7001ol	GTATTTTCCCTCATACCTGTAGTTTTATTTTTCTTATTTC	*petE* for pTHS83 (overlap PCR)
108	7001F_petEol	AAAACTACAGGTATGAGGGAAAATACGAAAAAC	*fm7001* for pTHS83 (overlap PCR)
109	7001R_SacI_C	AGCGAGCTCTAAGGCAGTCATTAAATAGTG	*fm7001* for pTHS83
110	7001F_NheI	AACTGCTAGCAGGGAAAATACGAAAAAC	*fm7001* for pTHS83
111	7001_3A	CTCTGGATCGGGTTCAGGAATGAGGGAAAATACGAAAAACATTGG	*fm7001* for pTHS84
112	7001_3B	CCTTTCGTCTTCAAGAATTCTTCAGACTAAGGCAGTCATTAAATAGTG	*fm7001* for pTHS84
113	pRL271_7up_F	AGAAATTCGATATCTAGATCTCGAGAGCAATGTGAGTGAGTTCGTGAGC	Upstream homology for pTHS126
114	7001KO_1B	GTGCTTGCGGCAGCGTGAAGCTTGGGGTTATCCTTAATAGAAGAAGAGTGC	Upstream homology for pTHS126
115	7001KO_2A	CGCCTTCTTGACGAGTTCTTCTGAATCAAGAGCATTCTTGATTTCTGTCTCA	Downstream homology for pTHS126
116	pRL271_7down_R	CAGGCATGCAAGCTTTCGCGAGCTCTGCTACCAAGACGATGCGTTTCATGTC	Downstream homology for pTHS126

117	7001KO_2A2	AATTCGATATCTAGATCTCGAGTTGCGTTTCAAAACACTACAAATTAGTACAAAC	Upstream homology for pTHS127
118	7001KO_2B2	AAGGTGCTGTGCACGGATCGGGGTTATCCTTAATAGAAGAAGAGTGC	Upstream homology for pTHS127
119	7001KO_4A2	CAAGGTAGTCGGCAAATAAATCAAGAGCATTCTTGATTTCTGTCTC	Downstream homology for pTHS127
120	7001KO_4B2	TGCAAGCTTTCGCGAGCTCCTGAAGACAAAGATGAAGTTTCGATATTACC	Downstream homology for pTHS127
121	trunc7001_2A	CTGAATAAGTGATAATAAGCGGTTGCGTTTCAAAACACTACAAATTAGTACAAA	Truncated *fm7001* for pTHS128
122	trunc7001_2B	TGCAAGCTTTCGCGAGCTCGTATTGATACTGGGTTGAGAATACTGC	Truncated *fm7001* for pTHS128
123	7001_gRNA_A	AGATGAGTTTTGCACAAAGTTGGA	*fm7001* gRNA for pTHS121 and pTHS123
124	7001_gRNA_B	AGACTCCAACTTTGTGCAAAACTC	*fm7001* gRNA for pTHS121 and pTHS123
125	Fm7001_HL1A	TTGTCTAGCTTTAATGCGGTAGTTGGTACCAGGAACATCGCGTCTCTACC	Downstream homology repair template for pTHS121 and pTHS123
126	Fm7001_HL1B	AAGAATGCTCTTGATGGGGTTATCCTTAATAGAAGAAGAGTGC	Upstream homology repair template for pTHS121 and pTHS123
127	Fm7001_HL2A	TATTAAGGATAACCCCATCAAGAGCATTCTTGATTTCTGTCTC	Upstream homology repair template for pTHS121 and pTHS123
128	Fm7001_HL2B	GATTACAGATCCTCTAGAGTCGACGGTACCTAAGGCAGCAACGTTTTCCG	Downstream homology repair template for pTHS121 and pTHS123
129	Syn017_NdeI_fwd	GCTACATATGACAAGTCAAAATTTTGTTTCTGAT	*slr7083* for pTHS61
130	Syn017_XhoI_wo_rev	GCTACTCGAGTGGTAAATAAGGGGGAGTGG	*slr7083* for pTHS61
131	pIGA_V_017_R	ACAAAATTTTGACTTGTCATTGAATTAATCTCCTACTTGACTTTATGAGTTGG	Amplification of pIGA with P_{cpc560} and T_{rbcL} for pTHS77
132	pIGA_V_017_F	CCACTCCCCCTTATTTACCAGCTAGTGCATCTGCTAGTGCT	Amplification of pIGA with P_{cpc560}

			and T_{rbcL} for pTHS77
133	pIGA_Syn017_F	TCAAGTAGGAGATTAATTCAATGACA AGTCAAAATTTTGTTTCTGATCAAG	*slr7083* for pTHS77
134	pIGA_Syn017_R	GCACTAGCAGATGCACTAGCTGGTA AATAAGGGGGAGTGGGAC	*slr7083* for pTHS77
135	Syn017_pRL25c_F	TAAAACTACAGGTTAGGAGAACGCC ATGACAAGTCAAAATTTTGTTTCTGA TCAAGATACC	*slr7083* for pTHS86
136	Syn017_pRL25c_R	CACTAGCACTAGCAGATGCACTAGC TGGTAAATAAGGGGGAGTGGGACG	*slr7083* for pTHS86
137	017_up_Fwd	GTCAGGGGGGCGGAGCCTATGGAA ATTTCCCAACAAATTAGTGAATGGCA GG	Upstream homology for pTHS120
138	017_up_Rev	CGTGCAATCCATCTTGTTCAATCATT GTTTTACCAGATTAAAATTAATGATT GAGACAGAATTGAAAAG	Upstream homology for pTHS120
139	017_down_Fwd	TCGCCTTCTTGACGAGTTCTTCTGA GATTTCCAGTCACTTCCGTTTTTTTA CTATTAGG	Downstream homology for pTHS120
140	017_down_Rev	TACGCGCAGAAAAAAAGGATCTCAA AATCCTAAAATTCGTGGTTCATCTTT CTTTGT	Downstream homology for pTHS120
141	Syn017_3A	CTCTGGATCGGGTTCAGGAATGACA AGTCAAAATTTTGTTTCTGATC	*slr7083* for pTHS85
142	Syn017_3B	CCTTTCGTCTTCAAGAATTCTCTATG GTAAATAAGGGGGAGTGGG	*slr7083* for pTHS85
143	Syn017_pET_2A	GTTTAACTTTAAGAAGGAGATATACA TATGACAAGTCAAAATTTTGTTTCTG ATCAAG	*slr7083* for pTHS69
144	017_Seq_A	CCACAGCGGAAACCTTTTTAGATC	Sequencing of Δ*slr7083* plasmids
145	017_Seq_B	AAACGAACAGAGTGGAACTTTGC	Sequencing of Δ*slr7083* plasmids
146	Syc484_2A	GTTTAACTTTAAGAAGGAGATATACA TATGAACTACGCTCTTACCCAAG	*syc2039* for pTHS87
147	Syc484_2B	AGTGGTGGTGGTGGTGGTGAGACC CTAACCAGCGGC	*syc2039* for pTHS87
148	Syc484_pIGA_2A	TAAAGTCAAGTAGGAGATTAATTCAA TGAACTACGCTCTTACCCAAGC	*syc2039* for pTHS80
149	Syc484_2A2	TACAGGTTAGGAGAACGCCATGAAC TACGCTCTTACCCAAG	*syc2039* for pTHS62
150	Syc484_2B2	CACTAGCAGATGCACTAGCAGACCC TAACCAGCGGC	*syc2039* for pTHS62
151	Syc484_pAM2991_2 A	CACACAGGAAACAGACCATGAACTA CGCTCTTACCCAAGC	*syc2039* for pTHS75
152	Syc484_KO_2A	TGTAGGAGATCTTCTAGAAAGATGT AGGCATCAAAGGCAGGC	Upstream homology for pTHS119
153	Syc484_KO_2B	CTTGCGGCAGCGTGAAGCTTAGCAA AGCAAAAGAAGCGATCG	Upstream homology for pTHS119

154	Syc484_KO_4A	TTCTTGACGAGTTCTTCTGATTCTGC TGCGATGCGTTAGG	Downstream homology for pTHS119
155	Syc484_KO_4B	CTCGAGTTTTTCAGCAAGATCAAGT AAGACTGGCTGCCATG	Downstream homology for pTHS119
156	Syc484_Seq_A	GATGCCACCGAGCAGAATTAG	Verification of Δ*syc2039*
157	Syc484_Seq_B	GGCAGATCAATCAGCAGCTC	Verification of Δ*syc2039*
158	Syc879_pET_2A	GTTTAACTTTAAGAAGGAGATATACA TATGCTCTATCTGGCTGAAGTCG	*syc1139* for pTHS66
159	Syc879_pET_2B	CAGTGGTGGTGGTGGTGGTGGGCT GCAATCAGTTGATGACT	*syc1139* for pTHS66
160	Syc879_pIGA_2A	TAAAGTCAAGTAGGAGATTAATTCA GTGCTCTATCTGGCTGAAGTCGG	*syc1139* for pTHS81
161	Syc879_2A	TACAGGTTAGGAGAACGCCATGCTC TATCTGGCTGAAGTCG	*syc1139* for pTHS93
162	Syc879_2B	CACTAGCAGATGCACTAGCGGCTGC AATCAGTTGATGACTG	*syc1139* for pTHS93
163	Syc879_pAM2991_2A	CACACAGGAAACAGACCATGCTCTA TCTGGCTGAAGTCGG	*syc1139* for pTHS74
164	Syc879_KO_2A	TGTAGGAGATCTTCTAGAAAGATCT GGAGCGATCGCTATGG	Upstream homology for pTHS133
165	Syc879_KO_2B	CTTGCGGCAGCGTGAAGCTTTATCG ATGCCTCGCCTTAATCAATC	Upstream homology for pTHS133
166	Syc879_KO_4A	CCTTCTTGACGAGTTCTTCTGAGCC AGTCCCCCGCGACTA	Downstream homology for pTHS133
167	Syc879_KO_4B	CTCGAGTTTTTCAGCAAGATGGCAA GCGCAACTGAATTCTTAC	Downstream homology for pTHS133
168	Syn708_NdeI_F	GCTACATATGCTCTATCTGGCTGAA ATTAAGAAA	*slr1301* for pTHS65
169	Syn708_XhoI_R_w/o	GCTACTCGAGACCGCCAAACAATAG GGTC	*slr1301* for pTHS65
170	Syn708_pET_2A	GTTTAACTTTAAGAAGGAGATATACA TATGCTCTATCTGGCTGAAATTAAGA AAC	*slr1301* for pTHS67
171	Syn708_pRL25c_Fwd	TAAAACTACAGGTTAGGAGAACGCC ATGCTCTATCTGGCTGAAATTAAGAA ACAAAC	*slr1301* for pTHS91
172	Syn708_pRL25c_Rev	CACTAGCACTAGCAGATGCACTAGC ACCGCCAAACAATAGGGTCT	*slr1301* for pTHS91
173	Syn708_3A	CTCTGGATCGGGTTCAGGAGTGCTC TATCTGGCTGAAATTAAG	*slr1301* for pTHS92
174	Syn708_3B	CCTTTCGTCTTCAAGAATTCTCTAAC CGCCAAACAATAGGGTC	*slr1301* for pTHS92
175	153Syn708_2A	AGAATTAAAGAGGAGAAATTAAGCA TGCTCTATCTGGCTGAAATTAAGAAA C	*slr1301* for pTHS82
176	153Syn708_2B	TCAGAGATGAGTTTCTGCTCACCGC CAAACAATAGGGTC	*slr1301* for pTHS82

177	pJET708_2A	TGTAGGAGATCTTCTAGAAAGATAATAGACTGCAATGTCAAAAAACTCAG	Upstream homology for pTHS131
178	708KO_CS3_2B	CAAGGTGCTGTGCACGGATCAAGTCGTTGTCCTGAGCAG	Upstream homology for pTHS131
179	708KO_CS3_4A	CCAAGGTAGTCGGCAAATAATTGGGTTGGTTGCCGAC	Downstream homology for pTHS131
180	pJET708_4B	CTCGAGTTTTTCAGCAAGATTTAGCAAGGTGGGGGGAATG	Downstream homology for pTHS131
181	708KO_1Aa	CCTGATTCTGTGGATAACCGTACGTCAAAATCGAATTCCCGGTC	Upstream homology for pTHS132
182	708KO_1B	TGCTTGCGGCAGCGTGAAGCTTAAGTCGTTGTCCTGAGCAGTG	Upstream homology for pTHS132
183	708KO_2A	CGCCTTCTTGACGAGTTCTTCTGATTGGGTTGGTTGCCGACTTC	Downstream homology for pTHS132
184	708KO_2B	GATTATCAAAAAGGATCTTCACCTTTAGCAAGGTGGGGGGAATGC	Downstream homology for pTHS132
185	Nos389_pET_2A	GTTTAACTTTAAGAAGGAGATATACATATGAATAGTGAGTTGTTCCAGAAGC	*all4981* for pTHS72
186	Nos389_NdeI_F	GCTACATATGAATAGTGAGTTGTTCCAGAAG	*all4981* for pTHS64
187	Nos389_XhoI_wo_R	GCTACTCGAGGATGTTACTATCACTACTTTGAATTTTT	*all4981* for pTHS64
188	Nos389_2A	CTACAGGTTAGGAGAACGCCATGAATAGTGAGTTGTTCCAGAAGCTAGC	*all4981* for pTHS89
189	Nos389_2B	GCACTAGCAGATGCACTAGCGATGTTACTATCACTACTTTGAATTTTTTTGAGTTTGGC	*all4981* for pTHS89
190	Nos389_3A	CTCTGGATCGGGTTCAGGAATGAATAGTGAGTTGTTCCAGAAGC	*all4981* for pTHS88
191	Nos389_3B	CCTTTCGTCTTCAAGAATTCTTTAGATGTTACTATCACTACTTTGAATTTTTTTGAG	*all4981* for pTHS88
192	Nos389_pIGA_2A	TAAAGTCAAGTAGGAGATTAATTCAATGAATAGTGAGTTGTTCCAGAAGC	*all4981* for pTHS79
193	Nos389_TrbcL_2B	CCGACAATCCAAACACCGGTTTAGATGTTACTATCACTACTTTGAATTTTTTTGAGTTTG	*all4981* for pTHS78
194	389KO_2A	ATTCGATATCTAGATCTCGAGTGTCAGATTTAGTACTTTAAATACAAGACTTACACAC	Upstream homology for pTHS129
195	389KO_2B	CAAGGTGCTGTGCACGGATCAGCTGTTCGCTCTTGAGGG	Upstream homology for pTHS129
196	389KO_4A	CCAAGGTAGTCGGCAAATAAAGTAACGCGATGTGCGACT	Downstream homology for pTHS129

197	389KO_4B	ATGCAAGCTTTCGCGAGCTCGATTA ATACCTTTGGTGTTCATGACACTGG	Downstream homology for pTHS129
198	trunc389_2A	CTGAATAAGTGATAATAAGCGGAAG CCATTTTAGATCGAGAGGCG	Truncated *all4981* for pTHS130
199	trunc389_2B	TGCAAGCTTTCGCGAGCTCGCTAAA TTCCAAAACTCACTGCCTT	Truncated *all4981* for pTHS130
200	Nos389_gRNA-A	AGATCAGAAGCTAGCAAAAGCACA	*all4981* gRNA for pTHS124 and pTHS125
201	Nos389_gRNA-B	AGACTGTGCTTTTGCTAGCTTCTG	*all4981* gRNA for pTHS124 and pTHS125
202	Nos389_HL1A	TTTGTCTAGCTTTAATGCGGTAGTTG GTACCGTGTGGGGTAATTTGCGGG	Upstream homology for pTHS124 and pTHS125
203	Nos389_HL1B	ATAAGTCGCACATCGCGTTACTTCA TAGCTGTTCGCTCTTGAGG	Upstream homology for pTHS124 and pTHS125
204	Nos389_HR2A	CCTCAAGAGCGAACAGCTATGAAGT AACGCGATGTGCGACTTATTC	Downstream homology for pTHS124 and pTHS125
205	Nos389_HR2B	GGATTACAGATCCTCTAGAGTCGAC GGTACCGGACACCACCAGCCATTTC	Downstream homology for pTHS124 and pTHS125
206	MB_1A	TGCCTGCAGGTCGACTCTAATGAAT AGTGAGTTGTTCCAGAAGC	*all4981* for pTHS107 and pTHS109
207	MB_1B	TCGGTACCCGGGGATCCTCGATGTT ACTATCACTACTTTGAATTTTTTTGA GT	*All4981* for pTHS107 and pTHS109
208	MB_2A	AGGGTCGACTCTAGAGGATATGAAT AGTGAGTTGTTCCAGAAGC	*all4981* for pTHS108
209	MB_2B	CTTACTTAGGTACCCGGGGGATGTT ACTATCACTACTTTGAATTTTTTTGA GT	*all4981* for pTHS108
210	MB_4A	TCTAGAGGATCCCCGGGTAATGAAT AGTGAGTTGTTCCAGAAGC	*all4981* for pTHS110
211	MB_4B	TCGATGAATTCGAGCTCGGGATGTT ACTATCACTACTTTGAATTTTTTTGA GT	*all4981* for pTHS110
212	MB_9A	TGCCTGCAGGTCGACTCTAATGCTC TATCTGGCTGAAATTAAGAAAC	*slr1301* for pTHS111 and pTHS113
213	MB_9B	TCGGTACCCGGGGATCCTCACCGC CAAACAATAGGGT	*slr1301* for pTHS111 and pTHS113
214	MB_10A	AGGGTCGACTCTAGAGGATATGCTC TATCTGGCTGAAATTAAGAAAC	*slr1301* for pTHS112

215	MB_10B	CTTACTTAGGTACCCGGGGACCGCC AAACAATAGGGTC	*slr1301* for pTHS112
216	MB_12A	TCTAGAGGATCCCCGGGTAATGCTC TATCTGGCTGAAATTAAGAAAC	*slr1301* for pTHS114
217	MB_12B	TCGATGAATTCGAGCTCGGACCGCC AAACAATAGGGTC	*slr1301* for pTHS114
218	MB_13A	TGCCTGCAGGTCGACTCTAATGACA AGTCAAAATTTTGTTTCTGATCAAG	*slr7083* for pTHS99 and pTHS101
219	MB_13B	TCGGTACCCGGGGATCCTCTGGTAA ATAAGGGGGAGTGGGAC	*slr7083* for pTHS99 and pTHS101
220	MB_14A	AGGGTCGACTCTAGAGGATATGACA AGTCAAAATTTTGTTTCTGATCAAG	*slr7083* for pTHS100
221	MB_14B	CTTACTTAGGTACCCGGGGTGGTAA ATAAGGGGGAGTGGGAC	*slr7083* for pTHS100
222	MB_16A	TCTAGAGGATCCCCGGGTAATGACA AGTCAAAATTTTGTTTCTGATCAAG	*slr7083* for pTHS102
223	MB_16B	TCGATGAATTCGAGCTCGGTGGTAA ATAAGGGGGAGTGGGAC	*slr7083* for pTHS102
224	MB_33A	TGCCTGCAGGTCGACTCTAATGCTC TATCTGGCTGAAGTCG	*syc1139* for pTHS115 and pTHS117
225	MB_33B	TCGGTACCCGGGGATCCTCGGCTG CAATCAGTTGATGACT	*syc1139* for pTHS115 and pTHS117
226	MB_34A	AGGGTCGACTCTAGAGGATATGCTC TATCTGGCTGAAGTCG	*syc1139* for pTHS116
227	MB_34B	CTTACTTAGGTACCCGGGGGGCTG CAATCAGTTGATGACT	*syc1139* for pTHS116
228	MB_36A	TCTAGAGGATCCCCGGGTAATGCTC TATCTGGCTGAAGTCG	*syc1139* for pTHS118
229	MB_36B	TCGATGAATTCGAGCTCGGGGCTGC AATCAGTTGATGACT	*syc1139* for pTHS118
230	MB_45A	TGCCTGCAGGTCGACTCTAATGAAC TACGCTCTTACCCAAG	*syc2039* for pTHS103 and pTHS105
231	MB_45B	TCGGTACCCGGGGATCCTCAGACC CTAACCAGCGGC	*syc2039* for pTHS103 and pTHS105
232	MB_46A	AGGGTCGACTCTAGAGGATATGAAC TACGCTCTTACCCAAG	*syc2039* for pTHS104
233	MB_46B	CTTACTTAGGTACCCGGGGAGACCC TAACCAGCGGC	*syc2039* for pTHS104
234	MB_48A	TCTAGAGGATCCCCGGGTAATGAAC TACGCTCTTACCCAAG	*syc2039* for pTHS106
235	MB_48B	TCGATGAATTCGAGCTCGGAGACCC TAACCAGCGGC	*syc2039* for pTHS106
236	708_Seq_A	CCAACAAACTACCTACCACCAGTC	Verification of *Δslr1301*
237	708_Seq_B	CCGTAGGGATGCCTGATAAACC	Verification of *Δslr1301*
238	Syc879_Seq_A	CATCAGGAATGGATGCAGGAGG	Verification of *Δsyc1139*

239	Syc879_Seq_B	GGCCGCTAATCACTTTCAGTG	Verification of *Δsyc1139*

1307 Restriction sites or overlapping sites are underlined.

1308

1309 **Supplementary Table 5: Employed and generated Plasmids**

Plasmids	Description	Resistance	Reference
pJET1.2/ blunt	*E. coli* subcloning vector	Amp	Thermo Fischer Scientific
pMAL-c2x	Bacterial vector for expressing N-terminal MBP-tagged proteins in *E. coli* with a Factor Xa cleavage site	Amp	A gift from Axel Scheidig (University of Kiel)
pet21a(+)	Bacterial vector for expressing C-terminal 6His-tagged proteins in *E. coli*	Amp	Novagen
pRL25C	Shuttle cosmid vector for cyanobacteria and *E. coli*	Km, Nm	Wolk *et al.*, 1988
pRL623	Methylation plasmid	Cm	Wolk *et al.*, 1988
pRL443	Conjugation plasmid	Amp	Wolk *et al.*, 1988
pRL271	*sacB* containing plasmid to select for double homologous recombination in *Anabaena*	Cm	Cai and Wolk, 1990
pRL278	*sacB* containing plasmid to select for double homologous recombination in *Anabaena*	Km, Nm	Cai and Wolk, 1990
pSL2680	Cpf1-mediated CRISPR editing plasmid	Km, Nm	Ungerer and Pakrasi, 2016
pRL25c-CRISPR	Functional CRISPR cassette from pSL2680 transferred into EcoRI and BamHI digested pRL25c by GIBSON assembly	Km, Nm	This work
pSM2-Pcpc560ter	pMD18-T derivate for insertion into *pta*, containing P_{cpc560}::*ter*::T_{rbcL} expression cassette	Km, Amp	A gift from Yin Li (Chinese Academy of Science). Zhou *et al.*, 2014
pIGA	Cyanobacterial vector for insertion into neutral locus (RS1 and RS2) of *slr0168* in *Synechocystis*	Amp, Km	A gift from Martin Hagemann (University of Rostock), Kunert, Hagemann and Erdmann, 2000
pRL153-GFP	Mobilizable broad host range vector, P_{trc}-*gfp*	Km, Nm	Tolonen, Liszt and Hess, 2006
pKNT25	P_{lac}::-*T25*	Km	Euromedex
pKT25	P_{lac}::*T25*-	Km	Euromedex
pUT18	P_{lac}::-*T18*	Amp	Euromedex
pUT18C	P_{lac}::*T18*-	Amp	Euromedex

pKT25-zip	pKT25; P_{lac}::*T25-zip*	Km	Euromedex
pUT18C-zip	pUT18C, P_{lac}::*T18-zip*	Amp	Euromedex
pAM2991	Cyanobacterial vector for expression of proteins under the control of P_{trc} that inserts into the NS1 site of *Synechococcus*	Sm, Sp	A gift from Susan Golden (Addgene plasmid # 40248)
pTHS1	pRL25C, P_{petE}::*alr4504-gfp*	Km, Nm	Springstein *et al*., 2019
pTHS33	pKNT25, P_{lac}::*sepJ-T25*	Km, Nm	Springstein *et al.*, 2019
pTHS34	pKT25, P_{lac}::*T25-sepJ*	Km, Nm	Springstein *et al*., 2019
pTHS35	pUT18, P_{lac}::*sepJ-T18*	Amp	Springstein *et al*., 2019
pTHS36	pUT18C, P_{lac}::*T18-sepJ*	Amp	Springstein *et al*., 2019
pTHS37	pKNT25, P_{lac}::*ftsZ-T25*	Km, Nm	Springstein *et al*., 2019
pTHS38	pKT25, P_{lac}::*T25-ftsZ*	Km, Nm	Springstein *et al*., 2019
pTHS39	pUT18, P_{lac}::*ftsZ-T18*	Amp	Springstein *et al*., 2019
pTHS40	pUT18C, P_{lac}::*T18-ftsZ*	Amp	Springstein *et al*., 2019
pTHS41	pKNT25, P_{lac}::*mreB-T25*	Km, Nm	Springstein *et al*., 2019
pTHS42	pKT25, P_{lac}::*T25-mreB*	Km, Nm	Springstein *et al*., 2019
pTHS43	pUT18, P_{lac}::*mreB-T18*	Amp	Springstein *et al*., 2019
pTHS44	pUT18C, P_{lac}::*T18-mreB*	Amp	Springstein *et al*., 2019
pTHS60	pIGA, P_{cpc560}::*fm7001-gfp*::T_{rbcL}	Amp, Km	This study
pTHS61	pET21a(+), P_{T7}::*slr7083-his*	Amp	This study
pTHS62	pET21a(+), P_{T7}::*syc2039-his*	Amp	This study
pTHS63	pET21a(+), P_{T7}::*fm7001-his*	Amp	This study
pTHS64	pET21a(+), P_{T7}::*all4981-his*	Amp	This study
pTHS65	pET21a(+), P_{T7}::*slr1301-his*	Amp	This study
pTHS66	pET21a(+), P_{T7}::*syc1139-his*	Amp	This study
pTHS67	pET21a(+); P_{T7}::*slr1301-gfp*	Amp	This study
pTHS68	pET21a(+), P_{T7}::*syc1139-gfp*	Amp	This study
pTHS69	pET21a(+), P_{T7}::*slr7083-gfp*	Amp	This study
pTHS70	pET21a(+), P_{T7}::*fm7001-gfp*	Amp	This study
pTHS71	pET21a(+), P_{T7}::*syc2039-gfp*	Amp	This study
pTHS72	pET21a(+), P_{T7}::*all4981-gfp*	Amp	This study
pTHS73	pMAL-c2x; P_{tac}::*mbp-fm7001-his*	Amp	This study
pTHS74	pAM2991, P_{trc}::*syc1139-gfp*	Sm, Sp	This study
pTHS75	pAM2991, P_{trc}::*syc2039-gfp-his*	Sm, Sp	This study
pTHS76	pIGA, P_{cpc560}::*yfp-fm7001*::T_{rbcL}	Amp, Km	This study

pTHS77	pIGA, P_{cpc560}::*slr7083-gfp*::T_{rbcL}	Amp, Km	This study
pTHS78	pIGA, P_{cpc560}::*yfp-all4981*::T_{rbcL}	Amp, Km	This study
pTHS79	pIGA, P_{cpc560}::*all4981-gfp*::T_{rbcL}	Amp, Km	This study
pTHS80	pIGA, P_{cpc560}::*syc2039-gfp*::T_{rbcL}	Amp, Km	This study
pTHS81	pIGA, P_{cpc560}::*syc1139-gfp*::T_{rbcL}	Amp, Km	This study
pTHS82	pRL153, P_{trc}::*slr1301-yfp*	Km, Nm	This study
pTHS83	pRL25C, P_{petE}::*fm7001-gfp*	Km, Nm	This study
pTHS84	pRL25C, P_{petE}::*yfp-fm7001*	Km, Nm	This study
pTHS85	pRL25C, P_{petE}::*yfp-slr7083*	Km, Nm	This study
pTHS86	pRL25C, P_{petE}::*slr7083-gfp*	Km, Nm	This study
pTHS87	pRL25C, P_{petE}::*syc2039-gfp*	Km, Nm	This study
pTHS88	pRL25C, P_{petE}::*yfp-all4981*	Km, Nm	This study
pTHS89	pRL25C, P_{petE}::*all4981-gfp*	Km, Nm	This study
pTHS90	pRL25C, P_{petE}-*creS-gfp*	Km, Nm	This study
pTHS91	pRL25C, P_{petE}::*slr1303-gfp*	Km, Nm	This study
pTHS92	pRL25C, P_{petE}::*yfp-slr1303*	Km, Nm	This study
pTHS93	pRL25C, P_{petE}::*syc1139-gf*	Km, Nm	This study
pTHS94	pRL25C, $P_{all4982}$::*all4982-ecfp*	Km, Nm	This study
pTHS95	pKNT25, P_{lac}::*fm7001-T25*	Km, Nm	This study
pTHS96	pKT25, P_{lac}::*T25-fm7001*	Km, Nm	This study
pTHS97	pUT18, P_{lac}::*fm7001-T18*	Amp	This study
pTHS98	pUT18C, P_{lac}::*T18-fm7001*	Amp	This study
pTHS99	pKNT25, P_{lac}::*slr7083-T25*	Km, Nm	This study
pTHS100	pKT25, P_{lac}::*T25-slr7083*	Km, Nm	This study
pTHS101	pUT18, P_{lac}::*slr7083-T18*	Amp	This study
pTHS102	pUT18C, P_{lac}::*T18-slr7083*	Amp	This study
pTHS103	pKNT25, P_{lac}::*syc2039-T25*	Km, Nm	This study
pTHS104	pKT25, P_{lac}::*T25-syc2039*	Km, Nm	This study
pTHS105	pUT18, P_{lac}::*syc2039-T18*	Amp	This study
pTHS106	pUT18C, P_{lac}::*T18-syc2039*	Amp	This study
pTHS107	pKNT25, P_{lac}::*all4981-T25*	Km, Nm	This study
pTHS108	pKT25, P_{lac}::*T25-all4981*	Km, Nm	This study
pTHS109	pUT18, P_{lac}::*all4981-T18*	Amp	This study
pTHS110	pUT18C, P_{lac}::*T18-all4981*	Amp	This study
pTHS111	pKNT25, P_{lac}::*slr1301-T25*	Km, Nm	This study
pTHS112	pKT25, P_{lac}:: *T25-slr1301*	Km, Nm	This study
pTHS113	pUT18, P_{lac}::*slr1301-T18*	Amp	This study
pTHS114	pUT18C, P_{lac}::*T18-slr1301*	Amp	This study
pTHS115	pKNT25, P_{lac}::*syc1139-T25*	Km, Nm	This study
pTHS116	pKT25, P_{lac}::*T25-syc1139*	Km, Nm	This study
pTHS117	pUT18, P_{lac}::*syc1139-T18*	Amp	This study
pTHS118	pUT18C, P_{lac}::*T18-syc1139*	Amp	This study
pTHS119	pJET1.2/blunt with ~1000 bp upstream and downstream of *syc2039* flanking *nptII*	Amp	This study
pTHS120	Circularized pUC ori with 1000 bp upstream and downstream of *slr7083*	Km, Nm	This study

	flanking *nptII* assembled by GIBSON assembly		
pTHS121	pSL2680 with *fm7001* gRNA and homologous repair templates 1000 bp upstream and downstream of *fm7001*	Km, Nm	This study
pTHS122	pRL25C containing *cpf1*, *lacZα* and pre-crRNA array with tandem spacer-repeat sequences from *Francisella novicida*	Km, Nm	This study
pTHS123	pTHS122 with *fm7001* gRNA and homologous repair templates 1000 bp upstream and downstream of *fm7001*	Km, Nm	This study
pTHS124	pSL2680 with *all4981* gRNA and homologous repair templates 1000 bp upstream and downstream of *all4981*	Km, Nm	This study
pTHS125	pTHS122 with *all4981* gRNA and homologous repair templates 1000 bp upstream and downstream of *all4981*	Km, Nm	This study
pTHS126	pRL271 containing 1000 bp upstream and downstream of *fm7001* flanking *nptII*	Km, Nm, Cm	This study
pTHS127	pRL278 containing 2000 bp upstream and downstream of *fm7001* flanking CS.3	Km, Nm, Sm, Sp	This study
pTHS128	pRL278 containing 2000 bp upstream of *fm7001* and the first 398 bp of *fm7001*	Km, Nm	This study
pTHS129	pRL278 containing 1000 bp upstream and downstream of *all4981* flanking CS.3	Km, Nm, Sm, Sp	This study
pTHS130	pRL278 containing 151 bp upstream of *all4981* and the first 449 bp of *all4981*	Km, Nm	This study
pTHS131	pJET1.2/blunt with ~1000 bp upstream and downstream of *slr1303* flanking CS.3 inserted by GIBSON assembly	Amp	This study
pTHS132	Circularized pUC ori with 1000 bp upstream and downstream of *slr1301* flanking *nptII* assembled by GIBSON assembly	Km, Nm	This study
pTHS133	pJET1.2/blunt with ~1000 bp upstream and downstream of *syc1139* flanking *nptII* inserted by GIBSON assembly	Amp	This study

Sm: streptomycin resistance; Sp: spectinomycin resistance; Amp: ampicillin resistance, Km: kanamycin resistance, Nm: neomycin resistance; Cm: chloramphenicol resistance.

- 1) The eYFP is C-terminally followed by a myc-tag, which is then followed by a heptapeptide of glycine and serine. Abbreviated: *yfp*.
- 2) Modified *gfpmut3.1* in which the internal NdeI site was removed by replacing CAT by the synonymous CAC codon. The GFP is N-terminally preceded by 12 alanine and serine residues. Abbreviated: *gfp*. (Stucken *et al.*, 2012).